COMPUTATIONAL FLUID DYNAMICS AND EXPERIMENTAL STUDY OF HYDRODYNAMICS IN AN INTERNAL AIRLIFT REACTOR

LIEW SHI YAN

MASTER OF SCIENCE

UNIVERSITI MALAYSIA PAHANG

UNIVERSITI MALAYSIA PAHANG

DECLARATION OF THESIS AND COPYRIGHT

Author's Full Name   : LIEW SHI YAN

Date of Birth   : 13 NOVEMBER 1990

Title   : COMPUTATIONAL FLUID DYNAMICS AND
EXPERIMENTAL STUDY OF HYDRODYNAMICS IN AN
INTERNAL AIRLIFT REACTOR

Academic Session   : SEM I 2019/2020

I declare that this thesis is classified as:

☐ CONFIDENTIAL (Contains confidential information under the Official Secret Act 1997)*

☐ RESTRICTED (Contains restricted information as specified by the organization where research was done)*

☒ OPEN ACCESS I agree that my thesis to be published as online open access (Full Text)

I acknowledge that Universiti Malaysia Pahang reserves the following rights:

1. The Thesis is the Property of Universiti Malaysia Pahang
2. The Library of Universiti Malaysia Pahang has the right to make copies of the thesis for the purpose of research only.
3. The Library has the right to make copies of the thesis for academic exchange.

Certified by:

_____   _____
(Student's Signature)   (Supervisor's Signature)

_____   Assoc. Prof. Dr. Jolius Gimbun
New IC/Passport Number   Name of Supervisor
Date: 15 November 2019   Date: 15 November 2019

NOTE : * If the thesis is CONFIDENTIAL or RESTRICTED, please attach a thesis declaration letter.

SUPERVISOR'S DECLARATION

I hereby declare that I have checked this thesis and, in my opinion, this thesis is adequate in terms of scope and quality for the award of the degree of Master of Science.

_____

(Supervisor's Signature)

Full Name : DR. JOLIUS GIMBUN

Position   : ASSOCIATE PROFESSOR

Date   : 15 NOVEMBER 2019

STUDENT'S DECLARATION

I hereby declare that the work in this thesis is based on my original work except for quotations and citations which have been duly acknowledged. I also declare that it has not been previously or concurrently submitted for any other degree at Universiti Malaysia Pahang or any other institutions.

_____

(Student's Signature)

Full Name　　: LIEW SHI YAN

ID Number　　: MKC 15031

Date　　　　 : 15 NOVEMBER 2019

COMPUTATIONAL FLUID DYNAMICS AND EXPERIMENTAL STUDY OF HYDRODYNAMICS IN AN INTERNAL AIRLIFT REACTOR

LIEW SHI YAN

Thesis submitted in fulfillment of the requirements
for the award of the degree of
Master of Science

Faculty of Chemical & Process Engineering Technology

UNIVERSITI MALAYSIA PAHANG

NOVEMBER 2019

ACKNOWLEDGEMENTS

ABSTRAK

Reaktor airlift berasaskan sistem gas-cecair baru-baru ini telah memperolehi perhatian daripada industri-industri tenaga yang boleh diperbaharui dan air kumbahan. Ini turut mendorong penggunaan kaedah komputasi bagi mengatasi had reka bentuk konvensional semasa dan menurunkan kos pengoptimuman. Kebanyakan kajian simulasi gas-cecair menggunakan kaedah dua-cecair model. Walaubagaimanapun, keupayaan ramalan model tersebut bergantung kepada pilihan *closure model* yang tepat untuk mengambil kira daya pertukaran momentum antara gas-cecair yang hilang akibat prosedur *ensemble-average*. Oleh itu, matlamat utama kerja ini adalah untuk membina sebuah computational fluid dynamics (CFD) model bagi reaktor *internal airlift* melalui penjelasan mantap *closure model* dalam dua-cecair model. Kajian ini boleh dibahagikan kepada dua bahagian utama. Pertama, penilaian *closure model* terhadap kuantiti aliran min telah dibuat di dalam reaktor *internal airlift* dengan gas sebahagian terlepas dalam *downcomer*. Simulasi ini menggunakan model turbulensi *k-ε dispersed* melalui model *Eulerian-Eulerian* untuk menyelesaikan medan aliran *transient*. *Closure model* yang dijelaskan dalam kajian ini merangkumi perbandingan model seretan, model daya penyebaran turbulen dan turbulen diinduksi oleh gelembung serta kesan model lif terhadap kuantiti aliran min. Keputusan menunjukkan bahawa hidrodinamik telah diprediksi dengan tepat apabila distorsi gelembung dan gerombolan gelembung diambil kira dalam model seretan melalui model Rayleigh-Taylor. Kuantiti aliran min yang diramalkan oleh *closure model* dengan data experimen segi purata permukaan gas, gas radial dan halaju cecair radial dimana kesilapan masing-masing yang diperolehi adalah 19.4%, 6.8% dan 13.5%. Bahagian kedua kajian ini adalah penilaian *closure model* dalam reaktor *internal airlift* dengan ketiadaan gas dalam *downcomer*. Kaedah model menggunakan dua-cecair model *Eulerian-Eulerian* dengan model turbulensi yang sama. Perbandingan diantara model seretan, kesan model lif dan model daya penyebaran turbulen dilaksanakan untuk prediksi halaju cecair paksi dalam *riser* dan *downcomer*. Prediksi disahkan dengan ukuran laser *Doppler* anemometri (LDA) yang diperolehi dari rig eksperimen. Dalam kajian ini, hasil simulasi menunjukkan ralat margin sebanyak 52.7% melalui model Rayleigh-Taylor, model lif dan model daya penyebaran turbulen. Secara keseluruhannya, keputusan simulasi memperoleh persetujuan yang munasabah dengan data eksperimen dengan ralat margin kurang daripada 20% dari segi gas pengedaran tempatan melalui model seret Rayleigh-Taylor, model lif fungsi nombor Reynolds dan Eötvös serta model daya penyebaran turbulen. Walaubagainmanapun, model dalam kajian ini adalah terhad kepada aliran homogen yang bergelora kerana ketiadaan model matematik yang mengira dinamik gelembung dalam aliran heterogen. Di samping itu, kesan lokasi *sparger* pada medan aliran juga dinilai menggunakan teknik pengukuran LDA. Didapati bahawa posisi $X_A = 0.125$ m adalah lebih cekap tenaga berbanding sparger pada kedudukan $X_B = 0.075$ m yang terletak berdekatan dengan dinding baffle. Posisi X_B menghasilkan *recirculation* dan magnitud halaju cecair yang lebih rendah dalam *downcomer*.

ABSTRACT

Gas-liquid airlift reactors have recently garnered interest from renewable energy and wastewater treatment industries, prompting the adoption of flexible computational method to elevate existing conventional scale-up constraints. Most gas-liquid simulation studies employed the two-fluid model owing to its computational affordability. However, the model's predictive capability depends on a proper choice of closure model to account the momentum exchange forces between the gas-liquid interphase lost during the trade-off. Hence, the main aim of this work is to develop a computational fluid dynamics (CFD) modelling approach in the gas-liquid internal airlift reactor via two-fluid model by elucidating the closure model. This study was divided into two main parts. Firstly, an assessment of the closure model on mean flow quantities was carried out in an internal airlift reactor with gas partially disengaged in the downcomer. The simulation employs the dispersed standard k-ε turbulence model through the Eulerian-Eulerian multiphase model to resolve the 3D transient flow field. The closure model elucidated in this work comprised of drag, lift, turbulent dispersion and bubble-induced turbulence forces. Results show that the hydrodynamics was accurately predicted when bubble distortion and bubble swarm were considered in the drag coefficient through the Rayleigh-Taylor model. Mean flow quantities predicted by the closure model were validated against literature data on surface-averaged gas holdup, radial gas holdup and radial liquid velocity of the flow field obtaining mean errors of 19.4%, 6.8% and 13.5%, respectively. Second part of this study extends the assessment of the closure model to an internal airlift reactor with total gas disengagement in the downcomer. The modelling approach employs the Eulerian-Eulerian two-fluid model with the same turbulence model. Comparison studies on different drag, the effect of lift and turbulent dispersion model were carried out to examine the mean axial liquid velocity in the riser and downcomer. Predicted results were validated against laser Doppler anemometry (LDA) measurements obtained from a fabricated experimental rig. It was found that the axial liquid velocity in the riser was severely under-predicted by the spherical drag model. In this study, the simulation results showed a margin error 52.7% when the Rayleigh-Taylor, lift and turbulent dispersion model was employed. Overall, the simulation results obtained reasonable agreement with experimental data with error less than 20% on local gas distribution results through the Rayleigh-Taylor drag model, lift model as a function of Reynolds and Eötvös number and drift velocity turbulent dispersion model. However, the modelling approach in this study is limited to bubbly homogeneous flow due to the absence of mathematical models to account the bubble dynamics in heterogeneous flow. In addition, the effects of sparger location on the flow field was also being evaluated using LDA measurement technique. It was found that the sparger with position $X_A = 0.125$ m is more energy efficient than sparger with position $X_B = 0.075$ m as the latter which is located slightly nearer to the baffle wall was producing recirculation flows within the downcomer and lower magnitudes of liquid velocity in the downcomer was observed.
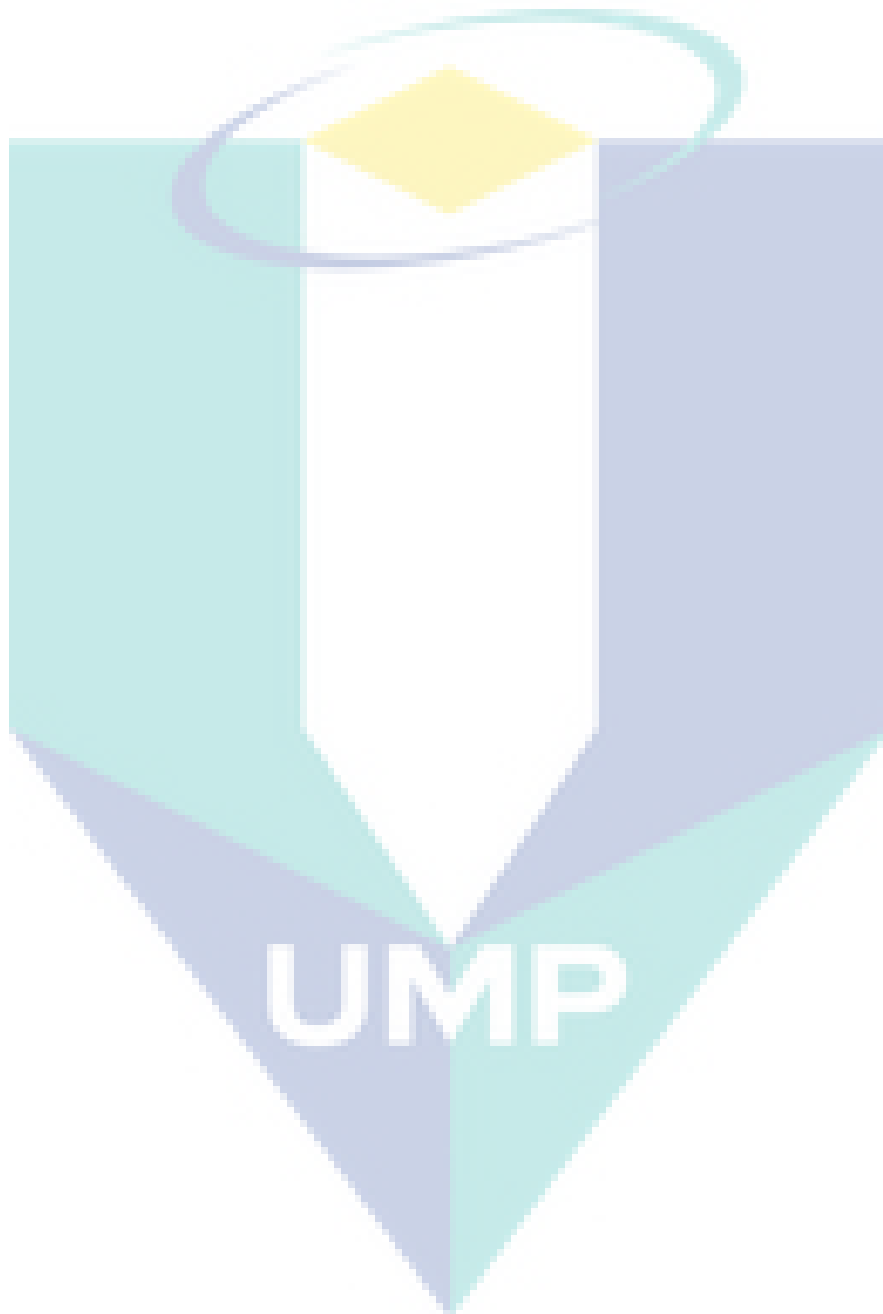
TABLE OF CONTENT

LIST OF TABLES

LIST OF FIGURES

LIST OF SYMBOLS

τ_l^t	Characteristic time of the turbulence in the liquid
$\tau_{l,g}^t$	Characteristic timescale of the turbulence
C	Coefficient value
A_d	Cross-sectional area in the downcomer
A_r	Cross-sectional area in the riser
v_d	Drift velocity
ε	Energy dissipation
Eö	Eötvös number
K_B	Frictional loss coefficient at the bottom clearance
K_T	Frictional loss coefficient at the top clearance
$\alpha_{g,d}$	Gas holdup in the downcomer
$\alpha_{g,r}$	Gas holdup in the riser
h_d	Gas-liquid dispersion height
$D_{l,g}^t$	Gas-liquid turbulent dispersion term
α_g	Global gas holdup
$\nabla \alpha_g$	Gradient of the dispersed phase volume fraction
g	Gravitational acceleration
$\overline{u_l u_g}$	Isotropic turbulence of the velocity correlation tensors
v	Kinematic viscosity
U_L	Liquid circulation velocity
ρ	Liquid density
v_l	Liquid velocity
μ	Liquid viscosity
d_a	Major dimension of the bubble
D_L	Mass diffusivity
μ_{ref}	Molecular viscosity of water.
Mo	Morton number

β	Piecewise function
σ_{TD}	Prandlt number
d_b	Sauter mean diameter or average spherical bubble size
v_{sg}	Superficial gas velocity
σ	Surface tension between the disperse and continuous phase
u_t	Terminal velocity
$\rho_k \overline{u}_k^{\text{I}} \overline{u}_k^{\text{I}}$	Turbulence stresses
k_l	Turbulent kinetic of the continuous phase
μ_c	Viscosity based on Casson model
$k_L a$	Volumetric mass transfer coefficient
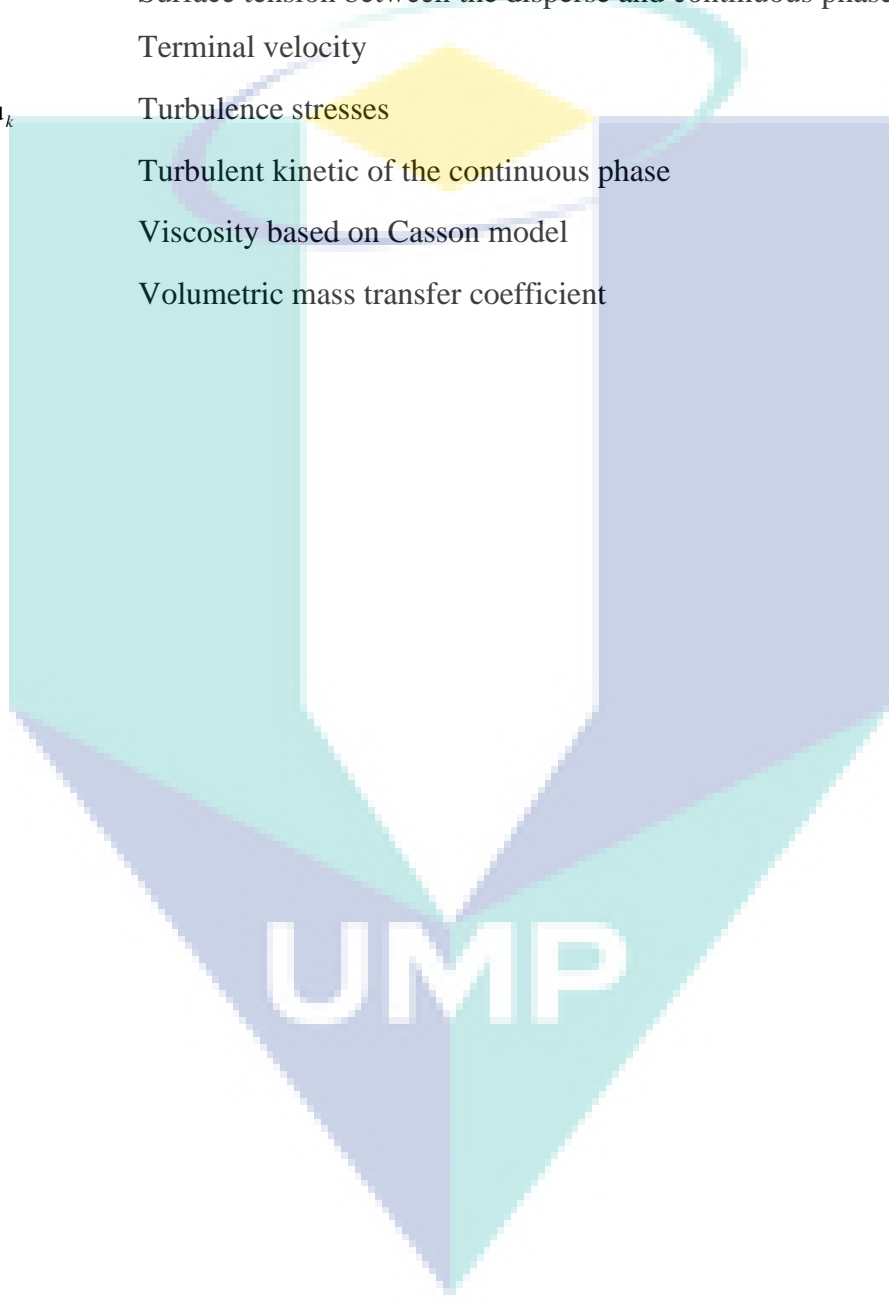
LIST OF ABBREVIATIONS

CARPT   Computer Automated Radioactive Particle Tracking

CCD   Charge-coupled Camera

CFD   Computational Fluid Dynamics

LDA   Laser Doppler Anemometry

PDA   Phase Doppler Anemometry

PI   Photographic Imaging

PIV   Particle Imaging Velocimetry
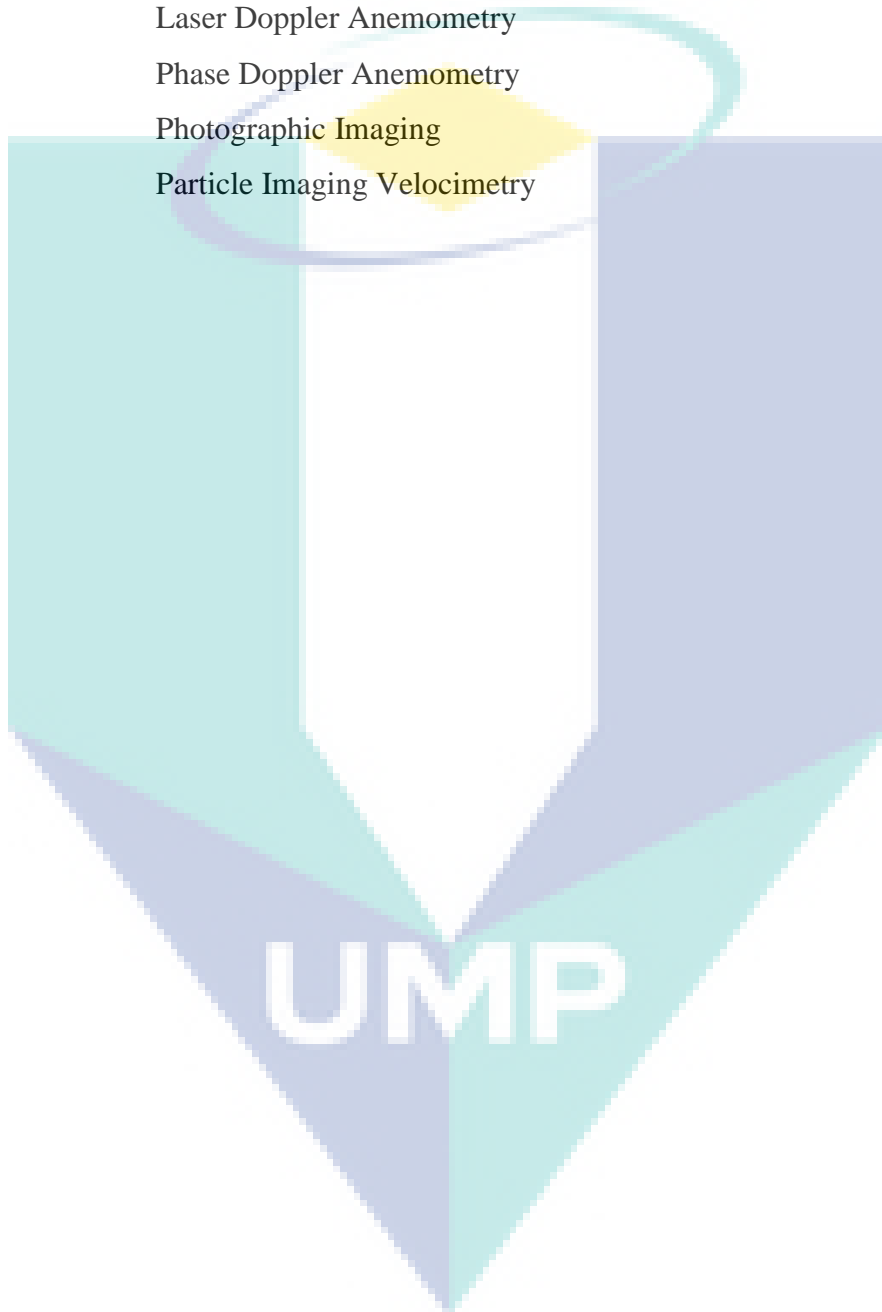
CHAPTER 1

INTRODUCTION

1.1 Introduction

Airlift reactors are pneumatically agitated devices that have initially been adapted for cell cultivation processes. First patented in 1955 by Lefrancois (1955) to succeed the bubble column, it was employed for single cell protein cultivation in England, USS Russia and Eastern Europe (Chisti and Moo-Young, 1987). As a result, numerous research papers regarding airlift reactor design have started to actively surface in the late 1970s as both the stirred tanks and bubble column technology were approaching maturity (Kadic and Theodore, 2014). The airlift reactor's hydrodynamics characteristic is attractive for shear-sensitive processes in comparison to its pneumatic predecessors as it exerts lower shear stress on cells and consumes lesser energy. Chao *et al.* (2000) found that the energy requirement of an airlift reactor to produce bacteria cellulose consumes only one-fifth energy of a stirred tank. Moreover, recent decade have extended the application of airlift reactors to wastewater treatment facilities (Zhang *et al*., 2017). Current breakthroughs in biological treatments of wastewater have narrowed down airlift reactor technology as a potential candidature for single stage bioreactors to accommodate various microbial in smaller operational footprint and improve mass transfer. It was found that the airlift reactor was able to reduce the hydraulic retention time (HRT) to degrade phenol by 10 h and obtain a 60% increment in volumetric mass transfer coefficient in comparison to the bubble column (Rayi and Anathula, 2014). Its application have also been studied in treating ammonium rich and phosphorus effluent from food industries such as milk processing plant (Asadi *et al.,* 2016).

The airlift reactor has also garnered interest from renewable energy industries in microalgae farming for the mass production of biofuel (Chisti, 2008). Microalgae

production is economically efficient when cultivated in vertical columns (i.e. bubble column and airlift reactors) with smaller aerial footprints in volumes ranging between 10^2 to 10^3 L in comparison to raceway ponds (Granata, 2017). Despite gaining wide exposure, ventures in airlift reactor application is still slow and restricted. The scale up process of the airlift reactor is still challenging due to inhomogeneous mixing.

Gas-liquid airlift reactors design are primarily being studied as the multiphase flow field can be extensively complex and can lead to inefficient mixing. The success of its design depends on gas-liquid mass transfer where the gas phase needs to be evenly dispersed and absorption to occur (Oldshue, 1983). This would require a hydrodynamics regime that promotes effective mixing for maximum mass transfer and minimal damage on the product due to shear force. The hydrodynamics of the airlift reactor is sensitive to the reactor configuration (i.e. downcomer-to-riser ratio, gas-liquid separator, top and bottom clearance, sparger type and position, reactor height) and fluid properties which leads to multiple design constraints to be considered. The airlift reactor structure is divided into an external airlift reactor and internal airlift reactor (i.e. a baffle or draft tube divides the structure inside the vessel). The former facilitates partial to total gas disengagement meanwhile, the latter has broader applications in bioprocesses which encourages minimisation of dead zones (Siegel and Robinson, 1992). Bioprocesses, which are sensitive to mass transfer would require a robust scale up and design method to capture the flow information accurately in order to maintain its yield performance. Thus, the scale up procedure is of concern in this study.

Early airlift reactor scale up procedure depended on correlations extrapolated from bubble columns (Hill *et al.,* 1976). This correlation is however valid at lower superficial gas velocities, requiring additional airlift reactor pilot plant experimentation studies to accommodate complex gas-liquid flows (Chisti and Moo-Young, 1993). Current industrial scale up procedures have diversified, relying on either optimisation and scale up, semi-fundamental or fundamental approaches (Merchuk *et al.,* 1999). Optimisation and scale up is often the approach used for scaling up industrial airlift reactors. It is traditionally reliant on empirical correlations obtained from laboratory or pilot scale airlift reactors (Bello *et al.,* 1984; Chisti *et al.,* 1988; Kawase *et al.,* 1995; Heijnen *et al.,* 1997). Notably, the immediate disadvantage of using highly empirical correlations can be traced back to its laboratory scale limitations. These correlations were

derived from sources that assumes well-mixed and homogeneous mixing of gas-liquid in laboratory scale vessels. This is thereby not valid when approximated in larger industrial scale airlift reactors where the homogeneity of the mixing differs. In addition, empirical correlations were based on both local and global parameters obtained from specific reactor geometry and operating conditions. These correlations can be unreliable when extended to other reactor configurations (Chisti *et al.,* 1988; Kilonzo *et al.,* 2007; Zhang *et al.,* 2012). Meanwhile, semi-fundamental approach simplifies fundamental concepts through the approximation of kinetic models and transport phenomena via mathematical models (Merchuk *et al.,* 1999). Several mathematical models have been proposed across literature to capture the mixing system within airlift reactor such as axial dispersion model (Dhaouadi *et al.,* 1997) and tanks-in-series approach (Znad *et al.,* 2004; Behin 2010). However, these approximations indicate the loss of information as the axial dispersion model cannot be extended to complicated mixing cases meanwhile the latter model is limited to the assumption of plug flow mixing (Znad *et al*., 2004).

Given these limitations, a fundamental approach through numerical methods is instead sought after to allow flexible scale and design on the airlift reactor as well as provide detailed local flow field information. Drastic improvements in computation power has led to the reliability of computational fluid dynamics (CFD) as a favourable tool often used to resolve the hydrodynamics within the airlift reactor. Over two decades worth of research have been devoted in developing a modelling strategy to accurately predict the flow field within the airlift reactor (Vial *et al,* 2002; Rzehak *et al.,* 2017). It has also been applied to optimise process design and industrial scale multiphase gas-liquid flows in both internal airlift reactors (van Baten *et al.,* 2003; McClure *et al.,* 2017; Chen and Bai, 2017; Ansoni and Paulo Seleghim Jr., 2019) and external airlift reactors (Massart *et al.,* 2014). Several case studies on novel modifications were also carried out using CFD (Bannari *et al.,* 2011; Zhang *et al.,* 2012). In addition, CFD has been the forefront of airlift reactor scale up and design for application in microalgae production of biofuel (Ali *et al.,* 2019) and astaxanthin production (Guler *et al.,* 2019). Commercial CFD software are extensively available equipped with numerous multiphase modelling. The two-fluid model through the pure Eulerian method in particular, was frequently adopted as a widely favourable approach to model the airlift reactor in bubbly flow regime (Talvy *et al.,* 2007; Liao *et al.,* 2016). This method adopts an ensemble averaging procedure on the forces between the continuous and dispersed phases for it to be

economical to simulate. Additional closure models were then included to account for the missing forces that were eliminated during the ensemble averaging process. This approach is deem computational cheaper and faster. Undoubtedly, numerical approach provides a flexible alternative in comparison to the highly empirical optimisation and scale up method and more detailed flow information than the semi-fundamental approach, so was thus considered in this study.

In order for the modelling approach to be considered reliable and robust, it should be validated against measurements obtained from experimental methods. Fluid flow measurements that have been conducted in the past have dated back as early as 1950s where photographic methods and probes were employed. However, their measurements were only able to provide global or macro spatial readings and may be intrusive to the flow field being investigated. With recent breakthrough in optical measurement technique, a paradigm shift towards the utilisation of the laser Doppler anemometry (LDA) to obtain velocity measurements was applied on single phase flow fields. It is a non-intrusive method and possesses high accuracy in recording local instantaneous velocities of the flow field. It is able to provide single point time-averaged measurements and study transient flow close to the wall (Mudde *et al.,* 1998; Ranade *et al.,* 2001). Several studies in the span of two decades have successfully implemented LDA to studythe multiphase flow within the airlift reactor (Tan *et al.,* 1995; Vial *et al.,* 2002). Hence, LDA was employed in this work to validate against predicted results obtained from the CFD two-fluid model.

1.2   Problem Statement

Efficient mixing in multiphase airlift reactors is essential for maximum performance. Poor mixing however, has the possibility to lead to unwanted losses in manufacturing and operating costs. U.S chemical industries alone suffered a loss estimated at $1 billion to $10 billion due to poor mixing (Paul *et al.,* 2004). Hence, efforts have been invested to improve current design and scale up methods via numerical approach to address those costly failures. The two-fluid model has gain wide recognition over the last two decades to simulate gas-liquid airlift reactor owing to its computational affordability. The two-fluid model through the pure Eulerian approach reduces the computational cost by resolving large-scale hydrodynamics and ensemble averaging smaller scales associated with phase interaction. This procedure however causes the loss

of information as a trade-off, requiring an additional closure model. The closure model consists of drag and non-drag forces (i.e. lift force, turbulent dispersion force and bubble-induced turbulence) which describes the momentum exchange forces to accurately capture the gas-liquid interphase in the airlift reactor. These forces are represented by mathematical and correlation models proposed across literature. However, there is a lack of consensus on a proper set of closure model to simulate the internal airlift reactor.

The wide discrepancy on the closure model in literature can be due to the lack of understanding on the underlying physics within the gas-liquid airlift reactor. For instance, the drag model in some studies still employed the spherical drag model to capture the effect of bubble wake on the liquid phase (Oey *et al.,* 2003; Chen and Bai, 2017). The limitations of the spherical model lies on its assumption that the bubbles are spherical in shape, which is unsuitable as bubbles tend to undergo deformation. There are also few studies which are split between employing the drag model as a function of bubble deformation (Šimčik *et al.,* 2011; Zhang *et al.,* 2012) and those that considered the effect of bubble swarm (Liao *et al.,* 2016; Rzehak *et al.,* 2017). Meanwhile, some studies have ignored the significance of the non-drag forces due to the uncertainty of its role (Zhang *et al.,* 2012; Bednarz *et al.,* 2017). The lift force was mostly omitted from the closure model, claiming the lack of understanding of its role or dismissed as being insignificant to the overall flow field (Talvy *et al.,* 2007; Bella *et al.,* 2007; Stritiba *et al.,* 2017). Whereas those that included the lift model found a reduction in phase velocities peak profile across the column (Masood and Delgado, 2014). In addition, the models considered to account the turbulent dispersion forces vary between the drift velocity model or the employment of singular turbulent dispersion coefficient model with no consensus yet to be obtained (Mohajerani *et al.,* 2012; Stritiba *et al.,* 2017). The bubble-induced turbulence on the other hand, is widely divided on the employment of its models and its effect on the predictive accuracy. The accuracy of individual models for each forces and the added effects of each forces requires a detailed study to narrow down a set of suitable closure model that provides an accurate prediction.

Aside from that, Šimčik *et al.* (2011) have pointed out that the discrepancy from past CFD studies in an internal airlift reactor is notably due to its flow regime. They have distinctly grouped the internal airlift reactor flow field into total gas disengagement, partial gas disengagement in the absence of bubble circulation and bubble circulating

regime configurations. Generally, the structure of the pneumatic internal airlift reactor is distinguished from its predecessor by a baffle or division separating the riser and the downcomer. Gas is sparged in the riser section with an upward flow, carrying the bubbles into the gas separator section. In the gas separator section, the gas is either fully disengaged above the liquid surface (i.e. total gas disengagement) or partially carried down into the downcomer at higher superficial liquid velocity. In the downcomer the fluid flows downward, carrying over smaller bubbles against the force of buoyancy until they achieve equilibrium in force (i.e. partial gas disengagement in the absence of bubble circulation). Increasing superficial liquid velocity allows the bubbles to overcome the buoyancy force and flow towards the bottom clearance of the airlift reactor before circulating back into the riser (i.e. bubble circulating regime). The flow regime in the downcomer is similar to plug flow in comparison to the heterogeneous mixing in the riser. Most internal airlift reactor CFD studies segregated these regimes and would fit in the best closure models for a particular configuration, albeit with limited cross-checking done with another configuration. It can be observed that CFD studies that employed the closure models in total gas disengagement configuration tend to have higher accuracy on the gas holdup and velocity predictions (Zhang *et al.,* 2012; Šimčik *et al.,* 2012). Whereas, CFD studies that employed closure models in internal airlift reactor configuration with bubbles present in the downcomer had wider difference between the simulation and experimental results (Liao *et al.,* 2016; Rzehak *et al.,* 2017). This opens an enquiry as to whether the predicted results by the closure models that have conformed with experimental results in total gas disengagement configurations were indeed robust enough to be employed in regimes with bubbles present in the downcomer.

In order for the modelling approach to be deem reliable, the simulation results should be validated against flow field information obtained from experimental measurements. Flow field information are described by their hydrodynamics parameters depending on the reactor design. In airlift reactors, the axial liquid velocity component dominantly affects the liquid circulation velocity induced by the gas sparger. Despite that the nature of the hydrodynamics in gas-liquid airlift reactor can be anisotropic, mean flow quantities is sufficient to capture the flow field for simulation validation. LDA technique is capable of obtaining velocity measurements, providing single point instantaneous measurements which can be conveniently time-averaged. This technique is also notably non-intrusive, giving high quality experimental measurements. Moreover, the LDA is

able to perform in multiphase system with high gas volume fraction of up to 25% in comparison to other optical such as PIV (Mudde *et al.,* 1997). Hence, in order to verify the validity of the modelling approach, experimental measurement through LDA technique is required.

On the other hand, there is also the open question about the influence of the sparger. Reactor hydrodynamics are sensitive to reactor configuration and the parameters that would influence the flow field being investigated. It is widely known that the downcomer-to-riser ratio has a crucial influence on the liquid circulation velocity as it determines the energy consumption of the mixing process and it is evident in most empirical correlations and had been well studied (Chisti *et al.,* 1988; Koide *et al.,* 1988; Kawase *et al.,* 1995). However, limited studies were conducted to evaluate the influence of sparger position despite being the source of the energy distributor (Behin and Ahmadi, 2010; Pirouzi *et al.,* 2014). Behin and Ahmadi (2010) found that gas sparged into the draft tube has relatively lower energy consumption in comparison to the gas sparged in annulus due to lesser wall effects. On the other hand, introducing additional sparger in the downcomer was able to produce a counter current flow which lead to an increase of mass transfer coefficient and effectively reducing the energy consumption (Pirouzi *et al.,* 2014). It is worth noting that, the position of the sparger may have some importance in bubble coalescence, gas distribution and reduction in energy consumption, thus should not be ignored (Chisti and Moo-Young., 1987). Thus, the effect of sparger position should be evaluated.

1.3   Research Objectives

The main aim of this study is to form a two-fluid CFD modelling approach in predicting the flow field within an internal airlift reactor. The following objectives of this research are:

i.   To elucidate a closure model for the CFD two-fluid model of a gas-liquid bubbly flow internal airlift reactor.

ii.   To evaluate the performance of the closure model on the CFD simulation in internal airlift reactor configurations with a partial gas disengagement in the absence of bubble circulation and total gas disengagement.

iii. To validate the CFD simulation with experimental validation of an internal airlift reactor with partial gas disengagement in the absence of bubble circulation and total gas disengagement.

iv. To carry out an experimental study on the influence of sparger position on a gas-liquid internal airlift reactor.

1.4   Scopes of Study

To meet the aforementioned objectives, the following scopes of the research have been identified:

i. Perform a grid independence study on the grid density of an internal airlift reactor.

ii. Elucidate the closure model by performing comparison studies between different drag models, effect of lift model, different turbulent dispersion models and bubble-induced models as well as their added effects in an internal airlift reactor with partial gas disengagement in the absence of bubble circulation configuration.

iii. Assess the closure model by evaluating the predictive accuracy on the surface-averaged gas holdup, radial gas holdup and axial liquid velocity of an internal airlift reactor with partial gas disengagement in the absence of bubble circulation configuration.

iv. Validate the predictive accuracy from the CFD simulation results of an internal airlift reactor with partial gas disengagement in the absence of bubble circulation configuration against experimental literature data.

v. Fabrication of an experimental rig of an internal airlift reactor with total gas disengaged configuration.

vi. Elucidate the closure model by performing comparison studies between different drag models, effect of lift model in an internal airlift reactor with total gas disengaged configuration.

vii. Assess the closure model by evaluating the predictive accuracy on the axial liquid velocity across the riser and downcomer in an internal airlift reactor with total gas disengaged configuration.

viii.   Validate the predictive accuracy from the CFD simulation results of an internal airlift reactor with total gas disengaged against experimental velocity measurements obtained via LDA technique.

ix.   Evaluate the influence of sparger position on the flow field using LDA measurement technique.

1.5   Overview of thesis

The structure of the remainder thesis is outlined as follows:

Chapter 1 elaborates the general background on the airlift reactor, the motivation to implement numerical scale up procedure, problem statement, objectives and scope of study.

Chapter 2 elaborates the literature review on the hydrodynamics and flow patterns of the internal airlift reactor. An overview of multiphase modelling, past CFD studies carried out on gas-liquid internal airlift reactor and comparison studies on the closure models have also been thoroughly reviewed. At the end of the chapter, effect of sparger configuration, experimental measurements and flow field information were also presented.

Chapter 3 describes the methodology to simulate the gas-liquid internal airlift reactor and carry out the optical measurement using LDA. The modelling approach, closure models adopted for the comparison study and LDA calibration setup were outlined. The reactor dimensions, grid density, fluid properties, boundary conditions and discretisation method were also provided in this chapter. In addition, a grid independence study was briefly conducted to determine a suitable grid density.

Chapter 4 presents the simulation results obtained from the comparison study of the closure models in the internal airlift reactor. A comparison study on the drag, lift, turbulent dispersion and bubble-induced turbulence models were evaluated to predict the gas holdup and axial mean liquid velocity in a partial gas disengaged internal airlift reactor. The simulation results were validated against literature data provided by Talvy et al. (2007). In the following segment of this chapter, the comparison study of the closure model in a total gas disengagement internal airlift reactor was also carried out. The predicted results were then validated against liquid velocity measurements obtained

through the LDA instrument. At the end of this chapter, the influence of the sparger position was evaluated through LDA velocity measurement.

Chapter 5 summarises the findings and contributions of the present work. The findings were concluded and recommendations for future work were outlined for further improvements at the end of this chapter.
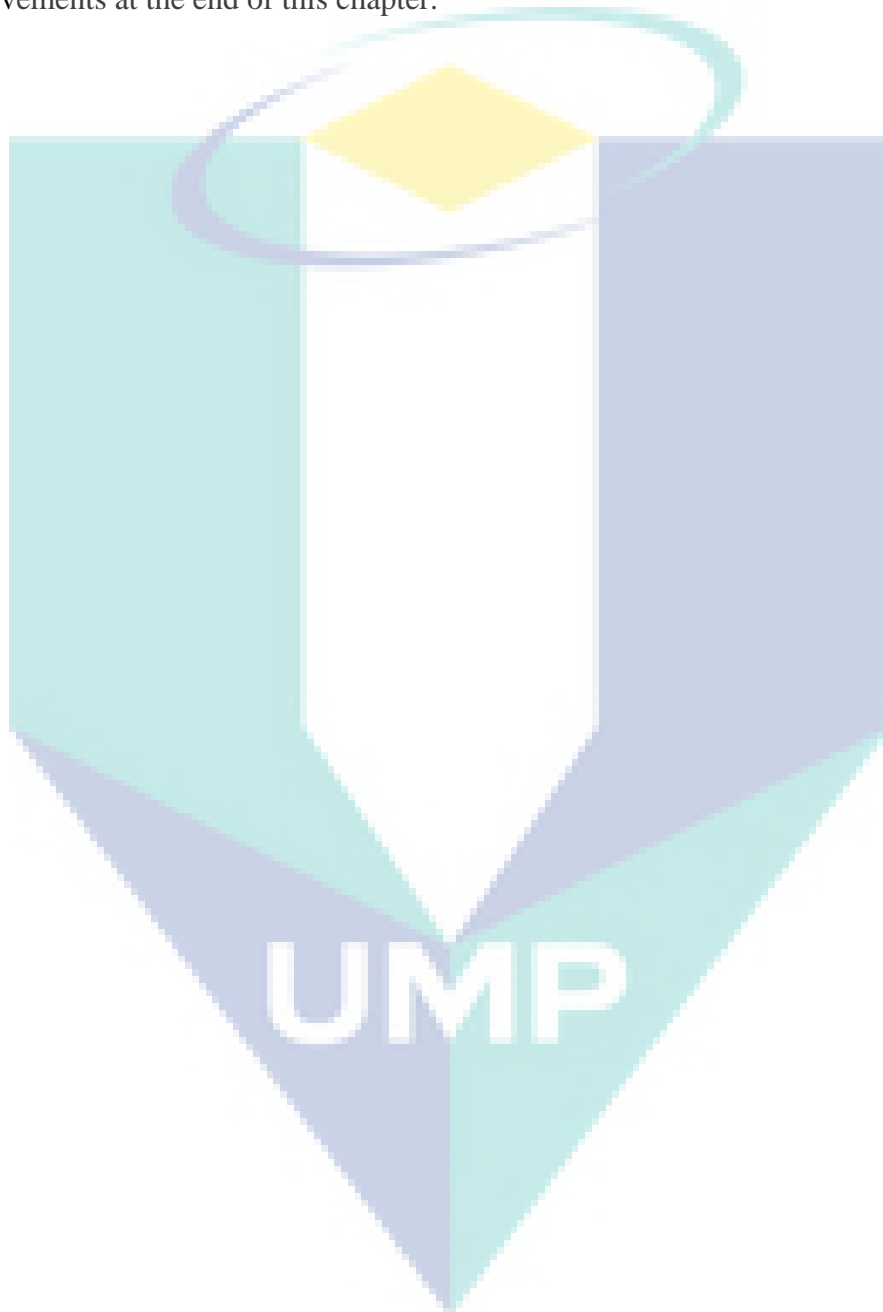
CHAPTER 2

LITERATURE REVIEW

2.1   Introduction

This chapter elaborates briefly on the hydrodynamics parameters and flow patterns found within the airlift reactor. Recent scale up methodologies employed by the industry and current developments in numerical method through the multiphase modelling, turbulence model, momentum exchange forces using CFD to resolve the flow field within the internal airlift reactor were also described. Moreover, the effect of sparger on the hydrodynamics of the airlift reactor was also discussed. Experimental validation is crucial to justify the robustness of the CFD model. Thus, an overview of the experimental measurements methods and the utilisation of optical measurement techniques using LDA were also discussed discretely in this chapter.

2.2   Brief Overview of Airlift Reactor

Airlift reactor belongs to a new class of pneumatic reactors that was designed through the modification of the bubble column to provide more control over the flow field (Kadic and Heindel, 2014). These modifications were done to address the limitations found within the bubble column such as complete back-mixing in the liquid phase and high pressure drop. The construction of a simple airlift reactor consists of a vessel equipped with an internal construction (i.e. baffle, draft tube) that divides the reactor into four sections; riser, downcomer, gas separator and bottom clearance as shown in Figure 2.1. The difference in the pressure distribution between the riser and downcomer becomes the driving force for the liquid circulation flow, inducing mixing in the airlift reactor. The presence of the internal baffle aids in controlling the liquid circulation through the gas flow rate and enhances the performance of the airlift reactor to operate at a wider range

of superficial velocities (Chisti and Moo-Young, 1987). The internal baffle also constrains the flow into a more cyclic pattern which aided in minimising liquid back-mixing within the reactor and withheld slugging regime at higher superficial gas velocities. This in turn reduces the gradient of the shear stress in the gas-liquid system while maintaining high turbulence profiles. This is highly attractive for bioprocesses which tend to be sensitive to shear stress.
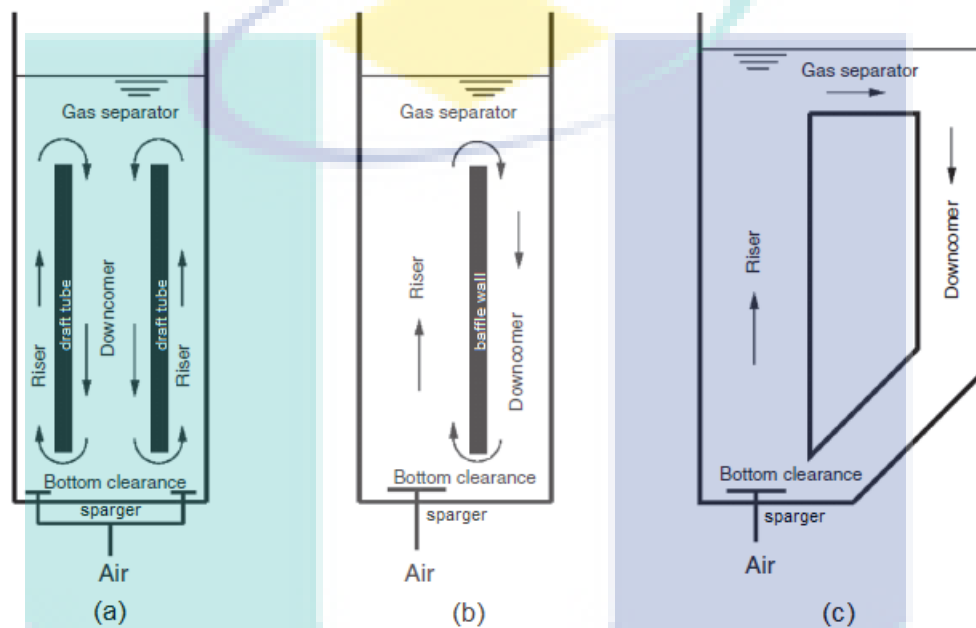
Figure 2.1   Types of airlift reactor structures, (a) internal airlift reactor with draft tube, (b) internal airlift reactor with baffle wall and (c) external airlift reactor

Source: Zhang *et al*. (2017).

Aside from that, energy consumptions are relatively lower in airlift reactors due to the absence of a mechanical agitator to disperse gas to the surrounding bulk. Instead, the airlift reactor relies on aeration from the sparger and the driving force of the liquid circulation to overcome the friction forces exerted by the wall.

2.3   Hydrodynamics within the Airlift Reactor

Comprehension on the influence of the hydrodynamics within the gas-liquid airlift reactors is essential. Earlier studies would identify scale independent global empirical correlations such as liquid circulation rate, mixing time and circulation time to reflect the mixing performance in the airlift reactor (Chisti *et al.,* 1988). They are then translated to multiple design parameters based on rule of thumb compiled by the engineer's

experience. During the early stages of scale up and design of the airlift reactors, empirical expression such as Equation 2.1 was commonly employed (Chisti *et al.,* 1988):

$$U_L = \left[\frac{2gh_d\left(\alpha_{g,r} - \alpha_{g,d}\right)}{\dfrac{K_T}{\left(1-\alpha_{g,r}\right)^2} + K_B\left(\dfrac{A_r}{A_d}\right)^2 - \dfrac{1}{\left(1-\alpha_{g,d}\right)^2}} \right]^{0.5} \qquad 2.1$$

where U_L is the liquid circulation velocity, h_d is the gas-liquid dispersion height, g is the gravitational acceleration, $\alpha_{g,r}$ is the gas holdup in the riser, $\alpha_{g,d}$ is the gas holdup in the downcomer, K_T is frictional loss coefficient at the top clearance, K_B is frictional loss coefficient at the bottom clearance, A_r is the cross-sectional area in the riser and A_d is the cross-sectional area in the downcomer.

The liquid circulation velocity reflects the overall distribution of the fluid flow in the gas-liquid airlift reactor system. It is interdependent with the gas holdup in the riser and downcomer. At lower superficial gas velocity, the liquid circulation velocity can be directly correlated to the density difference between the riser and downcomer denoted as $(\alpha_{g,r} - \alpha_{g,d})$ acting as the driving force to maintain the circulation loop as observed in Equation 2.1. However, increment in superficial gas velocity causes deviation from the correlation as the liquid circulation rate reduces with increasing bubble presences within the downcomer. This decrease is cause by the loss of energy required to overcome the resistant forces exerted by the bubbles, reactor geometry and gas compression (Jones and Heindel, 2010). By controlling the gas flow rate, we can manually increase the liquid circulation velocity resulting to a larger velocity gradient between the bulk fluid and the surface riser walls producing eddies near the wall region.

As further scale up challenges arise from different types flow patterns, identifying the hydrodynamics parameters is essential. These hydrodynamics parameters should be able to reflect the influence on the scale up criterion. Often, mass transfer rate is chosen as the main scale up criterion in gas-liquid chemical and aerobic bioprocesses. The mass transfer correlation in airlift reactors do not differ much between bioreactor components and can represent as an input for scaling up (Kadic and Heindel, 2014). Generally, the

mass transfer rate is directly proportional to the concentration gradient and the volumetric mass transfer coefficient. The concentration gradient translates to the difference between the equilibrium concentration at the fluid interface and the concentration in the bulk phase. Meanwhile, the volumetric mass transfer coefficient is defined as the product of the mass transfer coefficient, k_L and the specific interfacial area, a. As it is difficult to measure the mass transfer coefficient experimentally, they are typically based on theoretical models such as (Kawase and Moo-Young, 1990; Garcia-Ochoa and Gomez, 2004):

$$k_L = 0.301(\varepsilon \cdot v)^{1/4}\left(\frac{\mu}{\rho D_L}\right)^{-1/2}$$

2.2

$$k_L = \frac{2}{\sqrt{\pi}} \cdot \sqrt{D_L}\left(\frac{\varepsilon\rho\left(1-\sqrt{\alpha_r}\right)^2}{\mu_c/\rho}\right)^{1/4}$$

2.3

where ε is the energy dissipation, v is the kinematic viscosity, μ is the liquid viscosity, ρ is the liquid density, D_L is the mass diffusivity and μ_c is the viscosity based on Casson model. Instead, experimental measurements are more prone to measure volumetric mass transfer coefficient, $k_L a$ as a whole. A general expression has been proposed to evaluate the volumetric mass transfer coefficient by taking in the consideration of the superficial gas velocity, effective viscosity, downcomer-to-riser cross sectional area ratio, liquid velocity and gas holdup expressed in the correlation below (Bello *et al.,* 1984; Popovic and Robinson, 1989):

$$k_L a = C \cdot v_{sg}^a \mu_l^b \cdot \left(1 + \frac{A_d}{A_r}\right)^c \cdot v_l^d \cdot \alpha_g^e$$

2.4

where C is the coefficient value, v_{sg} is the superficial gas velocity, μ_l is the liquid viscosity, A_d is the downcomer cross-sectional area, A_r is the riser cross-sectional area, v_l is the liquid velocity and α_g is the global gas holdup. It can be observed few

factors influence the volumetric mass transfer coefficient. However, the gas holdup has a far more significant influence over the volumetric mass transfer coefficient expression. This can be justified by the observing the theoretical models for mass transfer coefficient in Equation 2.2 and Equation 2.3 which lack the hydrodynamics expressions in comparison to the volumetric mass transfer coefficient found in Equation 2.4. It can be seen that the mass transfer coefficient is a strong function dissipation energy associated with turbulence of the continuous phase. Meanwhile the gas holdup, α_g is directly correlated to the specific interfacial area which represents the area available for transfer of the reactants or nutrients in the liquid medium or substrates to take place. It is defined as the exchange surface per volume as follows:

$$a = \frac{6\alpha_g}{d_b}$$ 2.5

The expression d_b accounts the Sauter mean diameter or average spherical bubble size within the system. Moreover, as mentioned earlier the gas holdup also determines the liquid circulation velocity which in turn affects the mixing efficient of the overall system. Thus, gas holdup becomes a significant hydrodynamics parameter that need to be considered to not only represent the overall hydrodynamics of the system but it has significant influence on the scale up criterion through the mass transfer rate.

On the other hand, the expression axial liquid velocity is also a hydrodynamics parameter commonly observed within the flow field of the airlift reactor. As the airlift reactor flows within a cyclic loop redirected by the internal construction (i.e. draft tube, internal baffle), the axial component of velocity has major influence in comparison to its radial and tangential forces. The liquid velocity is vital as it translate to the shear stress exerted onto the system through the expression of the turbulence kinetic energy and dissipation energy. It was found that, the shear stress exerted by the airlift reactor was relatively lower in comparison to the stirred tank which allows shear sensitive cells to survive (Tan *et al.,* 1995).

As behaviour of the flow pattern within the airlift reactor may differ between the riser and downcomer, understanding the key hydrodynamics parameters alone is insufficient. Hydrodynamics within gas-liquid system can be complex requiring

fundamental understanding on the flow patterns existing within the airlift reactors. Flow patterns within the airlift reactor may differ locally based on amendments done onto the operating strategy and geometry design. It was found that through the incorporation of intermittent aeration and sparger-producing microbubbles, the diameter of the bubbles were small enough to be drag over into the downcomer and avoid being disengaged in the gas separator (Mahmood *et al.,* 2015). This increases the mass transfer greatly due to the increment of interfacial area. On the other hand, Moraveji et al. (2011) performed modifications by introducing a packed bed riser within the internal airlift reactor observed an increase of gas holdup in the riser. Modifications on the operating strategy (i.e. intermittent aeration) and geometrical aspects aside from riser-to-downcomer ratio could result to significant changes in the flow pattern behaviour within the airlift reactor which were not reflected by the empirical correlation.

2.4   Flow Pattern within the Airlift Reactor

Flow patterns in an airlift reactor differs widely from the bubble column where the latter would easily enter into a chaotic flow regime (i.e. slug flow) producing an array of vortices as a result of strong downflow region near the reactor walls. In the airlift reactor, the flow is less chaotic owing to the circulation pattern between the riser and downcomer. However, the cyclic pattern gives rise to the complexity of the flow patterns with increasing gas flow rate. According to Šimčik et al. (2011), the flow patterns in the airlift reactor can be classified into total gas disengagement, partial gas disengagement in the absence of bubble circulation and bubble circulating regime configurations. Total gas disengagement refers to the total absence of bubble within the downcomer as shown in Figure 2.2. This would result to a lower concentration of mass transfer within the downcomer as opposed to the riser. On the other hand, the partial gas disengagement in the absence of bubble circulations which happens to be a frequent occurrence within the internal airlift reactor as a result of drag force exerted on the bubble having equal or lesser force than buoyancy force. Even though the circulation of the liquid phase takes place, the bubbles would visually seem stagnant or eventually disengaged into the gas separator over time. Meanwhile, the bubble circulating regime configuration occurs when drag force exerted onto the bubble is greater than the resistance from the buoyancy force resulting to the cyclic movements of the bubbles within the internal airlift.
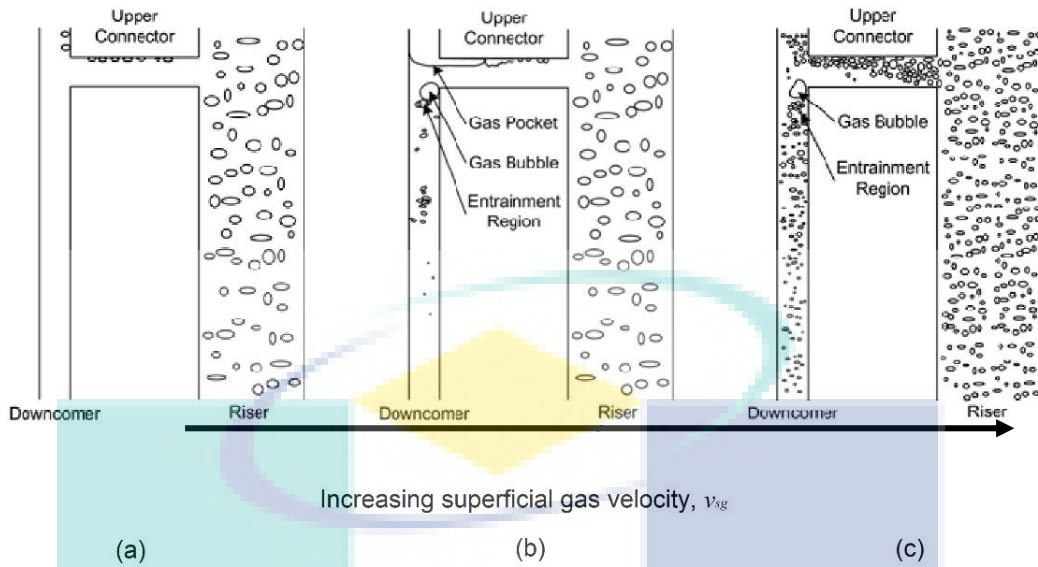
Figure 2.2　　Flow patterns classified into a) total gas disengagement, b) partial gas disengagement and c) bubble recirculation regime

Source: Jones & Heindel (2010).

Despite being generally classified into different flows based on its bubble regime, the flow pattern for each segment of the airlift reactor varies locally in the riser and downcomer.

2.4.1　Flow Pattern of Riser in an Airlift Reactor

The bulk fluid in the riser is driven dominantly by the gas emitting from the sparger. The fluid travels co-currently with the sparged gas in an upward motion into the gas separator before being recirculated back from the downcomer as shown in Figure 2.3. This greatly reduces the backflow issue in the riser, which is evident in the bubble column due to the lack of flow mitigation. The resultant bubble swarm from the gas sparging and liquid recirculation from the downcomer increases the resultant liquid velocity by an order magnitude higher in the airlift reactor in comparison to the bubble column (Merchuk and Siegel, 2007).
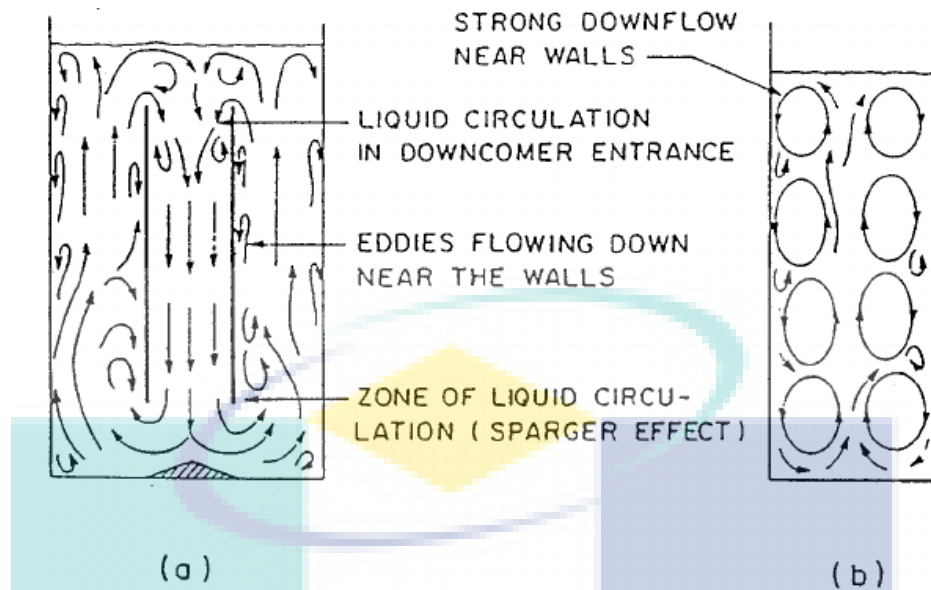
Figure 2.3   Flow patterns within (a) internal airlift reactor and (b) bubble column
Source: Chisti & Moo-Young (1987)

However, internal recirculation within the riser is also generated as a result of local circulations from the liquid phase. The flow near the vicinity of the riser wall tends to descend, causing eddies to form due to the difference in flow direction. These eddies are found across the length of the column, contributing to the internal recirculation. Small bubbles tend to be caught in these localised random loops and get drag down within the riser, increasing the bubble residence time within the riser. By increasing the gas flowing from the sparger, it introduces a steeper velocity gradient between the wall region and the bulk fluid which in turn increases the turbulence due to internal recirculation (Zhang *et al.,* 2019). Nevertheless, its effect on the general upward flow pattern is less influential on the bulk fluid in the airlift reactor than the ones in the bubble column.

2.4.2   Flow Pattern within Downcomer of Airlift Reactor

In the downcomer region, the bulk fluid flows from the gas separator and enters the downcomer in a downward flow. Figure 2.4 depict the evolution of the flow patterns within the downcomer with increasing liquid circulation velocity. At low superficial gas velocity, the gas are mostly disengaged at the gas separator therefore only the bulk fluid circulates into the downcomer. With increasing superficial gas velocity, small bubbles that were not fully disengaged in the gas separator get entrained by the bulk fluid in the downcomer. This flow pattern continues to develop into swirling flow patterns typically seen in bubble columns though the bubbles sizes that led to these swirls are much smaller

18

in the airlift reactor (Siegel *et al.,* 1986). The size distribution of the bubbles vary across the length of the column as buoyancy force is dependent on the bubble volume. In order for the bubbles to entrain or recirculate in the downcomer, the liquid circulation velocity must overcome the force exerted by the buoyancy force of the bubble swarm. As the liquid velocity in the downcomer increases, the swirling flow pattern starts to form into a wavy and straight flow. This results in the downcomer region to exhibit a plug flow pattern in comparison to the riser.
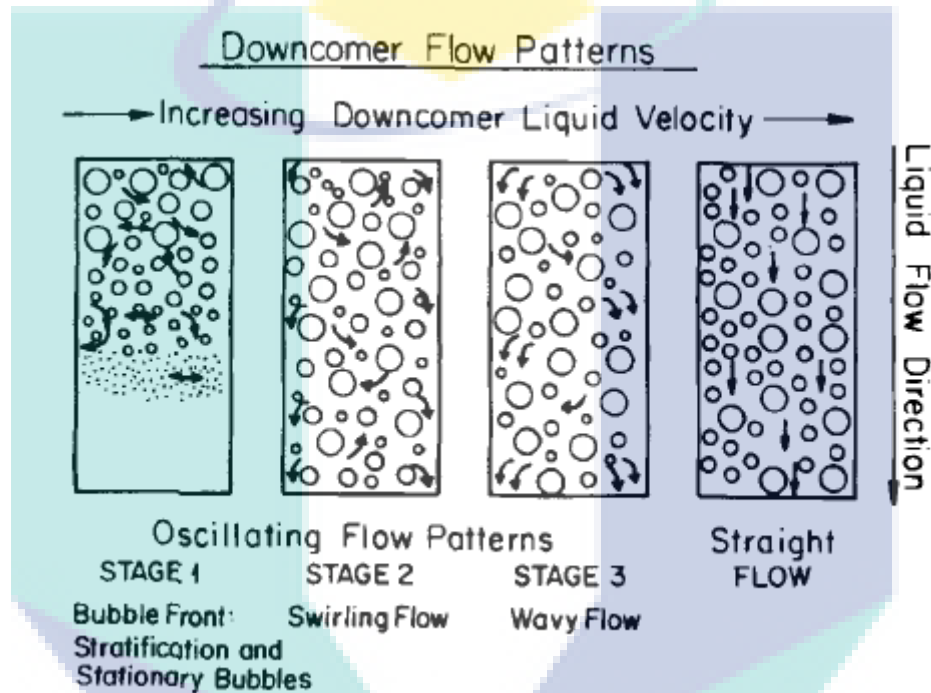
Figure 2.4:   Flow patterns existing in the downcomer with increasing liquid circulation velocity

Source: Siegel *et al.* (1986).

This flow pattern is uniform across the downcomer with exception at the entrance of the downcomer seen in Figure 2.3a. At the entrance, the bulk fluid carried from the riser causes the upper region of the downcomer to behave similar to that of an ideal continuous stirred tank reactor (CSTR) (García *et al.,* 2000). The ideal CSTR flow pattern is more prevalent at higher gas flow rates where the flow in the riser tends to behave heterogeneously causing stronger fluctuations to appear in the upper region of the downcomer. Hydrodynamics within the gas-liquid system can be complex requiring fundamental approach to obtain detailed flow phenomena within the airlift reactor. The hydrodynamics parameters can aid to identify the robustness of the numerical approach to represent the hydrodynamics within the two-phase system.

2.5   Fundamental Approach Using CFD

Fundamental approach through CFD is considered sophisticated yet is a more appropriate way to simulate industrial airlift reactors. It employs Navier-Stokes equation to capture the turbulence flows within the gas-liquid system. Though, direct application of the Navier-Stokes equation will be too computationally intensive as the variables within the equation captures instantaneous velocities locally for a whole flow map. Generally, an ensemble-averaging approach would be necessary to address these instantaneous values by enforcing statistical averaging and fluctuations from average value to allow it to be computationally viable to run. This ensemble averaged equation would then be expressed as Reynolds averaged Navier-Stokes (RANS) equation as shown in the following:

$$\frac{\partial}{\partial t}\left(\rho_k \vec{u}_k\right) + \frac{\partial}{\partial x_k}\left(\rho_k \vec{u}_k \vec{u}_k\right) = -\frac{\partial}{\partial x_k} p + \frac{\partial}{\partial x_k} \tau_k + \frac{\partial}{\partial x_k}\left(-\rho_k \overline{\vec{u}_k \vec{u}_k}\right) \qquad 2.6$$

Through the ensemble averaging procedure, it gives rise to an additional term $\rho_k \vec{u}_k \vec{u}_k$ (i.e. τ_k in this study) to the equation to represent the turbulence stresses due to fluctuating velocities. This term is known as Reynolds stresses which can be resolved by using functional expressions such as the turbulence model which will be further elaborated in Section 2.5.1. However, should the application of the procedure be extended to multiphase flows, generally it will undergo ensemble averaging procedure but the modelling methodology might vary based on flow regime.

2.5.1   Multiphase Modelling

The multiphase modelling approach depends on the nature of the flow regime. The flow regime within the gas-liquid airlift reactor adopted in this study behaves as a dispersed two-phase system in bubbly flow. Two phase system in gas-liquid flows are divided into continuous (i.e. bulk liquid) and dispersed phases (i.e. bubbles). Past CFD airlift reactor studies have commonly adopted either the Eulerian-Eulerian (i.e. two-fluid model) or the Eulerian-Lagrangian approach also known as discrete phase modelling to model these two phases.

The most widely adopted multiphase model is the Eulerian-Eulerian whereby it considers both the continuous and dispersed phases as interpenetrating media. The

Eulerian framework solves the mass, momentum and energy continuity for each phases separately, weighted by their corresponding volume fraction, which represents the ensemble averaged probability of the occurrence of each phase at certain point in time and space (Kleinstreuer, 2003). This ensemble averaged procedure will lead to the loss of microscopic information (i.e. averaging small length scales) associated with phase interface being eliminated as a trade-off for lower computational cost, only resolving large scales. Loss of vital information between the gas-liquid interaction can be resupplied with additional semi-empirical constitutive relations, which is also known as closure model to describe the absence of interfacial mass and momentum transfer within the continuity and conservation equations.

Meanwhile on the other hand, the Eulerian-Lagrangian framework traces particles as individual trajectories. It solves the Navier-Stokes equation by defining the continuous phase using the Eulerian framework and employing Lagrangian to represent the motion for the dispersed phase. The Eulerian frame divides the flow field into individual computational cells where each grid cell is treated as a fixed control volume. Inside the control volume, the fluid was allowed to flow through its boundary interface. The fluid field is solved through governing equations (i.e. continuity equation, conservation laws). Meanwhile, the dispersed phase is tracked through a trajectory model via the Lagrangian framework. The Eulerian-Lagrangian model accounts bubble interaction and the interfacial momentum forces on an Eulerian grid and convection algorithm. The drawback of this method is that its bubble count is limited under 100 000 and gas holdup lesser than 5% for Lagrangian to be affordable (Buwa *et al.,* 2006). Thus, it is unable to predict dense bubbly flows at industrial scale as it is computationally intensive to calculate each bubble position, shape and bubble interactions. Only few studies which employed the Eulerian-Lagrangian in gas-liquid airlift reactor have managed to surface in literature (Law *et al.,* 2008; Massart *et al.,* 2014).

Most of the studies would adopt the former Eulerian-Eulerian approach owing to its cheaper computational cost and practicality in industrial case studies in both bubbly and heterogeneous regimes (Vial *et al.,* 2002; *et al.,* 2003; Dhanasekharan *et al.,* 2005; Talvy *et al.,* 2007; Bannari *et al.,* 2011; McClure *et al.,* 2017). Flow field in a 200 L internal airlift reactor with over void fraction above 8% had been successfully predicted with good agreement with experimental results (Davarnejad *et al.,* 2012). Though, the

results were slightly under predicted at liquid circulation velocity above 0.03 ms^{-1} (Davarnejad *et al.,* 2012). This might be partly due to the closure model elaborated further in Section 2.4.4 that did not fully capture the physics occurring within the flow field. Nevertheless, the Eulerian-Eulerian multiphase modelling approach is suited for industrial flow applications where gas holdup may range above 5%.

2.5.2 Turbulence Model

Reynolds shear stress in the continuous phase due to fluctuation requires turbulence modelling to resolve the turbulence quantities within the flow field. Past studies in airlift reactor have commonly adopted the Reynolds averaged Navier-Stokes (RANS) turbulence model standard k-ε, RNG k-ε and RANS two-equation model SST k-ω. The standard k-ε is highly favoured in airlift reactor CFD studies and have been extensive employed across literature with earlier studies obtaining good agreement with experimental studies on total gas holdup, overall axial liquid velocity within the downcomer and riser (van Baten *et al.,* 2002; Dhanasekharan *et al.,* 2005). It was also reported that the predicted liquid circulation velocity, mixing time and axial dispersion coefficient obtained through the employment of the standard k-ε model were able to similarly achieved good agreement with experimental data (Roy *et al.,* 2006; Balleda *et al.,* 2007). However, Lestinsky et al. (2012) noted that the discrepancy between the predicted total gas holdup in both the riser and downcomer as well as the axial liquid velocity using the same model is much less significant at lower gas flow rate. This may be due to the model which assumes isotropic turbulence which might not always be the case for experimental turbulence which are anisotropic in nature. So, although good agreement on the gas holdup and liquid velocity predictions were obtained through the employment of the standard k-ε, the turbulence kinetic and energy dissipation quantities were not validated. Meanwhile, the RNG k-ε was adopted by fewer airlift reactor studies (Cao *et al.,* 2007; Huang *et al.,* 2010; Jiang *et al.,* 2016). The model employs correction on the dissipation rate to consider the distortion of the mean flows. Although the accuracy of the RNG k-ε on turbulence quantities has not been fully disclosed in airlift reactor literature yet, in the case of similar pneumatic reactor flows it was able to obtained better estimations of break up rates in the bubble column when RNG k-ε was applied (Laborde-Boutet *et al.,* 2009). Meanwhile, SST k-ω has also been applied onto two phase flows in airlift reactors but also in fewer cases (Liao *et al.,* 2016; Rzehak *et al.,* 2017). It was not

explicitly disclosed on the choice of their turbulence model in their study but the SST k-ω model is more appropriate for resolving boundary layers near walls through the viscous sublayers and conveniently switches to k-ε in the bulk region. The results were not obviously better than the results from standard k-ε with major discrepancy (i.e. error at 44%) in $\sqrt{k}$ obtained near the walls (Liao *et al.,* 2016). Rzehak et al. (2017) on the other hand had employed the SST k-ω model across different dimensions of reactors (i.e. pipe, bubble column and airlift reactor). Their model were able to satisfactory predict local gas holdup, axial liquid velocity and turbulent kinetic energy in the pipe and bubble column reactor but obtained a large discrepancy in the airlift reactor.

In the airlift reactor flow field, the bubble rise induced flow is the predominant force while other external forces are limited due to the absence of any mechanical moving parts (i.e. impeller) which may cause strong anisotropic turbulence. Standard k-ε variants assume a pseudo-homogeneous turbulence which can adequately resolve the turbulence flow in an airlift reactor. For instance, most of the previous work (e.g. Zhang *et al.,* 2012; Chen and Bai, 2017) reported a minimal error (6.7 %) on global liquid velocity from a CFD simulation with standard k-ε based model.

2.5.3   Past CFD Studies

Extensive CFD studies have been employed in airlift reactor across literature in the last two decades. Table 2.1 describes the CFD studies that were employed to predict flow field details within internal and external airlift reactors across laboratory scale and pilot scale plants. Initial CFD study employed a one-dimensional model (1D) internal airlift reactor model resolved through a momentum balance equation (Cockx *et al.,* 1997). However, the essential directions (i.e. radial flow) might affect the predictions of the gas holdup which tend to migrate radially towards the wall. The 1D model was then extended to a two-dimensional models (2D) and managed to achieve good agreements on the prediction of liquid velocity and gas holdup locally (Vial *et al.,* 2002; van Baten *et al.,* 2003). Though, it is widely agreed upon that 2D would be sufficient enough to resolve the mean quantities of the flow field (i.e. liquid velocity and gas holdup) (Balleda *et al.,* 2007; Law *et al.,* 2008; Huang *et al.,* 2010; Lestinsky *et al.,* 2012; Zhang *et al.,* 2012; Mohajerani *et al.,* 2012; Liao *et al.,* 2016; Bednarz *et al.,* 2017; Rzehak *et al.,* 2017) however spatial dispersion has an impact over the axial dispersion responsible for the transport phenomena in the airlift reactor. Spatial dispersion involves extending the 2D

simulation into a three-dimensional (3D) model instead to take into account a third direction. It was found that the accuracy of the axial dispersion is affected majorly by the spatial dispersion which precedes over the turbulent dispersion (Talvy *et al.,* 2007). This finding was also supported by Liao et al. (2016) study which had ruled that 3D gave rise to a slight increase of accuracy over the 2D model in predicting the liquid velocity and gas holdup. With increment of computational power, more studies were leaning towards the simulation of 3D airlift reactor models using two-fluid model (i.e. Eulerian-Eulerian approach).

Two-fluid model simulations would adopt closure model to account the momentum exchange forces between the dispersed and continuous phase. Many combinations of closure model have been proposed across literature with some studies employing a general two-fluid model across pneumatic reactors (i.e. bubble column, pipe and airlift reactor) (Rzehak *et al.,* 2017). This may be invalid as the bubble columns tend to experience backflows which produces an array of vortices not present in airlift reactors.

Major discrepancy was found in the prediction results in the airlift reactor in comparison to the bubble column when the same closure models were applied (Rzehak *et al.,* 2017). As the combinations on the selections of forces (i.e. drag, lift, turbulent dispersion and bubble-induced turbulence) varies across literature, a consensus has yet to be achieved on a robust two-fluid model approach.

2.5.4   Momentum Exchange Closure

The fundamental criteria for choosing these closure models should be adaptable in similar gas-liquid systems of different flow regime since these interphase forces are governed by similar physics (Liao *et al.,* 2016). The ideal closure model would be able to describe the momentum exchange between the gas-liquid phase and the additional effects of the dispersed bubbles on the turbulence from the continuous phase. Momentum exchange closures comprise of drag and non-drag forces (i.e. lift force, turbulent dispersion force and bubble-induced turbulence). These forces are added through models that were proposed across literature.

Table 2.1   List of all past studies perform in airlift reactors performed in two phase simulations

Author	Reactor type/volume (dimensions)/sparger/operating conditions	Simulation setup/multiphase/ turbulence model/ interfacial momentum forces (IMF)/others	Remarks
Vial et al. (2002)	EL-ALR cylindrical (2D) $A_d/A_r = 0.28$, 6.00 m height Riser: 0.15 m dia. Orifice sparger $v_{sg} = 0.012$ to 0.117 ms^{-1}	FLUENT 4.51, 20 x 200 rectangular cells[a] t_{step} = not reported Eulerian-Eulerian, standard k-ε model, IMF: Drag model	• The turbulent kinetic energy was overestimated in the core region riser at higher superficial gas velocity probably due to the absence of bubble-induced turbulence in the normal direction. • At homogeneous regime, the radial liquid velocity and gas velocity was in good agreement.
van Baten et al. (2003)	IL-ALR cylindrical (axi-2D, 3D) A_d/A_r[b] = 1.5, 3.02 m height Riser: 0.24 m dia. Perforated plate sparger $v_{sg} = 0.02$ to 0.16 ms^{-1}	CFX 4.2, 3D: 138500 cells t_{step} = 0.00005 to 0.01s (10000 time steps) Eulerian-Eulerian, standard k-ε model, IMF: Drag model	• Simulation predictions using axi-2D shown an overestimation of gas distribution exhibiting core peaking profile (i.e. mostly exist at slug regimes) in comparison to the 3D simulation exhibiting intermediate peak patterns. • Gas holdup in the riser is underpredicted meanwhile the axial liquid velocity in the downcomer is overpredicted at lower superficial gas velocity.
Oey et al. (2003)	IL-ALR rectangular (3D) $A_d/A_r = 1.67$, 1.75 m height Riser: 0.0144 m^2 Sparger not specified $v_{sg} = 0.00375$ to 0.0075 ms^{-1}	ESTEEM (in-house), 65 x 100 x 18 cells[a] t_{step} = 0.01s (300s) Eulerian-Eulerian, standard k-ε model, IMF: Drag, turbulent dispersion, bubble-induced interaction models	• The oscillation period in the downcomer decreases with increasing gas flow rate. • Simulation predictions on the oscillation period were agreeable at low superficial gas velocity however begins to diverge slightly at higher

Table 2.1   continued

Author	Reactor type/volume (dimensions)/sparger/operating conditions	Simulation setup/multiphase/ turbulence model/ interfacial momentum forces (IMF)/others	Remarks
Dhanasekharan et al. (2005)	EL-ALR cylindrical (3D) $A_d/A_r = 4.90$, height not reported $V_{working}$: 23 L Sparger not specified $v_{sg} = 0.01$ to 0.05 lms^{-1}	FLUENT 6.0, 23000 cells[a] t_{step} = not reported Eulerian-Eulerian, standard k-ε model, IMF: Drag model, PBM: Class method	• Global gas holdup was underpredicted at higher superficial gas velocity with a maximum error of 13%. • This error was magnified when the hydrodynamic parameter was employed to predict the mass transfer data with a maximum error of 25% despite discretizing the gas phase into 9 bubble sizes in the PBM model.
Roy et al. (2006)	EL-ALR cylindrical (3D) $A_d/A_r^b = 0.02$-0.042, 1.37 to 10 m height[b] Riser[b]: 0.1 to 0.155 m dia. Sparger not specified $v_{sgr} = 0.01$ to 0.26 ms^{-1}	CFX 5.7.1, 50000 tetrahedral nodes t_{step} = not reported (120s) Eulerian-Eulerian, standard k-ε model, IMF: Drag, lift, turbulent dispersion and bubble-induced turbulence models	• Predicted liquid circulation velocity and mixing time are in good agreement with experimental data. • Local gas holdup near the walls of the riser were underpredicted at lower superficial gas velocity.
Cao et al. (2007)	EL-ALR cylindrical (3D) $A_d/A_r = 0.06$, 2.50 m height Riser: 0.47 m dia. Multi-orifice sparger $v_{sg} = 0.02$ to 0.35 ms^{-1}	FLUENT 6.0, 66334 cells $t_{step} = 0.5$s (10s) Eulerian-Eulerian, RNG k-ε model, IMF: not reported	• Local gas holdup, axial liquid velocity and gas velocity were in good agreement with experimental data at lower superficial gas velocity. The discrepancy occurs at higher superficial gas velocity. • The lack of agreement of the experimental results can be due to the influence of the bubble-induced turbulence in normal directions not taken into account or as poor mesh.

Table 2.1   continued

Author	Reactor type/volume (dimensions)/sparger/operating conditions	Simulation setup/multiphase/ turbulence model/ interfacial momentum forces (IMF)/others	Remarks
Talvy et al. (2007)	IL-ALR rectangular (3D) $A_d/A_r = 1$, 3.00 m height Riser: 0.125 m^2 Cylindrical membrane sparger $v_{sg} = 0.005$ to 0.045 ms^{-1}	FLUENT 6.0, 62900 cells t_{step} = not reported Eulerian-Eulerian, modified k-ε model, IMF: Drag, turbulent dispersion, bubble-induced turbulence and virtual mass models	• The inclusion of drift velocity significantly improved the local gas distribution prediction in the riser, meanwhile the effect of virtual mass is negligible. • Drag model as a function of Eötvos number showed accurate predictions of local gas holdup in the riser.
Balleda et al. (2007)	IL-ALR cylindrical (2D) $A_d/A_r = 1$, 0.60 m height Riser: 0.004 m^2 Porous sparger $v_{sgr} = 0.003$ to 0.0067 ms^{-1}	FOTRAN, 40 x 55 cells t_{step} = not reported (75s) Eulerian-Eulerian, standard k-ε model, IMF: Drag and bubble-induced turbulence models	• The axial liquid velocity in the bottom clearance was overpredicted at higher gas flow rate with experimental data. • This led to the overprediction of the liquid circulation rate with increasing gas flow rate.
Law et al. (2008)	EL-ALR cylindrical (2D) A_d/A_r = not reported, not reported Riser: not reported Plate sparger $v_{sg} = 0.01$ to 0.20 ms^{-1}	CFDLib (In-house), 7574 cells t_{step} = not reported (90s) Eulerian-Lagrangian, modified k-ε model, bubble-pressure model IMF: Bubble-induced turbulence	• Bubble-induced turbulence introduced in the form of slip-production energy term and the inclusion of bubble-pressure model obtained a good agreement on the predicted overall gas holdup at lower superficial gas velocity.

27

Table 2.1   continued

Author	Reactor type/volume (dimensions)/sparger/operating conditions	Simulation setup/multiphase/ turbulence model/ interfacial momentum forces (IMF)/others	Remarks
Hekmat et al. (2010)	IL-ALR cylindrical (3D) $A_d/A_r{}^b = 0.44$, 1.8 m height Riser: 0.25 m dia. Sparger not specified $v_{sg} = 0.012$ ms^{-1}	FEMLAB, 120000 tetrahedral cells $t_{step} = 0.001$s (100s) Eulerian-Eulerian, standard k-ε model, IMF: Drag and bubble-induced turbulence models	• Their study evaluates the effect of draft tube position. The accuracy of the simulation increases as the draft tube approaches the wall due to the decreasing liquid velocity which operates similar to a reactor in the absence of a draft tube.
Huang et al. (2010)	IL-ALR cylindrical (2D) $A_d/A_r = 1.16$, 3.03 m height Riser: 0.10 m dia. Perforated plate sparger $v_{sg} = 0.01$ to 0.06 ms^{-1}	In-house code, 72 x 666 cells t_{step} = not reported Eulerian-Eulerian, RNG k-ε model, IMF: Drag, lift, turbulent dispersion model, wall lubrication and bubble-induced turbulence models	• The total gas holdup was slightly underpredicted at lower superficial gas velocity but overall in good agreement with experimental data.
Silva et al. (2011)	EL-ALR cylindrical (3D) $A_d/A_r = 0.68$, 5.76 m height Riser: 0.23 m dia. Perforated plate sparger $v_{sg} = 0.05$ to 0.08 ms^{-1}	CFX 11.0, 179000 cells $t_{step} = 0.00001$ to 0.001s (170s) Eulerian-Eulerian, standard k-ε model, IMF: Drag and bubble-induced turbulence models, PBM: MUSIG model	• Radial gas holdup in the riser was underpredicted in comparison with literature data at heterogeneous regime. • When the sparger employed the perforated plate, the radial gas holdup predicted in the riser was in closer agreement with experimental results except near the riser wall.

28

Table 2.1   continued

Author	Reactor type/volume (dimensions)/sparger/operating conditions	Simulation setup/multiphase/ turbulence model/ interfacial momentum forces (IMF)/others	Remarks
Šimčik et al. (2011)	IL-ALR rectangular (3D) $A_d/A_r{}^b$ = 1.66, 1.713 m height V_{working}: 50 L Porous plate sparger v_{sgr} = 0.01 to 0.075 ms^{-1}	FLUENT 6.3, 49100 cells[a] t_{step} = 0.005s (not reported) Eulerian-Eulerian, standard k-ε model, IMF: Drag and turbulent dispersion models	• Comparison on drag models as a function of Reynolds and Eötvös number obtained similar results on the prediction of axial liquid velocity and global gas holdup in the riser. • However, discrepancy in the drag models were more obvious in the downcomer as the downcomer is flowing counter current against buoyancy force. The effect of changing the predicted slip velocity from the models caused significant changes on the simulation results.
Lestinsky et al. (2012)	IL-ALR cylindrical (axi-2D) $A_d/A_r{}^b$ = 7.05, 1.50 m height Riser: 0.06 m dia. Sparger not specified v_{sgr} = 0.022 to 0.112 ms^{-1}	COMSOL 3.5a, mesh not reported t_{step} = 0.001s (60s) Eulerian-Eulerian, standard k-ε model, IMF: Drag, lift, turbulent dispersion, bubble-induced turbulence, virtual mass and friction force models	• Prediction on global liquid velocity and gas holdup were within 10% error. • The model is especially less accurate when high gas flow rate is flowing through a small draft tube in the internal airlift reactor.
Zhang et al. (2012)	IL-ALR cylindrical (axi-2D) A_d/A_r = 1.90, 1.482 m height Riser: 0.11 m dia. Perforated plate sparger v_{sgr} = 0.001 to 0.03 ms^{-1}	FLUENT 6.3, 4 mm triangle cells t_{step} = 0.00005 to 0.05s (140s) Eulerian-Eulerian, standard k-ε model (dispersed), IMF: Drag model	• The global liquid velocity and gas holdup were predicted within less than 5% and 10.2% error, respectively.

Table 2.1   continued

Author	Reactor type/volume (dimensions)/sparger/operating conditions	Simulation setup/multiphase/ turbulence model/ interfacial momentum forces (IMF)/others	Remarks
Karcz et al. (2013)	EL-ALR cylindrical (3D) $A_d/A_r = 0.19$, 1.932 m height Riser: 0.1056 m dia. Orifice sparger $v_{sgr} = 0.003$ ms^{-1}	CFX 13.0, 768287 tetrahedral cells[a] $t_{step} = 0.01$s (not reported) Eulerian-Eulerian, SST k-ω model and zero equation model, IMF: not mentioned	• Studied the on the effect of number of orifices in perforated plate on the hydrodynamics.
Massart et al. (2014)	EL-ALR cylindrical (3D) $A_d/A_r = 0.017$, 0.60 m height $V_{working}$: 12.8 L Orifice sparger $v_{sg} = 0.022$ to 0.301 ms^{-1}	FLUENT 6.3, 32227 cells t_{step} = not reported Eulerian-Lagrangian, standard k-ε model	• The liquid flow rate predicted in the riser starts to deviate with increasing air flow rate.
Mohajerani et al. (2012)	IL-ALR rectangular (axi-2D) $A_d/A_r{}^b = 0.54$, 3.06 m height[b] Riser: not reported Sparger not specified $v_{sg} = 0.02$ to 0.12 ms^{-1}	COMSOL 3.5, 3704 cells[a] $t_{step} = 0.1$ (10s) Eulerian-Eulerian, standard k-ε model, IMF: Drag, lift, turbulent dispersion and bubble-induced turbulence models	• The spherical drag model heavily underpredicted in the riser and downcomer. It also overpredicted the overall gas holdup. • Drag model as a function of Reynolds and Eötvös number was more accurate at predicting the global hydrodynamics even with increasing superficial gas velocity.

Table 2.1　　　continued

Author	Reactor type/volume (dimensions)/sparger/operating conditions	Simulation setup/multiphase/ turbulence model/ interfacial momentum forces (IMF)/others	Remarks
Jiang et al. (2016)	EL-ALR cylindrical (3D-riser) A_d/A_r not reported, 5.00 m height Riser: 0.15 m dia. Perforated plate sparger $v_{sgr} = 0.023$ to 0.117 ms^{-1}	FLUENT, mesh not reported $t_{step} = 0.0005$ to 0.005s (130s) Eulerian-Eulerian, RNG k-ε model, IMF: Drag model	• Spherical drag model underpredicted the gas holdup. This is also reflect on the gas distribution across the height of the riser. • The model as a function of bubble deformation and superficial gas velocity
Liao et al. (2016)	IL-ALR cylindrical (2D, 3D) A_d/A_r 0.25, 1.16 m height Riser: 0.04 m dia. Ring sparger $v_{sg} = 0.01$ ms^{-1}	CFX 14.5, 2D: 4000, 3D: 210000 cells $t_{step} =$ not reported Eulerian-Eulerian, SST k-ω mode, IMF: Drag, lift, turbulent dispersion, wall lubrication and bubble-induced turbulence models	• Mean flow quantities predicted near the sparger region is affected slightly by the spatial dispersion with 3D obtaining slightly better prediction. • The radial gas holdup in the downcomer were overpredicted, notably in the lower part of the downcomer.
Bednarz et al. (2017)	IL-ALR cylindrical (axi-2D) $A_d/A_r^c = 1.04$, 0.459 m height $V_{working}$: 40 L Ring sparger $v_{sgr} = 0.00035$ to 0.0016 ms^{-1}	FLUENT 15.0, 17632 cells $t_{step} = 0.001$s (50s) Eulerian-Eulerian, standard k-ε model, IMF: Drag and turbulent dispersion models	• Global gas holdup was in good agreement with experimental results through the implementation of spherical drag model. • However, the entrainment of the polyamide spheres which was used to trace the liquid flow field was severely overpredicted.

31

Table 2.1   continued

Author	Reactor type/volume (dimensions)/sparger/operating conditions	Simulation setup/multiphase/ turbulence model/ interfacial momentum forces (IMF)/others	Remarks
Chen and Bai (2017)	IL-ALR cylindrical (3D) $A_d/A_r{}^c = 5.32$, 1.90 m height Riser: 0.094 m dia. Ring sparger $v_{sgr} = 0.0059$ to 0.0179 ms^{-1}	FLUENT 14.5, mesh not reported t_{step} = not reported Eulerian-Eulerian, standard k-ε model, IMF: Drag, lift and turbulent dispersion models	• The turbulent dispersion model significantly improved the overall gas holdup and liquid velocity prediction. • Though the accuracy reduces with increasing superficial gas velocity.
Stiriba et al. (2017)	IL-ALR rectangular (3D) $A_d/A_r = 1$, 2.00 m height $V_{working}$: 63 L Orifice sparger $v_{sg} = 0.01$ to 0.08 ms^{-1}	FLUENT 15.0, 60398 tetrahedral cells $t_{step} = 0.0005$s (180s) Eulerian-Eulerian, standard k-ε model (dispersed), IMF: Drag and turbulent dispersion models	• The predicted superficial liquid velocity and superficial gas velocity in the riser were within 12% error. However, the discrepancy increases with increasing gas flow rate.
Rzehak et al. (2017)	IL-ALR cylindrical (axi-2D) $A_d/A_r{}^c = 0.61$, 1.16 m height Riser: 0.008 m^2 Ring sparger $v_{sg} = 0.01$ ms^{-1}	CFX 14.5, 2.5 x 20 mm^a t_{step} = Courant-Friedrichs-Lewy Eulerian-Eulerian, SST k-ω model, IMF: Drag, lift, turbulent dispersion, wall lubrication, bubble-induced turbulence and virtual mass models	• Extended the closure model from bubble columns to internal airlift reactor but obtained an overprediction in its liquid velocity. • The gas distribution in both the riser and downcomer were also overpredicted. • In addition, the square root turbulent kinetic energy was severely underpredicted.

32

Table 2.1   continued

Author	Reactor type/volume (dimensions)/sparger/operating conditions	Simulation setup/multiphase/ turbulence model/ interfacial momentum forces (IMF)/others	Remarks
McClure et al. (2017)	IL-ALR cylindrical (3D) $A_d/A_r = 1$, 2.00 m height Riser: 0.119 m^2 Orifice sparger $v_{sg} = 0.07$ to 0.34 ms^{-1}	FLUENT 18.0, 125284 cells $t_{step} = 0.001$s (100s) Eulerian-Eulerian, standard k-ε model and and zero equation model, IMF: Drag, turbulent dispersion and bubble-induced turbulence models	• The mixing time was under predicted by the model even at the lowest superficial gas velocity. • The discrepancy could be due to the use of single bubble size model.

[a]Mesh structure may vary in different regions of the airlift reactor, thus only the notable region was reported.
[b]Study may have more than one geometry structure, only the notable dimensions were reported.
[c]Gas is sparged in the annulus of the cylindrical airlift reactor.

2.5.4.1 Drag Force

Amongst these forces, the drag force is found to be the most predominant force. In bubble columns, it was found that the drag force is 100 times in magnitude higher than the lift force (Chen *et al.,* 2004). Various drag models have been employed in airlift reactor studies citing sources from single bubble experiments; spherical bubbles (i.e. Schiller and Naumann, 1935), bubble deformation (i.e. Tomiyama *et al.,* 1998; Grace *et al.,* 1976; Ishii and Zuber, 1979) and models derived based on operating parameters (Chen *et al.,* 2005). The spherical drag model employed in the gas-liquid system is the most controversial model whereby sources that employed it have obtained both good and dissatisfactory predictions on the gas holdup and liquid velocity. Schiller and Naumann (1935) model was derived based on the assumption of single rigid spherical particle moving in a stagnant fluid.

$$C_D = \max\left(\frac{24}{\mathrm{Re}_b}(1 + 0.15\,\mathrm{Re}_b^{0.687}),\ 0.44 \right)$$

2.7

where at higher bubble Reynolds number, $\mathrm{Re}_b > 1000$ the drag coefficient converges at a constant value of 0.44. Dhanasekharan et al. (2005) and Law et al. (2008) were able to obtain great agreement through the employment of the spherical drag model with errors within 15.4% and 7.3%, respectively. However, a comparison study carried out by Mohajerani et al. (2012) obtained poor predictions across all superficial gas velocity through the employment of the Schiller and Naumann (1935) model. The difference between these studies may be a result of Dhanasekharan et al. (2005) employing population balance model in their study which significantly increases the accuracy.

Aside from that, it is common to observe Schiller and Naumann (1935) drag model being successfully employed in external airlift reactor which are known to be effective at disengaging gas in the gas separator. This implies that the role of the drag models might be less influential in the riser. However, the drag force as a result of bubble deformation have influence within the downcomer in the presence of bubbles (Šimčik *et al.,* 2012). Grace et al. (1976) model considers the effects bubble deformation in modelling the drag coefficient. Bubble deformation is expected to occur when the bubble

is larger than 3 mm (Gimbun *et al.,* 2009). The expression of the correlation was given as:

$$C_\text{D} = \max\left(\min\left(C_\text{D,ellipse}, C_\text{D,cap}\right), C_\text{D,sphere}\right)$$ 2.8

Bubbles with very low bubble Reynolds number, have spherical shape bubbles and tends to behave close to Stokes regime where $C_\text{D,sphere} = 24/\text{Re}_b$ meanwhile at slightly higher bubble Reynolds number, $C_\text{D,sphere}$ similar to Schiller and Naumann (1935) model in viscous regime was employed.

$$C_\text{D,sphere} = \min\left(\frac{24}{\text{Re}_b}\left(1 + 0.15\,\text{Re}_b^{0.687}\right), \frac{24}{\text{Re}_b}\right)$$ 2.9

However, when external forces were applied on the dispersed phase it causes the bubble to lose its spherical-like shape. Bubbles with non-spherical shapes affect the drag coefficient where deformed bubbles generates more drag. Instead, the correlation $C_\text{D,ellipse}$ derived based on the terminal velocity, u_t of a single bubble moving in a stagnant fluid is incorporated to account the effect of ellipsoidal bubbles on the drag coefficient. The ellipse drag correlation is dependent through the Eötvös number, $\text{Eö} = gd_b^2(\rho_l - \rho_g)/\sigma$ which represents the ratio of gravitational to surface tension forces and Morton number, $\text{Mo} = g\mu_l^4(\rho_l - \rho_g)/\rho_l^2\sigma^3$ which accounts the fluid properties.

$$C_\text{D,ellipse} = \frac{4gd_b}{3u_t^2\rho_l}\left(\rho_l - \rho_g\right)$$ 2.10

$$u_t = \frac{\mu_l}{\rho_l d_b}\text{Mo}^{-0.149}\left(\beta - 0.857\right)$$ 2.11

where σ refers to the surface tension between the disperse and continuous phase and β is a piecewise function expressed in terms of *b*.

$$\beta = \begin{cases} 0.94b^{0.757} & 2 < b \le 59.3 \\ 3.42b^{0.441} & b > 59.3 \end{cases} \qquad 2.12$$

$$b = \frac{4}{3}\text{EöMo}^{-0.149}\left(\frac{\mu_g}{\mu_{\text{ref}}}\right)^{-0.14} \qquad 2.13$$

Given μ_{ref} is the molecular viscosity of water. At higher Eötvös number, $\text{Eö} \ge 40$ the bubbles are capped in shape which has the tendency to have higher drag than both spherical and ellipse bubbles, thus converges to a single constant value:

$$C_{\text{D,cap}} = \frac{8}{3} \qquad 2.14$$

Meanwhile, Tomiyama et al. (1998) model is similar to the Grace et al. (1976) model in which it considers the bubble deformation. The empirical data were obtained from Clift et al. (1978) which segregates the correlations into degrees of contamination (i.e. pure liquid, slightly contaminated liquid and contaminated liquid). Industrial airlift reactor tap waters are typically categorised as slightly contaminated water thus, the following expression was adopted based on the derivation of a single bubble moving in a stagnant fluid:

$$C_D = max\left(min\left(\frac{24}{Re_b}(1 + 0.15Re_b^{0.687}), \frac{72}{Re_b}\right), \frac{8}{3}\frac{\text{Eö}}{\text{Eö} + 4}\right) \qquad 2.15$$

There is a notable slight difference in the Stokes regime expression, $C_D = 72/\text{Re}_b$ for low bubble Reynolds number which takes into account that the water was slightly contaminated. The correlation to account the viscous regime adopts the similar rigid sphere model. Meanwhile, their model also implemented a generalised correlation on distorted and capped bubble regimes with respect to Eötvös.

The correlation is valid within the range of $10^{-3} < \text{Re}_b < 10^5$, $10^{-2} < \text{Eö} < 10^3$ and $10^{-14} < \text{Mo} < 10^7$. Šimčik et al. (2011) has conducted a comparison study between spherical drag model and bubble deformation drag model and found that both were equally good at predicting the riser but the latter outperformed the former in the downcomer. The implementation of other models (i.e. bubble deformation) may require

some comparison study to be carried out as generally it is well understood bubble diameter has a significant influence on the selection of the drag models. For instance, bubble diameter with less than 3 mm typically employs spherical drag models (Gimbun *et al.,* 2009), 3 to 9 mm which are a mixed of deformed bubbles (i.e. spherical cap) employs Tomiyama et al. (1998).

It is worth noting most of the drag models were derived from single bubble rising in stagnant continuous phase experiments. However, single bubbles may have lower C_D than the drag coefficient obtained from a swarm of bubbles of the same radius (Tomiyama, 2004). Thus, an additional correction term that accounts the effect of bubble swarm was introduced through the Universal drag model (Kolev, 2005) so long as the following conditions were satisfied:

$$C_{D,dis} = \frac{2}{3}\left(\frac{d_b}{\lambda_{RT}}\right)\left(\frac{1+17.67\left((1-\alpha_g)^{1.5}\right)^{6/7}}{18.67\left(1-\alpha_g\right)^{1.5}}\right)^2 \qquad 2.16$$

where $C_D = C_{D,dis}$ if, the value of $C_{D,dis}$ is higher than the drag coefficient value in the viscous regime but lower than then drag coefficient value in capped regime (i.e. $C_{D,vis} < C_{D,dis} < C_{D,cap}$). The distorted regime here indicates the wake region produced by the trailing vortex behind the bubble causing the distortion to itself and surrounding bubbles. $\lambda_{RT} = \left(\sigma / g\left(\rho_l - \rho_g\right)\right)^{0.5}$ refers to the Rayleigh-Taylor instability.

$$C_{D,vis} = \frac{24}{\text{Re}_b}\left(1+0.1\text{Re}_b^{0.75}\right) \qquad 2.17$$

where $C_D = C_{D,vis}$ if, the value of $C_{D,dis}$ is lesser than the drag coefficient value in viscous regime (i.e. $C_{D,dis} < C_{D,vis}$).

$$C_{D,cap} = \frac{8}{3}\left(1-\alpha_g\right)^2 \qquad 2.18$$

where $C_D = C_{D,cap}$ if, the value of $C_{D,dis}$ is more than the drag coefficient value in capped regime (i.e. $C_{D,dis} > C_{D,cap}$).

2.5.4.2 Non-drag Forces

On the other hand, the non-drag forces which consists of lift, turbulent dispersion and bubble-induced forces can be observed to be widely employed in internal airlift reactors but is quite uncommon in external airlift reactors as outlined in Table 2.2 and Table 2.3. The significance of the lift force is highly debatable in literature as some studies have neglected it (Oey *et al.,* 2003; Talvy *et al.,* 2007; Balleda *et al.,* 2007; Zhang *et al.,* 2012; Bednarz *et al.,* 2017).

The role of the lift force is believe to assist in the radial migration of the bubbles with larger size towards the centre and bubbles of smaller size towards the wall. The effect of the lift model is minor in comparison to the drag model but is needed to correct the radial profiles of the gas holdup, turbulent kinetic energy, axial liquid velocity and capture bubble plume oscillations to accurately predict instantaneous gas velocity (Bhole *et al.,* 2008; Gupta and Roy, 2013).

However, a wide discrepancy has occurred whether to consider lift force in the gas-liquid CFD simulation due to lack of proper guidelines. The lift force can be expressed by a constant value obtained from experimental data or identified through a lift model. The lift coefficient value, $C_L = 0.5$ have shown to be great at capturing axial liquid and gas velocities, motioning bubbles to migrate in a lateral direction to the wall which reduces the profile peaks of the phase velocities across the column (Masood and Delgado, 2014; Masood *et al.,* 2015). However, lift models contribute to a more dynamic bubble plume oscillation in comparison to lift coefficient (Masood *et al.,* 2015). Tomiyama (1998) model that accounts the bubble deformation has been widely implemented in past studies (Liao *et al.,* 2016; Bannari *et al.,* 2011; Rzehak *et al.,* 2017). The model is a function of bubble Reynolds number and Eötvös number derived from a single bubble moving in a glycerol-water solution. The validity of the model extends within the defined regions of $1.39 \leq \text{Eö} \leq 5.74$ and $-5.5 \leq \log_{10}\text{Mo} \leq -2.8$. The model was also proven to be capable of being employed in air-water systems as well (Lucas and Tomiyama, 2011).

Given that the function $f(\text{Eö}_a)$ is expressed as:

$$C_L = \begin{cases} min(\,0.288\,tanh(\,0.121\,Re_b),f(\text{Eö}_a) & \text{Eö}_a < 4 \\ f(\text{Eö}_a) & 4 < \text{Eö}_a < 10 \\ -0.27 & 10 < \text{Eö}_a \end{cases} \qquad 2.19$$

where in the modified Eötvös number, $E\ddot{o}_a = gd_a^2(\rho_l - \rho_g)/\sigma$, the d_a is the major dimension of the bubble which can defined through the empirical correlation of the aspect ratio as (Wellek et al., 1966):

$$d_a = d_b\big(1 + 0.163\text{Eö}^{0.757}\big)^{\frac{1}{3}} \qquad\qquad 2.20$$

The lift coefficient sign changes to a negative value at bubble diameter greater than 5.8 mm. For bubble sizes below that value, the gas-liquid system would rely on a constant lift coefficient whereby the value $C_L = 0.28$. Past studies however have shown slight over-predictions profile near walls or higher peaks at the centre of the column due to low lift coefficient values which weakens the dispersion of bubbles towards the walls (Rzehak and Krepper, 2013a; Masood and Delgado, 2014).

Meanwhile, the employment of different turbulent dispersion models has not been fully disclosed yet in literature. The turbulent dispersion is found to be significant affect the dispersed phase as it describes the effect of eddies from the continuous phase on the bubbles. Few turbulent dispersion models have been proposed across literature to account those effects. One such is the Lopez de Bertodano (1991) model which is based on molecular movement analogous to the thermal diffusion of particles in the atmosphere. The dispersion term is simplified to a singular constant known as the turbulent dispersion coefficient, C_{TD} derived from empirical data. The model can be expressed as:

$$M_{l,g}^{\text{TD}} = C_{\text{TD}}\rho_l k_l \nabla \alpha_g \qquad\qquad 2.21$$

Table 2.2   Past CFD studies that employed interfacial momentum forces in internal airlift reactors

Author	Interfacial momentum models				Accuracy
	Drag	Lift	Turbulent dispersion	Turbulence interaction	
Oey et al. (2003)[a]	Schiller and Naumann (1935)	-	Burns et al. (2004)	Gosman et al. (1992) Issa and Oliveira (1993)	-
Talvy et al. (2007)[a]	Karamanev and Nikolov (1992)	-	Simonin and Viollet (1990)	Bel Fdhila and Simonin (1992) Elgobashi and Abou-Arab (1983)	11.9%
Balleda et al. (2007)	Schwarz and Turner (1988)	-	-	Kataoka and Serizawa (1989)	-
Mohajerani et al. (2012)	Dijkhuizen et al. (2010)	$C_L = 0.5$	Lopez de Bertodano (1991)	Bel Fdhila and Simonin (1992) Elgobashi and Abou-Arab (1983)	17.1%
Šimčik et al. (2012)	Tomiyama et al. (2002)	-	Burns et al. (2004)	-	11.2%
Zhang et al. (2012)	Tomiyama (1998)	-	-	-	8.2%
Liao et al. (2016)[a,b]	Ishii and Zuber (1979)	Tomiyama et al. (2002)	Burns et al. (2004)	Troshko and Hassan (2001)[c]	17.3%
Stritiba et al. (2017)	Karamanev and Nikolov (1992)	-	Simonin and Viollet (1990)	Bel Fdhila and Simonin (1992) Elgobashi and Abou-Arab (1983)	16.3%
Chen and Bai (2017)	Schiller and Naumann (1935)	$C_L = 0.5$	Burns et al. (2004)	-	8.9%
Bednarz et al. (2017)	Schiller and Naumann (1935)	-	Simonin and Viollet (1990)	-	-
Rzehak et al. (2017)[c]	Ishii and Zuber (1979)	Tomiyama et al. (2002)	Burns et al. (2004)	Troshko and Hassan (2001)[c]	24.0%

[a]Considered virtual mass effect, $C_{VM} = 0.5$.

[b]Considered wall lubrication effect using Tomiyama et al. (1995) model in their study.

[c]Implements mixed scale ($d_b / \sqrt{k_l}$) in their study (Rzehak and Krepper, 2013).

where k_l is the turbulent kinetic of the continuous phase and $\nabla\alpha_g$ is the gradient of the dispersed phase volume fraction. This model is however limited by its singularity coefficient value obtained from empirical data. On the other hand, another turbulent dispersion model by Simonin and Viollet (1990) places emphasis on the dominance of the momentum from the dispersed phase whereby the dispersion gives rise to a term that appears as diffusion of the dispersed units relative to the liquid. This model is expressed through the drift velocity model as a function of gas-liquid turbulent dispersion term, $D_{l,g}^t$ relating to the turbulence characteristics scale and volume fraction gradient expressed as follows:

$$v_d = -D_{l,g}^t \left(\frac{\nabla\alpha_g}{\alpha_g} - \frac{\nabla\alpha_l}{\alpha_l} \right) \qquad 2.22$$

$$M_{l,g}^{\text{TD}} = \frac{\kappa C_{\text{TD}}}{\sigma_{\text{TD}}} D_{l,g}^t \left(\frac{\nabla\alpha_g}{\alpha_g} - \frac{\nabla\alpha_l}{\alpha_l} \right) \qquad 2.23$$

where κ is obtained from Equation 2.23, v_d is the drift velocity and σ_{TD} is the Prandlt number given as 0.75. The turbulent dispersion term, $D_{l,g}^t$ can be defined as:

$$D_{l,g}^t = \frac{1}{3}\tau_{l,g}^t \overline{u_l u_g} \qquad 2.24$$

and $\tau_{l,g}^t$ is the characteristic timescale of the turbulence seen by the dispersed phase and $\overline{u_l u_g}$ is the isotropic turbulence of the velocity correlation tensors as shown below:

$$\tau_{l,g}^t = \frac{\tau_l^t}{\sigma_{k,l}}\left(1 + C_\beta \zeta_r^2\right)^{-\frac{1}{2}} \qquad 2.25$$

$$\overline{u_l u_g} = 2k_l\left(\frac{b+\eta_r}{1+\eta_r}\right) \qquad 2.26$$

41

Meanwhile, the characteristic time of the turbulence in the liquid τ_l^t, expression b and the ratio of the characteristic timescale of the turbulence seen by the dispersed phase and the bubble entrainment by the liquid motion η_r were defined as shown in the following:

$$\zeta_r = \frac{|V_r|}{\sqrt{\frac{2}{3}k_l}}$$

2.27

$$\tau_l^t = \frac{3}{2}C_\mu \frac{k_l}{\varepsilon_l}$$

2.28

$$b = \frac{1+C_{VM}}{\rho_g/\rho_l + C_{VM}}$$

2.29

$$\eta_r = \frac{\tau_{l,g}^t}{\tau_{l,g}^e}$$

2.30

The turbulent dispersion force in other pneumatic reactors (i.e. bubble column) have been concluded to be essential with increasing superficial gas velocity (Tabib *et al.,* 2008). As a basis to this, studies on the roles of the turbulent dispersion forces in the airlift reactor were found to significantly increase the accuracy of predicting the global gas holdup (Chen and Bai, 2017). It was also found that the turbulent dispersion model greatly increased local predictions of the gas holdup in the riser (Talvy *et al.,* 2007). However, there is a lack of direct comparison between different turbulent dispersion models. Moreover, models empirical constant should be kept without adjustments being made for them to be qualified as versatile enough to be employed in airlift reactors across different configurations.

The bubble-induced turbulence model is essential and one of the fewer developed forces that may have an impact on the turbulent dispersion force and bubble dynamics (Rzehak *et al.,* 2013). The bubble-induced turbulence model may be introduced by adding to effective viscosity terms as shear-induced turbulent or through an additional source term in the turbulence model (i.e. turbulence kinetic energy and dissipation energy). The bubble-induced turbulence models employed are equally divided as evident in Table 2.2 and Table 2.3. The bubble-induced turbulence can be incorporated as an additional

viscosity term. Sato and Sekoguchi (1975) bubble-induced model is extensively known for its added bubble-induced contribution to the turbulent viscosity expressed as:

$$\mu_b = C_\mu \frac{k_l^2}{\varepsilon_l} + C_b \alpha_g d_b \left| \vec{u}_g - \vec{u}_l \right|$$

2.31

On the other hand, the bubble-induced turbulence can alternatively be included as an additional source terms $S_{k,l}$ and $S_{\varepsilon,l}$ in the dispersed standard k-ε turbulence model. Troshko and Hassan (2001) model derived source terms that were added into the two-equation dispersed standard k-ε turbulence model to account the effects of bubble-induced turbulence on both the turbulence kinetic energy and the dissipation energy of the liquid phase. The k source term assumes that all the energy lost due to drag acted upon a bubble is converted into turbulence kinetic energy in the wake region behind the bubble. Thus, the term is defined as:

$$S_{k,l} = C_k \sum_{g=1}^{M} \frac{K_{l,g}}{\alpha_l \rho_l} \left| \vec{u}_g - \vec{u}_l \right|^2$$

2.32

Meanwhile, the ε source term for the dissipation equation is taken as the k source term divided by the characteristic timescale:

$$S_{\varepsilon,l} = \frac{C_{\mathrm{TD}}}{\tau_b} S_{k,l}$$

2.33

The bubble scale time was employed as the characteristic time of induced turbulence, τ_b in this work as shown in Equation 2.34:

$$\tau_b = \frac{2C_{VM} d_b}{3C_D \left| \vec{u}_g - \vec{u}_l \right|}$$

2.34

43

Table 2.3　　Past CFD studies that employed interfacial momentum forces in external airlift reactors

| Author | Interfacial momentum models | | | | Accuracy |
	Drag	Lift	Turbulent dispersion	Turbulence interaction	
Vial et al. (2002)	Schiller and Naumann (1935)	-	-	-	57.4%
Dhanasekharan et al. (2005)[a]	Schiller and Naumann (1935)	-	-	-	15.4%
Roy et al. (2006)	Zhang and Vanderheyden (2002)	$C_L = 0.1$	Lopez de Bertodano (1991)	-	3.7%
Law et al. (2008)[b]	Schiller and Naumann (1935)	-	-	Sato et al. (1981)	7.3%
Bannari et al. (2011)[a,b]	Schiller and Naumann (1935)	Tomiyama et al. (2002)	-	-	-
Silva et al. (2011)[a]	Ishii and Zuber (1979)	-	-	Sato and Sekoguchi (1975)	14.7%
Jiang et al. (2015)	Dual-bubble size (Chen *et al.*, 2009)	-	-	-	19.2%

[a]Implemented population balance model.

[b]Considered virtual mass effect, $C_{VM} = 0.5$.

[c]Considered bubble swarm effect in their study

2.5.4.3   Past Studies on Closure Models in Airlift Reactors

Comparison studies on a good closure model has been carried out before in the past (Talvy *et al.,* 2007; Mohajerani *et al.,* 2012; Jiang *et al.,* 2015). Talvy et al. (2007) and Jiang et al. (2015) have conducted drag model comparison studies and found that the Karamanev and Nikolov (1992) and dual-bubble size models gave better predictions in their studies, respectively. Mohajerani et al. (2012) on the other hand have compared across different drag models available in literature and concluded Dijkhuizen et al. (2010) model with the best accuracy. As Table 2.2 and Table 2.3 illustrate, they have not agreed upon a similar set of models as well as their forces to account for the flow fields within the airlift reactor. Šimčik et al. (2011) has noted that this disagreement is common as the bubble presence within the airlift reactor configuration were not taken into account in their evaluations. They argued that comparison studies on the closure models should be separated between airlift reactor configurations with bubble present in the downcomer (partial gas disengagement in the absence of bubble circulation) and bubble absent in the downcomer (total gas disengagement). This has a significant effect due to counter-current forces (i.e. bubble buoyancy and liquid circulation from the opposing direction) in the downcomer experienced by the bubbles (Šimčik *et al.,* 2011). This bubble configuration is typically found in internal airlift reactors, which as mentioned earlier tend to include both the drag and non-drag forces in their closure models. For instance, Zhang et al. (2012) has an exceptional minimal error of 8.2% by only employing the Tomiyama et al. (1998) drag model. This would be valid as Zhang et al. (2012) reactor configuration adopts a total gas disengagement internal airlift reactor (i.e. bubbles absent in downcomer) and operates below a superficial gas velocity of 0.03 ms^{-1} which is relatively low in comparison to Vial et al. (2002). When no proper comparison on closure models was conducted, most of the partial gas disengagement in the absence of bubble circulation airlift reactor configuration errors were above 15% (Liao *et al.,* 2016; Stritiba *et al.,* 2017). On the other hand, there are a handful of studies that have adopted robust models by other researchers' work and obtained higher discrepancy in their results (i.e. 16.3% error) than the predecessors (i.e. 11.9% error) (Stritiba *et al.,* 2017).

Another complexity added to narrow down the choice of proper closure model is the proposed theoretical or semi-empirical models to represent individual forces. There are various models across literature and their accuracy varies with different airlift reactor

settings. As of current, there has yet to be a systematic analysis on a set of closure model carried out with in different airlift reactor configurations. Šimčik et al. (2011) work only elucidated the closure model based on two drag models in a partial gas disengagement in the absence of bubble circulation airlift reactor and total gas disengagement. Further works on other non-drag forces were not elucidated. As different models has significant role in capturing the physics behind the hydrodynamics and flow patterns in the riser and downcomer of the airlift reactor, suitable models for both drag and non-drag forces should be taken into account and systematically reviewed.

2.6   Effect of Sparger

The construction of a simple airlift reactor consists of a vessel equipped with an internal baffle that divides the reactor into four sections; the riser, downcomer, top clearance and bottom clearance. The presence of the internal baffle enhances the performance of the airlift reactor to operate at a wider range of superficial velocities and provide more control over the flow field than the bubble column (Chisti, 1987; Kadic and Theodore, 2014). Aeration and mixing in the airlift reactor is solely dependent on the sparger in the absence of mechanical agitation.
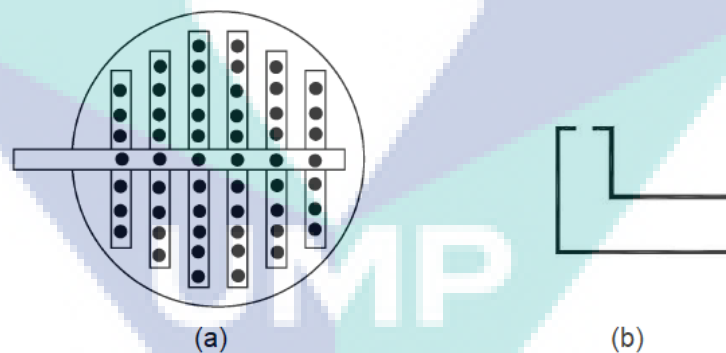
Figure 2.5   (a) Multi orifice and (b) single orifice spargers equipped in airlift reactors

Source: Vial *et al.* (2002); Gumery *et al.* (2009).

Various kinds of sparger types such as the multi orifice and single orifice sparger as shown in Figure 2.5 have been employed across literature. The effect of different sparger configurations (i.e. multi orifice, single orifice) may influence the distribution of the bubbles in the flow field (Vial *et al.,* 2002; Cao *et al.,* 2007; Karcz *et al.,* 2013; Massart *et al.,* 2014; Stritiba *et al.,* 2017; McClure *et al.,* 2017). It was found that the multi orifice

sparger produced a broader swarm of bubble hence more uniform riser velocity was observed. In contrast, a single orifice study showed a narrow bubble swarm and higher velocity at the middle of the riser.

It can be seen here the spargers which acts as gas injectors into the airlift reactor system influence the dispersion of the gas due to kinetic energy distribution. Thus, it is clear the sparger design and configuration may affect the gas-liquid flow and its hydrodynamics. Apart from sparger type, sparger location may also influence the gas-liquid hydrodynamics in airlift reactors because the bubble rise occurs at the immediate vicinity of the sparger.

Since in airlift reactor the liquid velocity is affected mainly by the bubble rise, therefore the sparger location potentially has a significant effect on the gas-liquid flow. Chisti and Moo-Young (1987) have noted the sparger to have influence on the distribution of the bubbles which would also affects the shear forces and dead zones. They observed that when sparger was placed inside the riser, the gas was better distributed as illustrated in Figure 2.6.

However, raising the sparger height from the bottom of the riser can also lead to the decrease of gas holdup in the riser due to recirculation (Siegel *et al.,* 1986). Moreover, it was found that the volume of the dead zone within the airlift reactor increases with increasing height of the sparger (Mahmood *et al.,* 2015). Meanwhile when the sparger was placed in the downcomer, it was found at heights halfway or greater distance from the bottom of the downcomer the power consumption of the airlift reactor reduces (Kubota *et al.,* 1978). Behin and Ahmadi (2010) on the other hand identified sparger placed within the annulus has a better liquid mixing time and circulation time than the sparger placed within the draft tube. It is notable that no previous study on the effect of sparger location across the radial riser is currently available in the literature.
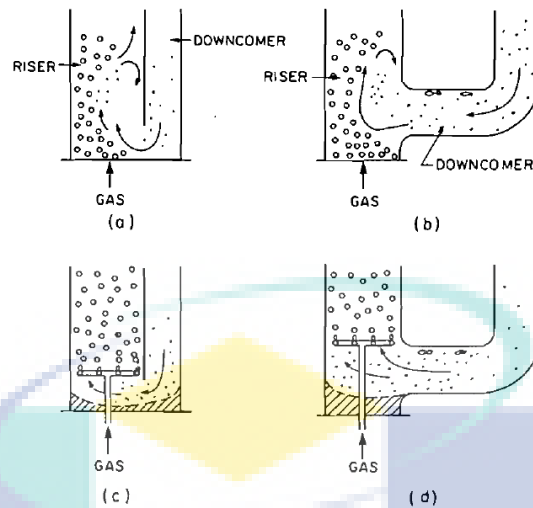
Figure 2.6:   Influence of sparger location on the gas holdup in airlift reactors

Source: Chisti & Moo-Young (1987).

2.7   Experimental Measurement Techniques in Airlift Reactor

Determination on the robustness of a CFD model should be validated against experimental measurements. As the gas-liquid is a complex two phase system, special tools are required to detect the intrinsic hydrodynamics phenomena. One of the hydrodynamic parameter that is being focused in this study is the liquid velocity which reflects the turbulence within the two phase system. Numerous measurement techniques have been applied across literature to measure the flow field within the airlift reactor including photographic imaging (PI), measurement probes (i.e. conductivity, convection or pressure probes), laser Doppler anemometry (LDA), particle imaging velocimetry (PIV) and computer automated radioactive particle tracking (CARPT). These methods, their past studies and limitations are briefly discussed to understand their applications in the flow phenomena.

2.7.1   Photographic/Digital Imaging

Photographic imaging is the most basic method to perform the flow measurement. It was applied back in the 1950s to capture the fluid velocities within gas-liquid systems. As of current, there exist high speed imaging system which have been employ to visualise the flow field within gas-liquid flows. They are cheaper, simple to handle and possessed the ability to capture overall flow field and mean liquid velocities through post-processing over the images. Behin and Farhadian (2013) employed digital image processing to

capture the residence time distribution which were then processed using advanced image processing software to extract the data. However, data collected are mostly global data which has limitations in providing the intrinsic details of the hydrodynamic that might influence the transport phenomena locally. Moreover, concerns over bubbles overlapping at high gas volume fractions would interfere with measurements.

2.7.2   Measurement Probes

Further advancement in data processing, analysing and computers had allowed the used of measurement probes to conduct flow field measurements locally in the 1960s. This method is the most widely adopted approach in measuring liquid velocity in airlift reactors as of current for their ability to capture both mean and fluctuating flows locally. The type of probes varies between pressure probes, conductivity probes, convection probes (i.e. hot wire and hot film) and pH probes with selected tracers inserted into the gas-liquid system.

The conductivity probe was often applied to measure liquid velocity in most airlift reactor studies (Vial *et al.,* 2001; van Baten *et al.,* 2003; Couvert *et al.,* 2004; Zhang *et al.,* 2012; Luo *et al.,* 2013). Two or more conductivity probes will be preinstalled during the fabrication of the rig at selected locations to locally measure the liquid velocity. A salt tracer (i.e. sodium chloride and potassium chloride) is then dissolved into the airlift reactor system and the data is collected for further analysis to remove the background noise. On the other hand, pH probes which are rarely used to capture the liquid velocity due to its sensitivity to change of environment (i.e. fermentation processes) has also been successfully employed to study laboratory scale model of an internal airlift reactor using a sulphuric acid tracer (Šimčik *et al.,* 2011).

2.7.3   Laser Doppler Anemometry (LDA)

Advancement in optical measurement technique has brought breakthroughs in the application of laser to measure signals from the flow phenomena. One of the instruments that were further developed into the current optical measurement tool is the LDA. The LDA emits dual laser beams to form a volume probe to measure the fluid particles and transmits the signals detected within the volume probe back to the sensor. A workstation validates and post processed the data to be further analysed. This instrument is highly attractive for its non-intrusive instantaneous velocity measurements. One of the many

advantages of using this equipment is its high resolution single point measurements which measures up to three velocity components.

Studies using LDA to measure gas-liquid flow first begun to emerge in the late 1970s. As this instrument is relatively new, only few studies of LDA measurements have been applied into airlift reactor studies to study phase velocities (Becker *et al.,* 1994; Tan *et al.,* 1995; Vial *et al.,* 2002). Becker et al. (1994) study was amongst the first to employ LDA in an airlift reactor to measure the axial time-averaged and periodic liquid velocity measurements across the riser and downcomer of an external-loop airlift reactor. Meanwhile, Tan et al. (1995) measured both the axial time-averaged liquid velocity and fluctuating velocities to study the influence of the flow field on a 10 L animal cell cultivating bioreactors using two component LDA. Vial et al. (2002) on the other hand obtained both the axial and tangential time-averaged liquid velocity and the root-mean-square (r.m.s.) velocity using a back-scattered one component LDA. They were able to obtained two components by traversing the LDA to capture the tangential velocity of the flow.

2.7.4   Particle Image Velocimetry (PIV)

In conjunction with the advancement in laser and imaging techniques, the technologies have extended itself to capture flow field maps through the particle image velocimetry (PIV). The PIV instrument came out slightly later than the LDA, equipped with charge-coupled camera (CCD) and a laser sheet over the flow field. They are capable of capturing snapshots of instantaneous and time-averaged flow field in a vector map, bubble velocity via particle tracking and the determination of the bubble size distribution. Most importantly, they too are non-intrusive on the flow field when obtaining measurements and provide a map of the flow field.

Some studies were also carried out using PIV to measure the liquid velocity although specialised equipment for additional features were added to their setup (Cockx *et al.,* 1997; Lin and Chen, 2005; Ziegenhein *et al.,* 2016). The first study to employ the PIV was by Cockx et al. (1997) where the radial profile of the time-averaged liquid velocity was measured across the downcomer. Lin and Chen (2005) on the other hand, measured additional shear stress and vortices from the flow field through a particle image analyser (PIA) which works similarly to the PIV for liquid velocities. Meanwhile,

Ziegenhein et al. (2016) equipped a particle tracking device to track bubbles using particle tracking velocimetry (PTV) which was also extended to measure the liquid velocity using similar concept. Despite the PIV being able to provide numerous flow field information, the setup of the PIV system as well as the post-processing snapshots captured are technically sophisticated. Aside from that, this instrument is only limited to measure gas-liquid flow fields with gas holdup no more than 5% (Deen, 2001).

2.7.5 Computer Automated Radioactive Particle Tracking (CARPT)

CARPT is the most modern measurement instrument available to measure flow field over the last two decades. It consists of radioactive particles which are release into the flow and tracked over their movements for flow mapping especially in complex multiphase processes with high gas holdup. It has been employed to measure the instantaneous and time-averaged velocities as well as turbulent parameters. Limited literature on its application in airlift reactors are available on this instrument as it is highly sophisticated to conduct and relatively expensive. Liao et al., (2016) applied CARPT to measure the time-averaged liquid velocities and the averaged across the height of the airlift reactor. Meanwhile, Luo and Al-Dahhan (2011) has also employed CARPT in their study but was used to track particles to study cell trajectory rather than flow phenomena.

2.7.6 Comparison between Experimental Measurement Techniques

The selection of a proper measurement technique depends on the flow field applied and the key process within the gas-liquid system. The nature of the flow field within the airlift reactor tends to be a cyclic pattern which is influenced by the liquid circulation indicating the importance of the liquid velocity. Measurement probes are most commonly used in airlift reactor studies to measure liquid velocity owing to their low cost setup, ability to measure time-averaged and fluctuating phase velocities (Zhou, 1997). Despite its versatility, using measurement probes tends to intrude the actual reading carried out on the flow field. The probes are required to be inside the flow field in order to capture readings on the liquid velocity of the gas-liquid system. This would bring unnecessary discrepancy on the actual flow in the presence of the probe. The probes could also potentially introduce unwanted contamination into the reactor process if not sterilised properly as the probes tend to be fragile. In addition, they are preposition to only capture specific locations at a time unless manually moved, requiring extra dismantling and

reassembling work. This would pose as inconvenience if flow mapping is part of the objective. Thus, non-intrusive method is highly sought after. The CARPT is one of the latest non-intrusive techniques that have been introduced to measure the flow phenomena and turbulent quantities. It can be applied in opaque fluids which are mostly found in wastewater or fermentation processes and gas-liquid systems with high gas holdup. However, the CARPT is costly and sophisticated to calibrate which outweighs the advantages to measure liquid velocity alone.

Breakthroughs in optical measurement techniques has brought the advancement of LDA and PIV as non-intrusive flow measurement instruments. Both the LDA and PIV employ laser technology to illuminate the flow field. However the latter is highly limited to void fractions below 5% (Deen *et al.,* 2001). Vector maps obtained from PIV have relatively lower resolution than LDA due to a fixed range spatial flow field being captured. The PIV would then be not that ideal for industrial flow regime analysis where high gas holdup is a common occurance. The LDA on the other hand is able to operate at high gas holdup (i.e. over 25%) providing accurate measurements (Mudde *et al.,* 1997). It is worth noting that one of the major drawbacks of employing optical measurements is that the fluid needs to be transparent and clear which will not be applicable in measuring real industrial fluids. Nevertheless, these instruments would be ideal over simple fluid case (e.g. air, oxygen, nitrogen, water, CMC, salt solution) studies in laboratory gas-liquid reactor setups.

2.7.7   Principle of Laser Doppler Anemometry Technique

The working principle behind the LDA is based on the Doppler's shift whereby two laser beams of a fixed wavelength are channelled onto the fluid to form a volume probe consisting of fringes as a result of wave interference as demonstrated in Figure 2.7. Seeding particles will then be scattered into the flow field as tracers for the lasers to capture. The moving particles enter the volume probe and scatter the light which results to changes in frequency. The new changes in frequency known as the Doppler's shift is signalled back to the photodetector. The photodetector receives and collects these signals and stores them into a workstation (i.e. see Figure 2.8). The collection of instantaneous velocities obtained were filtered according to the threshold set for validated data over time. Data analysis is carried out through the post-processing to extract instantaneous velocity measurements.
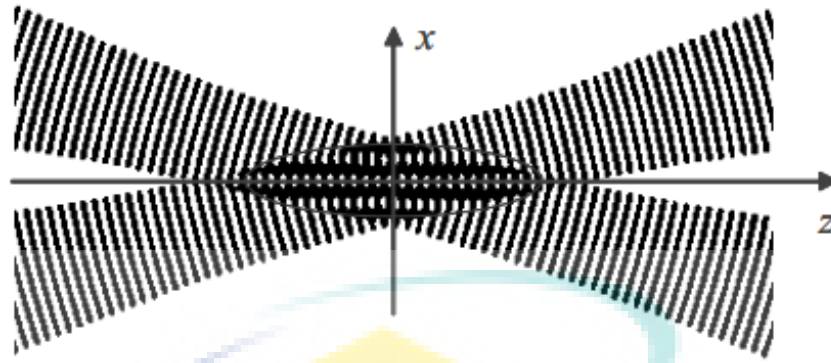
Figure 2.7   Volume probe consisting of fringes as a result of wave interference.

The LDA is divided into two modes denoted respectively as the forward-scattered mode LDA and the back-scattered mode LDA. The forward-scattered mode LDA is more sensitive to the flow field allowing it to measure instantaneous velocity, bubble velocity and bubble size distribution. It is able to generate larger data rates without requiring additional seeding particles as the bubbles themselves can behave as seeding particles within the flow. However, the forward-scattered mode is limited to lower gas holdup (Groen et al., 1996). The back-scattered mode on the other hand, predominantly measures the liquid velocity. The bubble velocity do not interfere with the results obtained and can measure flow fields at higher gas holdup although the data rate is lower in comparison to the forward-scattered mode (Groen *et al.,* 1996). This is because back-scattered mode setup causes the rejection of bubbles with diameter larger than 1 mm, which does not recognised them as seeding particles. Thus it removes larger bubbles as background noise, lowering the data rate accepted. In order to trace the flow field within the airlift reactor, seeding particles are required in order for the back-scattered mode to detect the flow.

On the other hand, calibration is foremost required to obtain accurate measurements from LDA. As the measurements obtained tend to be instantaneous, a sufficient duration of run time is needed in order to capture the mean flow quantities. Becket et al. (1994) conducted liquid velocity measurements in an external airlift reactor for a duration of 30 to 60 s and obtained a measured bubble swarm periodic time of 41 s which is in good agreement with the time range employed. Meanwhile, Vial et al. (2002) found that a duration of 120 to 180 s was sufficient to obtained mean flow values within an accuracy of ± 0.1 ms^{-1} in an external airlift reactor.

Furthermore, the amount of seeding particles should also be sufficient in order to undergo a selective threshold and provide sufficient amount of valid data. Vial et al.

(2002) observed the data rate in the presence of seeding particles were able to go up to 1 kHz near the wall. However, upon approaching the centre of the column the data rate tends to approach near zero due to the presence of the bubbles causing the reflection of the laser. In addition, the seeding particles must small enough that is has almost no slip properties on the fluid to prevent inaccurate measurement results. In Vial et al. (2002) study, a particle diameter of 5 μm was used to attain the effect of no slip through the measurement of radial liquid velocity. Meanwhile, Jia et al. (2007) used spherical glass particles with diameter of 10 μm and density of 1020 kgm^{-3} to measure the liquid velocity in a rectangular internal airlift reactor. Seeding particles the size of micrometres with a density close to liquid density would be an ideal for the particles to follow the fluid flow.
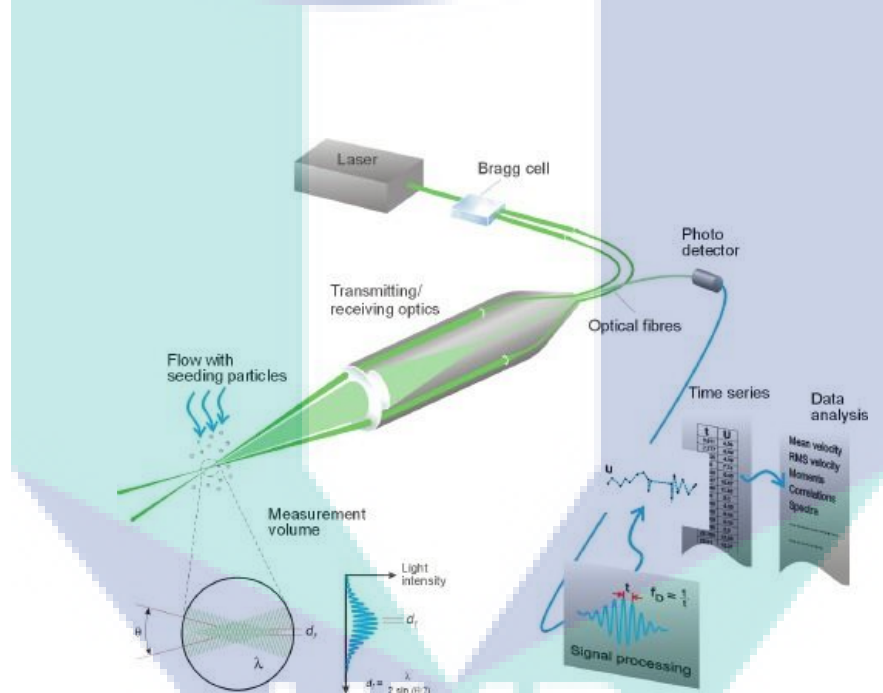
Figure 2.8   Schematic diagram of the working principles of the laser Doppler anemometry

Source: Blocken *et al.* (2016).

2.8   Summary

The hydrodynamics and flow patterns in an airlift reactor has been outlined in this chapter. Design and scale-up of an internal airlift reactor depends on its scale criterion. In chemical and bioprocesses, the distribution of the mass transfer within the airlift reactor is essential for successful scale up and are highly dependent on few hydrodynamics parameters. The first is the distribution of the gas holdup within the riser and downcomer. The gas holdup is interdependent with the liquid circulation velocity, responsible for

driving the bulk fluid and overall mixing within the internal airlift reactor. In addition, the mass transfer correlations are governed by the interfacial area of the bubbles, directly correlated to the gas holdup within the airlift reactor. The second key hydrodynamics parameter is the liquid velocity exerted by the bulk fluid. It reflects the shear stresses exerted onto the bulk fluid through the expression turbulence kinetic energy and dissipation energy of the system. Hence, both the intrinsic hydrodynamics parameters plays an important role to represent the overall hydrodynamics within the internal airlift reactor in macroscale.

Meanwhile, fundamental approach for scale up and design of an internal airlift reactor using CFD was also discussed. Robustness of a CFD model requires an affordable computational model to reflect the flow phenomena within the internal airlift reactor. The pure Eulerian multiphase model is a widely used two-fluid model, which requires lesser computational power to simulate the fluid flow up to industrial internal airlift reactors with reasonable accuracy. However, the model's predictive capability requires the addition of closure model to account the momentum exchange forces lost during the trade-off for less intensive computation. Several past studies have studied on a selection of closure model to capture the fluid flow in the internal airlift reactor but was unable to come to a consensus. One of the reasons can be traced back to the difference in flow configuration, where the closure models were tailored for similar flow configurations rather than a broader spectrum. Thus, the difference in the configuration resulted to the discrepancy on the proposed closure models across literature. There is a need for a systematic evaluation on the closure model in different flow configurations (i.e. total gas disengagement and partial gas disengagement in the absence of bubble circulation). As of current, there is a lack of study on a systematic evaluation on the closure model in different flow configurations in terms of drag and non-drag forces as most past studies are focus on individual flow configurations.

In order to ensure the robustness of the CFD model, experimental validation is needed. Several experimental measurement techniques have been employed across literature have been described in this chapter. Advancement in optical measurements through the laser technology has allowed non-intrusive methods with high resolution measurements. The LDA is a promising tool to study the fluid flow phenomena by obtaining single point measurements of mean flow quantities. Meanwhile, the effect of

sparger on the distribution of the flow cannot be ignored also. Sparger location can affect the dead zone region and the energy consumption in an internal airlift reactor. The effect of sparger location across the length of the column and in the region of the downcomer has been studied previously. However, the effect of sparger radially especially near the flow of the liquid circulation has not been studied previously. Hence, the effect of sparger location is important to improve the energy consumption within the system.
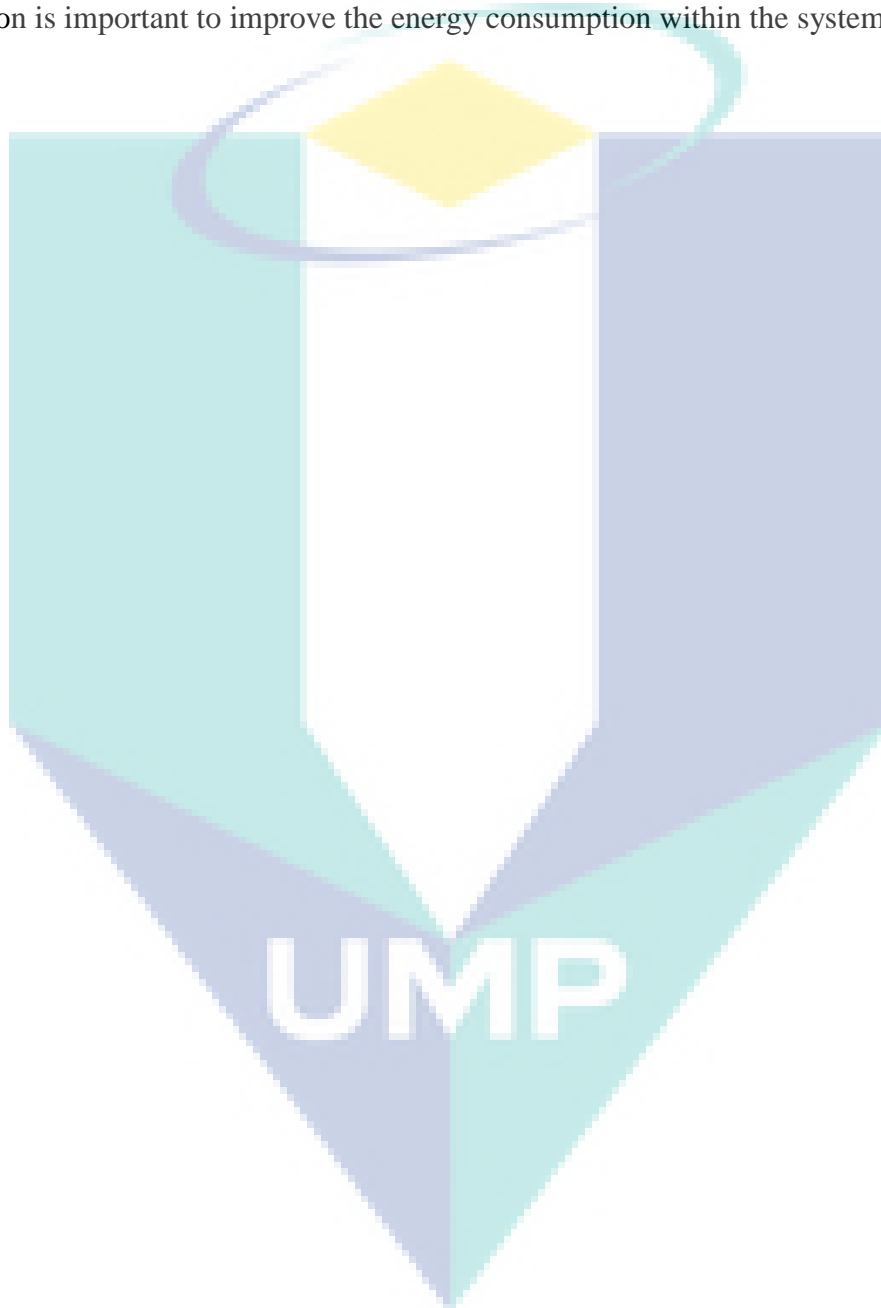
CHAPTER 3

METHODOLOGY

3.1 Introduction

This chapter discusses on the methods carry out to study the CFD simulation using two-fluid model on an internal airlift reactor and carry out an experimental validation on the predicted results using LDA measurement techniques. Firstly, a 3D internal airlift reactor geometry was setup using GAMBIT 2.4.6 and grid generation was conducted. CFD modelling approach was then setup by including the multiphase model, turbulence model and closure model which accounts the momentum exchange forces (i.e. drag, lift, turbulent dispersion and bubble-induced turbulence) using FLUENT 16.2. Prior to the actual simulation, a grid independence study was carried out in order to ensure that the predicted results are not influenced by the grid density. An adequate grid density will then be selected and used to run the simulations. The simulations are subjected to study the interfacial momentum force models two different reactors (i.e. partial gas disengaged in the downcomer and total gas disengagement in the airlift reactor). The first phase of the study evaluates the closure model by performing comparison studies between the drag models, turbulent dispersion models and bubble-induced turbulence in a non-zero downcomer internal airlift reactor. The effect of the lift model was also being evaluated. The results were validated against existing literature experimental pressure measurements on local gas holdup by Couvert (2000) and PIV data on liquid velocity by Cockx et al. (1997). In the second phase of this study, the closure model was then extended to a zero downcomer internal airlift reactor. In order to ensure the CFD model employed is valid, an experimental validation was carried out. A lab scale internal airlift reactor rig was built and setup with the LDA. The airlift reactor was filled with tapped water and 4g/L of salt to minimise bubble coalescence to match with CFD simulation (Deen, 2000). LDA was calibrated (i.e. photodetector voltage, time sampling, velocity range, sampling rate,

sample size and run time) and the liquid velocity were measured. The experimental measurements obtained were to validate the CFD simulation from the zero downcomer internal airlift reactor. Lastly, the sparger position was also being evaluated to assess its influence on the flow field. LDA measurements were obtained on the influence of the sparger on the liquid velocity.
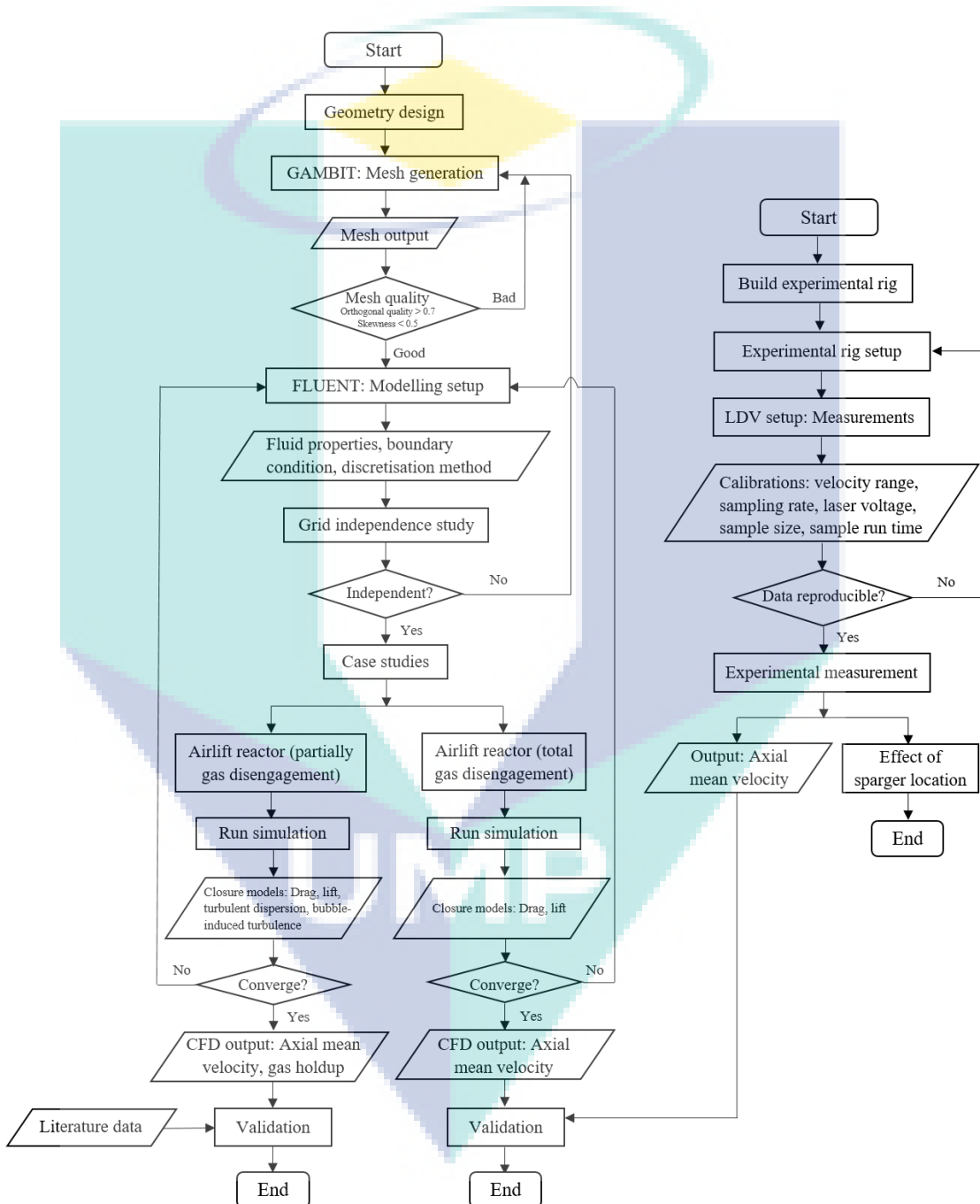
Figure 3.1   Flow chart on the research methodology of this work.

3.2   Geometry Construction

This work employs two different internal airlift reactor geometries. The first airlift reactor adopts Talvy et al. (2007) work with geometry dimensions of 0.50 m width, at a height of 3.00 m and a depth of 0.50 m as shown in Figure 3.2. An internal baffle separates the riser and downcomer region with a length of 2.35 m. A 0.15 m bottom clearance was left between the internal baffle wall and the bottom of the reactor. Gas enters through two cylindrical membrane spargers located 0.10 m above the bottom of the reactor. The unaerated water was filled up to 2.60 m of the reactor. Meanwhile, the second airlift reactor is based on a laboratory scale internal airlift reactor with a measurement of 0.40 m width, 0.60 m in height and 0.25 m in depth. An internal baffle with a height of 0.26 m is positioned 0.10 m from the bottom of the reactor. These geometries were prepared in three dimensional (3D) using GAMBIT 2.4.6.
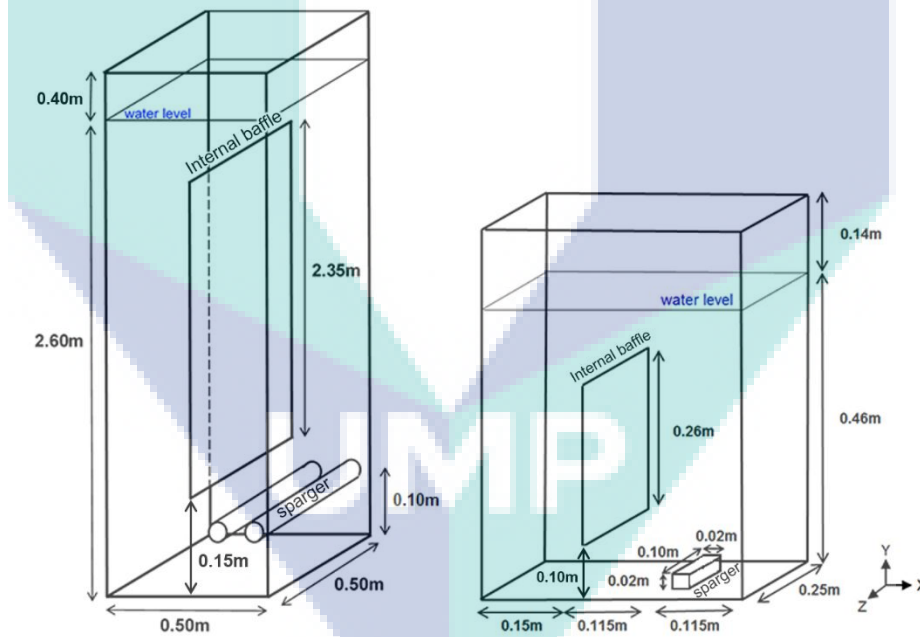
Figure 3.2   (a) Talvy et al.'s geometry (b) Laboratory scale internal airlift reactor

Prior to the CFD simulation in the internal airlift reactors, the grid generation was prepared. A coarse grid (236071 cells), an intermediate grid (373146 cells) and fine grid (717058 cells) were prepared. Figure 3.3 shows the difference in surface mesh surrounding the sparger which consists of hexahedral cells prepared using GAMBIT

2.4.6. The boundary layer on the sparger consists of three layers with a width of 0.005 m, 0.001 m and 0.0008 m for the coarse, intermediate and fine grid, respectively. The length of the mesh was set at 0.004 m, 0.0085 m and 0.0007 m for coarse, intermediate and fine grid with a growth factor set at 1.2, propagating towards the top of the internal airlift reactor. The depth of the grid was set at 0.05 m, 0.025 m and 0.01 m for the coarse, intermediate and fine grid.
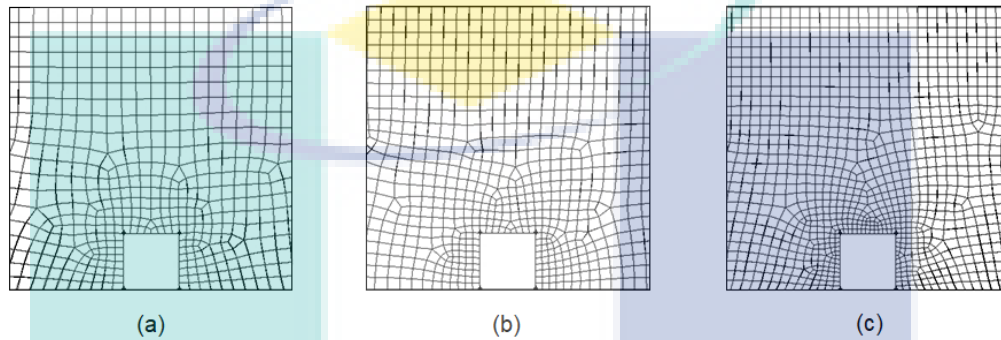
Figure 3.3   Surface mesh of the sparger (a) coarse, (b) intermediate and (c) fine grid.

3.3   CFD Modelling Approach

Eulerian-Eulerian multiphase model was employed in this study to represent the continuous and disperse phases as interpenetrating media, weighted by their local volume fractions. The variable k in Eq. 3.1 represents the continuous (liquid) phase, l and disperse (gas) phase, g. The total sum of the phase volume fraction should satisfy to a unity and is governed by the following mass continuity:

$$\frac{\partial}{\partial t}\left(\alpha_k \rho_k\right) + \nabla \cdot \left(\alpha_k \rho_k \vec{u}_k\right) = 0 \qquad 3.1$$

where α is the phase volume fraction, t is the time, ρ is the density and $\vec{u}$ is the velocity of the respective phases. The mass source term on the right side of Equation 3.1 is zero as the interphase mass transfer is neglected in the scope of this study. The momentum balance for the phase k is:

$$\underbrace{\frac{\partial}{\partial t}\left(\alpha_k \rho_k \vec{u}_k\right)}_{\text{time derivative}} + \underbrace{\nabla \cdot \left(\alpha_k \rho_k \vec{u}_k \vec{u}_k\right)}_{\text{convection}} = \underbrace{-\alpha_k \nabla p}_{\text{pressure gradient}} + \underbrace{\nabla \cdot \tau_k}_{\text{stress-strain tensor}} + \underbrace{\alpha_k \rho_k g}_{\text{external acceleration}} + \underbrace{M_{l,g}^{\mathrm{D}} + M_{l,g}^{\mathrm{L}} + M_{l,g}^{\mathrm{TD}}}_{\text{momentum exchange}} \qquad 3.2$$

where p is the pressure gradient, τ_k is the kth stress-strain tensor, g is the acceleration due to gravity, $M_{l,g}^{\mathrm{D}}$ is the drag force, $M_{l,g}^{\mathrm{L}}$ is the lift force and $M_{l,g}^{\mathrm{TD}}$ is the turbulent dispersion forces considered in this study. Virtual mass is neglected in this study as it has negligible effect on the overall flow behaviour and would result in increment of computational cost (Sokolichin *et al.,* 2004; Talvy *et al.,* 2007; Liao *et al.,* 2016).

$$\tau_k = -\alpha_k \mu_{\mathrm{eff},k}\left(\nabla \vec{u}_k + \left(\nabla \vec{u}_k\right)^t - \frac{2}{3} I\left(\nabla \vec{u}_k\right)\right) \qquad 3.3$$

where $\mu_{\mathrm{eff},k}$ is the effective viscosity of the respective phases. The effective liquid viscosity as shown in Equation 3.4 consists of three contributions; the molecular viscosity, turbulent viscosity and bubble-induced turbulence term.

$$\mu_{\mathrm{eff},l} = \mu_{\mathrm{m}} + \mu_{\mathrm{t}} + \mu_{\mathrm{b}} \qquad 3.4$$

where the value of μ_{m} was taken as 0.00005 m^{2}s^{-1} and μ_{b} represents the bubble-induced turbulence. Meanwhile, the effective gas viscosity was based on the effective liquid viscosity (Jakobsen et al., 1997) as shown:

$$\mu_{\mathrm{eff},g} = \frac{\rho_g}{\rho_l} \mu_{\mathrm{eff},l} \qquad 3.5$$

The eddy viscosity or turbulence viscosity, μ_{t} can be resolved through many approaches such as turbulence model or Reynold shear stress model. In this study, the eddy viscosity is resolved through the standard *k-ε* turbulence model proposed by Launder and Spalding (1974).

3.4　Turbulence Modelling

This study employed the dispersed standard k-ε turbulence model based on Tchen-theory for systems with dilute concentration of the dispersed phase. The transport equations for turbulence kinetic energy, k and dissipation energy rate, ε are given by:

$$\underbrace{\frac{\partial}{\partial t}\left(\alpha_l \rho_l k_l\right)}_{\text{time derivative}} + \underbrace{\frac{\partial}{\partial x_i}\left(\alpha_l \rho_l \vec{u}_l k_l\right)}_{\text{convection}} = \underbrace{\frac{\partial}{\partial x_i}\left(\alpha_l\left(\mu_l + \frac{\mu_{t,l}}{\sigma_k}\right)\frac{\partial k_l}{\partial x_i}\right)}_{\text{diffusion}} + \underbrace{\alpha_l G_{k,l}}_{\text{generation}} - \underbrace{\alpha_l \rho_l \varepsilon_l}_{\text{dissipation}} + \underbrace{\alpha_l \rho_l S_{k,l}}_{\text{source term}} \qquad 3.6$$

$$\underbrace{\frac{\partial}{\partial t}\left(\alpha_l \rho_l \varepsilon_l\right)}_{\text{time derivative}} + \underbrace{\frac{\partial}{\partial x_i}\left(\alpha_l \rho_l \vec{u}_l \varepsilon_l\right)}_{\text{convection}} = \underbrace{\frac{\partial}{\partial x_i}\left(\alpha_l\left(\mu_l + \frac{\mu_{t,l}}{\sigma_\varepsilon}\right)\frac{\partial \varepsilon_l}{\partial x_i}\right)}_{\text{diffusion}} + \underbrace{\alpha_l \frac{\varepsilon_l}{k_l}\left(C_{1,\varepsilon} G_{k,l} - C_{2,\varepsilon}\rho_l \varepsilon_l\right)}_{\text{generation and dissipation}} + \underbrace{\alpha_l \rho_l S_{\varepsilon,l}}_{\text{source term}} \qquad 3.7$$

The source terms $S_{k,l}$ and $S_{\varepsilon,l}$ were included to consider the bubble-induced turbulence between the dispersed phase and the continuous phase. The values of the constants in Equation 3.6 and Equation 3.7 were given by $\sigma_k = 1$, $\sigma_\varepsilon = 1.3$, $C_{1,\varepsilon} = 1.44$ and $C_{2,\varepsilon} = 1.92$ as recommended by Launder and Spalding (1974) based on experiments conducted on free turbulent flows. The eddy viscosity is expressed by combining k and ε as shown below:

$$\mu_t = \rho C_\mu \frac{k_l^2}{\varepsilon_l} \qquad 3.8$$

where $C_\mu = 0.09$. On the other hand, $G_{k,l}$ is the production rate of the turbulent kinetic energy and its form is similar to the single phase flow:

$$G_{k,l} = -\mu_t S^2 \qquad 3.9$$

$$S = \sqrt{2 S_{ij} S_{ij}} \qquad 3.10$$

3.5   Interfacial Momentum Exchange

3.5.1   Drag Model

Drag force is the resistance force acting on the bubble moving in the surrounding continuous phase. The drag force is governed by inertia whereby the force becomes increasingly significant at higher bubble Reynolds number expressed as follows:

$$M_{l,g}^{D} = \kappa(\vec{u}_g - \vec{u}_l) \qquad\qquad 3.11$$

where $\vec{u}$ is the velocity of the respective phases and κ is the interphase exchange coefficient as expressed below:

$$\kappa = \frac{C_D \, \mathrm{Re}_b \, A_i \mu_l}{8d_b} \qquad\qquad 3.12$$

The d_b represents the Sauter mean bubble diameter and μ_l is the molecular viscosity of the continuous phase in the equation above. Meanwhile, A_i is the interfacial area concentration and Re_b is the bubble Reynolds number governed by the slip velocity, $\vec{u}_{slip} = \left|\vec{u}_g - \vec{u}_l\right|$ as expressed in the following:

$$A_i = \frac{6\alpha_g \alpha_l}{d_b} \qquad\qquad 3.13$$

$$\mathrm{Re}_b = \frac{\rho_l d_b \vec{u}_{slip}}{\mu_l} \qquad\qquad 3.14$$

The C_D in Equation 3.12 denotes the drag coefficient used to quantify the drag force between phases. The drag coefficient can be obtained from the drag model. This study, four drag models (Schiller and Naumann (1935), Grace et al. (1976), Tomiyama et al. (1998) and Universal drag model) were chosen to evaluate on their performance in predicting local gas holdup and axial liquid velocity as shown in Equation   2.7-2.18.

3.5.2 Lift Model

Lift force is the interfacial forces acting in the lateral direction, perpendicular to the direction of the flow. This resulted to the migration of larger bubbles to the centre of the wall and smaller bubbles towards the walls induced by the traverse lift force. The migration of the bubbles is expressed in the following lift model as given by (Zun, 1980; Auton 1987; Drew and Lahey, 1987):

$$M_{l,g}^{L} = \alpha_g \rho_l C_L \left(\vec{u}_g - \vec{u}_l \right) \times \nabla \times u_l \qquad 3.15$$

where C_L is the lift coefficient that can be identified through the Tomiyama et al. (2002) model as shown in Equation   2.19-   2.20. The model is a function of bubble Reynolds number and Eötvös number derived from a single bubble moving in a glycerol-water solution. The validity of the model extends within the defined regions of $1.39 \leq \text{Eö} \leq 5.74$ and $-5.5 \leq \log_{10} \text{Mo} \leq -2.8$.

3.5.3 Turbulent Dispersion Model

The effect of turbulent dispersion force has significant contribution on the distribution of the dispersed phase. It describes the effect of turbulent eddies of the liquid phase on the bubbles. This force is derived through the ensemble averaging of the fluctuating component of the drag forces between the dispersed and continuous phase. Two models were chosen for comparison in this study which are the Lopez de Bertodano (1991) model and Simonin and Viollet (1990) model as described in Equation   2.21-2.30.

In the Lopez de Bertodano (1991) model, studies in airlift reactor gas-liquid systems normally adopted the value of turbulent dispersion coefficient $C_{TD} = 0.1$ as recommended by Lahey et al. (1993) (Roy *et al.,* 2006; Mohajerani *et al.,* 2012). However, since no empirical support is available to modify the current default value, $C_{TD} = 1.0$ was employed instead in this work. On the other hand, in the Simonin and Viollet (1990) the values for Prandlt number, C_β, C_μ and C_{VM} employed in this study were $\sigma_{TD} = 0.75$, $C_\beta = 0.45$, $C_\mu = 0.09$ and $C_{VM} = 0.5$, respectively.

3.5.4   Bubble-induced Turbulence Model

Bubble-induced turbulence which describes the influence of the dispersed phase over the liquid phase turbulence was accounted in this study. The bubble-induced turbulence can be incorporated through additional source terms $S_{k,l}$ and $S_{\varepsilon,l}$ in the dispersed standard k-ε turbulence model or through an additional viscosity term. In this study, both the approaches were considered using Sato and Sekoguchi (1975) and Troshko and Hassan (2001) proposed bubble-induced turbulence models as shown in Equation   2.31-   2.34.

In the Sato and Sekoguchi (1975) model, the value $C_{b} = 0.6$ was employed. Meanwhile, Troshko and Hassan (2001) model constant values employed in this study were $C_{k} = 0.75$ and $C_{TD} = 0.45$.

3.6   Numerical Solution

The numerical simulations in this work were performed based on the equation above using ANSYS FLUENT 16.2. These simulations were carried out using HP Compaq Pro 6300 MT Quad-core 3.4 GHz processors (i7-3770) with 4 GB RAM. Two assessment studies on the closure model in two different reactor configurations were being evaluated. Both the studies were conducted in a 3D transient simulation in gas-liquid internal airlift reactors.

In the first segment, Talvy et al. (2007)'s geometry of a partial gas disengagement internal airlift reactor configuration was setup within the FLUENT 16.2. The physical properties were assigned to describe the fluid properties (i.e. air as the dispersed phase and water as the continuous phase) employed and the mean bubble size of the dispersed phase (i.e. 3.4 mm according to Talvy et al.'s work). The membrane spargers in the simulation were treated as a continuous source of gas with a gas flow rate of $Q_{g} = 0.00212 \text{ m}^{3}\text{s}^{-1}$. No-slip boundary conditions were applied on the walls and the top of the headspace region was set as pressure outlet. The temperature and pressure were set to ambient condition. The discretisation scheme for the pressure-velocity coupling employs the SIMPLE method. The spatial discretisation employs the Green-Gauss node based method and first order upwind for all variables with exception the momentum which employed the second order upwind. All residuals were set below $1 \, x \, 10^{-8}$ for each

time step to achieve a good convergence. The time step was set at 0.001 s. The facet average of the gas holdup at 2.125 m and the local axial liquid velocity in the downcomer at 1.125 m were monitored. The data was averaged once a pseudo-steady condition was achieved around 50 s and the iterations were halted once a constant value was observed.

In the second segment of this work, the closure model was extended the simulation in a zero downcomer internal airlift reactor with the same geometry as the laboratory rig. The steps of setting up the simulation was similar to the non-zero downcomer internal airlift reaction where it was performed in FLUENT 16.2. The physical properties described the air and water as the dispersed and continuous phase, respectively. The mean bubble size is based on Wilkinson (1991) correlation. The sparger which is the source of the dispersed phase exerts a volumetric flow rate of $Q_g = 0.30 \text{ m}^3\text{h}^{-1}$. The boundary conditions of the outlet and wall, discretisation scheme, spatial discretisation and residual adopted similar approaches as the previous setup. The time step for this work, was set at 0.0001 s. The axial liquid velocity at height 0.30 m was monitored and the data was averaged around 20 s. The iterations were halted once a constant value was observed.

3.7   Data Extraction

The data extracted from the simulation are mean flow quantities in terms of gas holdup and axial liquid velocity. In the first part of the simulation, the surface-averaged gas distribution, local radial gas holdup in the downcomer and the liquid velocity across the downcomer were validated with experimental data obtained from literature. The gas holdup extrapolated was surface-averaged across the height of the riser and downcomer between $0 \text{ m} \le H \le 2.5 \text{ m}$. Meanwhile the local gas holdup at height 1.125 m was extracted radially across the downcomer. The liquid velocity on the other hand was acquired radially across the riser at height 2.125 m. In the second part of this simulation work, the axial liquid velocity across the riser and downcomer were obtained. The predicted results extracted were radially taken at heights $Y_1 = 0.20$ m, $Y_2 = 0.30$ m and $Y_3 = 0.38$ m. Comparison on the predicted and experimental results of the surface-averaged gas distribution were obtained based on relative error. Meanwhile, the comparison results for the radial gas holdup and axial liquid velocity were based on mean error obtain across the radial riser and downcomer.
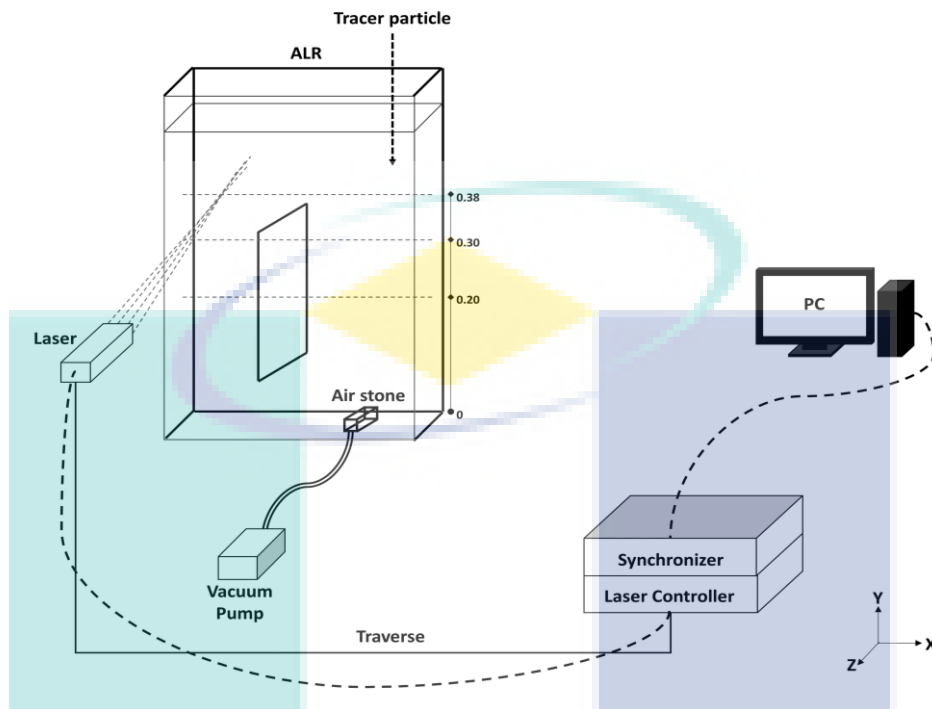
3.8   Experimental Setup

Figure 3.4   Schematic diagram of the experiment rig and LDA measurements.

In order to study the flow in a gas-liquid zero downcomer internal airlift reactor and the influence of sparger position, a laboratory scale internal airlift reactor was constructed made of transparent Perspex materials. The reactor was filled with tap water and sparged with air through a 4" Classica air stone with dimensions of 0.10 m in length and 0.20 m in height located at the based on the reactor. A rotameter was used to control the flow rate of the air supplied from a vacuum pump. A two component FlowExplorer back-scattered mode LDA system from Dantec Dynamics was employed to carry out the liquid velocity measurements on the flow field. Both 15 mW He-Ne and 5 W Ar-ion lasers manufactured by Spectra-Physics were used as light sources emitting wavelengths of 532 nm and 561 nm which produces a 2.1 mm^3 volume probe. The laser and focal lens were mounted on a bi-directional traverse and was controlled using a workstation. Figure 3.4 and Figure 3.5 illustrates the general setup of the experimental rig.
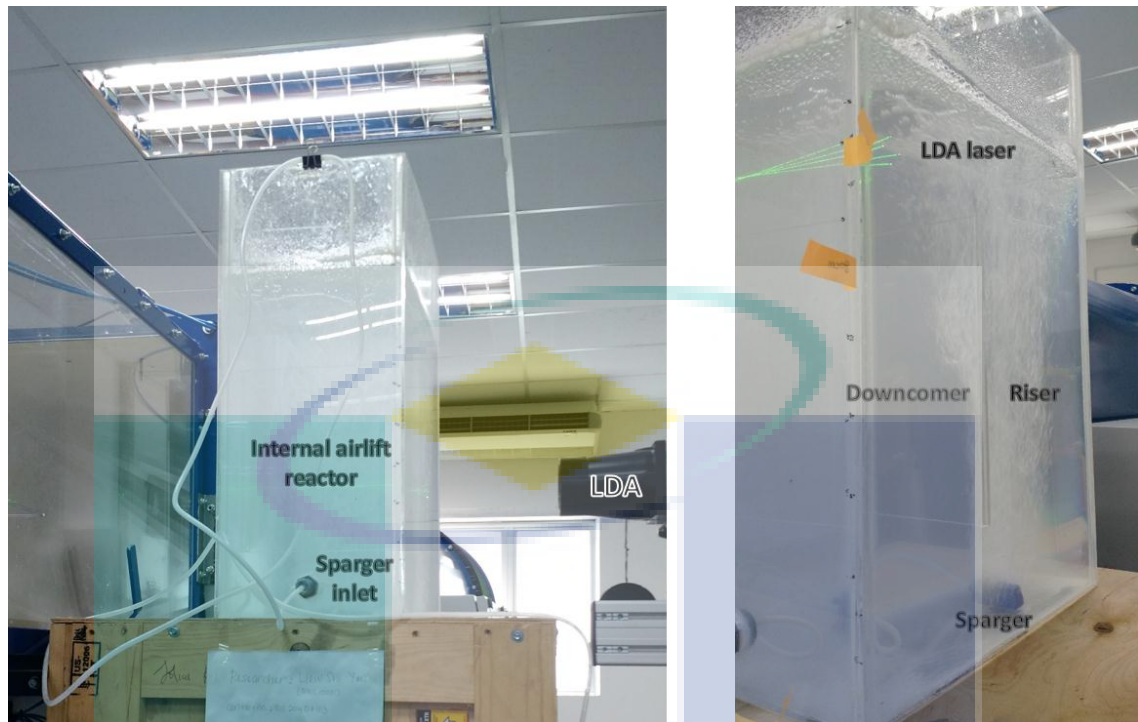
Figure 3.5   Laboratory setup of the experimental rig and LDA.

3.8.1   Seeding Particles and Calibration

In order to capture the flow field within the lab scale internal airlift reactor, seeding particles are required. The gas-liquid internal airlift reactor is seeded with polyamide seeding particles of diameter size 20 μm and density of 1030 kgm^{-3} from Dantec Dynamics. The density of the seeding particles must be close enough to the density of the bulk fluid in order to accurately capture the flow field. In addition, calibration is compulsory to ensure that the types of data collected from the flow field are valid.

Calibration was initially performed on the LDA prior to the experimental run as summarised in Table 3.1. A laser intensity of 40 mW for both the lasers were employed. The voltage from the photodetectors determines the sensitivity and intensity of the laser on the flow field. Although high voltage would be helpful to increase the sensitivity of the reading, it would also over exhaust the photodetector. Burst mode data collection method was selected for data collection with a sample size of 10 000 data and run time of 300 s. In order to calibrate the velocity range, data samples collected from the internal

airlift reactor will be analysed by the BSA3 Processor v6.10 software. A threshold of the velocity is set to reject unwanted measurements and narrow the range of valid data collected from the flow to increase the precision of the equipment. The data samples collected must behave with a Gaussian distribution. Several measurements were performed repetitively by adjusting the gain, sensitivity and anode to improve the accuracy of the time-averaged liquid velocity.

Table 3.1   Calibration setting of LDA setup

Calibration	Setting
Mode	Burst mode
Laser intensity	40 mW
Sampling size	10 000 data
Run time	300 s

It is worth noting that the data rate of acquisition drops as the laser approaches the bubble region. This is especially observed when the laser moves from the wall to the bubble plume region in the riser. When light hits the bubble, the intensity of the light reflected will be higher (Groen et al., 1999). However, these lights are reflected and scattered, lowering the probability of the lights hitting the photodetector. This results in the reduction of sample count obtained.

3.8.2 LDA Measurement and Processing

The liquid velocity within the riser and downcomer were collected radially across the internal airlift reactor. The spatial space between two data points across the radial riser and downcomer taken were 0.01 m. Three heights (i.e. $Y_1 = 0.20$ m, $Y_2 = 0.30$ m and $Y_3 = 0.38$ m) across the riser and downcomer were measured. The duration of the run time specified is sufficient enough to obtain time-averaged values within an accuracy of ± 0.01 ms^{-1} as shown in Figure 3.6.
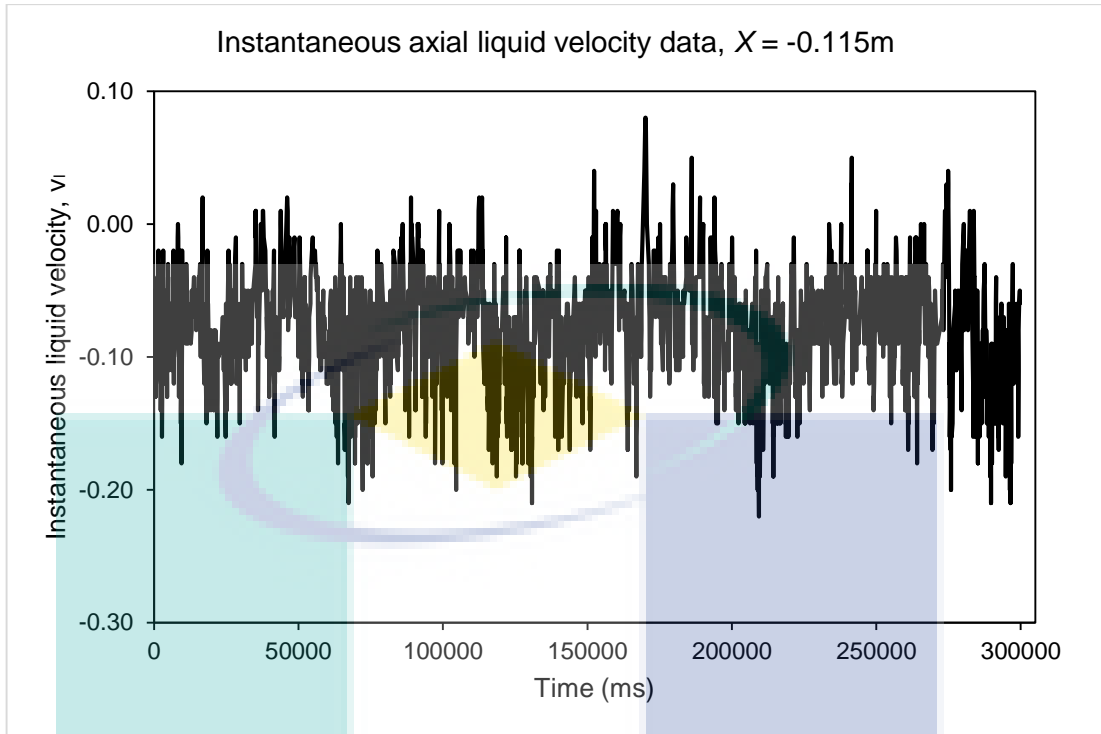
Figure 3.6   Instantaneous axial liquid velocity data obtained at radial position X = 0.115 m of the riser at height Y3 = 0.38 m.

The time-averaged values, mean axial liquid velocity, v_l were obtained using Equation 3.16 as shown below:

$$v_l = \frac{1}{N} \sum_{n=i} v_{l,i} \qquad\qquad 3.16$$

where N is the total number of realizations, $v_{l,i}$ is the instantaneous axial liquid velocity of the nth term. This post-processing was done using BSA3 Processor v6.10 software. Within that timeframe and setup as described earlier, 10^2 to 10^3 amount samples were obtained. Although longer sampling time would be encouraged for high quality data, it was found that large data quantities would not result to significant improvements in accuracy.

CHAPTER 4

RESULTS AND DISCUSSION

4.1   Introduction

This chapter describes the findings obtained from comparison studies on the closure model applied to simulate gas-liquid internal airlift reactors in two distinguished configurations. Prior to the simulation, a grid sensitivity study was conducted through the preparation of a coarse, intermediate and fine grid. It was followed by the evaluation of the closure models on the partial gas disengaged airlift reactor simulation. The two-fluid model approach through the Eulerian-Eulerian model was selected to perform the multiphase simulation owing to its lower computational demands. The lower computational cost is a consequent of ensemble averaging the multiphase model, requiring closure models to account the missing interfacial momentum forces. These forces comprise of drag and non-drag forces (i.e. lift model, turbulent dispersion model and bubble-induced turbulence) and would require suitable models. Comparison studies on the models for drag, turbulent dispersion and bubble-induced forces were conducted to evaluate the best model to describe each forces, respectively. Moreover, the effect of lift model on gas-liquid internal airlift reactor was also being studied. The comparison studies were carried out in an internal airlift reactor with bubble presence in the downcomer to predict the gas hold up and axial liquid velocity. Predicted results were validated against pressure (i.e. gas holdup) and PIV (i.e liquid velocity) measured data by Talvy et al. (2007). Subsequently, the comparison studies were extended to an internal airlift reactor in the absence of bubbles in the downcomer (i.e. total gas disengagement). The drag and lift models were assessed to predict the axial liquid velocity across the riser and downcomer. The predicted results were validated against LDA measurements attained from a laboratory scale internal airlift reactor. Lastly, the evaluation of the effects

of the sparger position was carried out to determine its effect on the airlift reactor hydrodynamics.

4.2   Grid Independency Study

Prior to the CFD simulation in the internal airlift reactors, a grid sensitivity should be conducted to ensure the accuracy of the result is not influenced by the grid density. In this segment, the grid sensitivity study on a zero downcomer airlift reactor was presented. A grid sensitivity study was conducted by preparing a coarse grid (236071 cells), an intermediate grid (373146 cells) and fine grid (717058 cells).
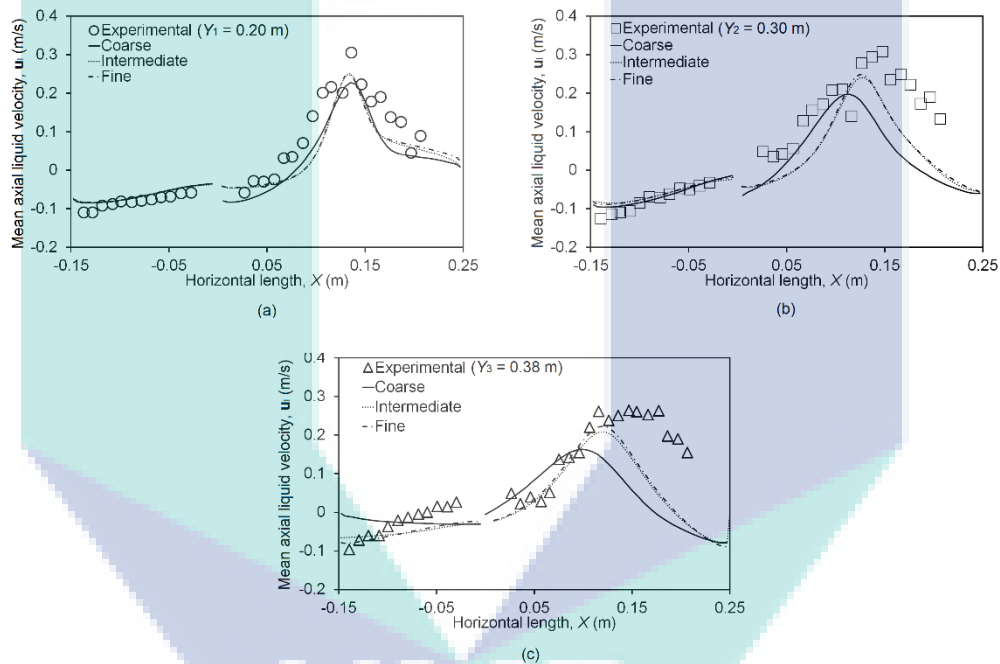

Figure 4.1   Results on grid sensitivity study on the mean axial liquid velocity at different heights, (a) $Y_1 = 0.20$ m, (b) $Y_2 = 0.30$ m and (c) $Y_3 = 0.38$ m.

Grid independence study was performed by employing the Universal drag model, lift model by Tomiyama et al. (2002) and drift velocity by Simonin and Viollet (1990). Figure 4.1 illustrates the result from the grid independence study. It can be seen at height $Y_1 = 0.20$ m, all grids were in close agreement with the experimental data especially in the downcomer. At higher heights where the liquid velocity of more driven by the buoyancy of the bubble, both the intermediate and fine grid achieved good agreement with experimental data obtained from LDA. Meanwhile, a large discrepancy occurs when coarse grid was employed at higher heights. This suggest, the grids in the buoyancy regions were not enough to resolve the flow field.

On the other hand, the computational time spent by each grids were, coarse grid (0.12 s/iterations), intermediate grid (0.26 s/iterations) and fine grid (0.35 s/iterations), respectively. From the overall results, the intermediate grid (373146 cells) yielded to be sufficient grid independent as considering the fine grid (717058 cells) will be computationally costly with no significant improvements to the result. Thus, the intermediate grid was considered to be sufficient enough to be employed in the comparison studies.

4.3   Internal Airlift Reactor with Partial Gas Disengagement

Consideration of an appropriate closure model plays an essential role in predicting the gas holdup profiles accurately in the airlift reactor. Gas holdup profiles reflect the pressure distribution in the airlift reactors which is the driving force behind the liquid circulation. Thus, a non-zero downcomer internal airlift reactor is being evaluated prior. Closure models proposed in internal airlift reactors have wider discrepancy on the models chosen to capture the individual interfacial momentum forces. In this work, the comparisons between different drag models, effects of lift model, comparison between different turbulent dispersion models and bubble-induced turbulence models were assessed.

4.3.1   Comparison between Drag Models on Prediction of Local Gas Holdup

Initially, the performance between four different drag models namely, Schiller and Naumann (1935), Grace et al. (1976), Tomiyama et al. (1998) and Universal drag model were compared. The simulation results were validated against experimental literature data acquired from Talvy et al. (2007) partial gas disengaged internal airlift reactor at $v_{sg} = 0.017 \text{ ms}^{-1}$. For this two-fluid CFD model, the monodispersed bubble size of 3.40 mm measured by Talvy et al. (2007) was employed. Figure 4.2 shows the corresponding predicted gas holdup profiles at different heights across the riser and downcomer. The riser gas holdup profile is more uniform with increasing height meanwhile in the downcomer, the gas holdup is not zero and the profile decreases at lower regions of the reactor.

Results in Figure 4.2 (a) showed that the gas holdups predicted was almost two-folds lower than the experimental data in the riser when only the drag model was

considered. Aside from that, there is an observable minimal discrepancy between the riser gas holdup results using different drag models. This is because of the co-current flow of the gas and liquid phases within the riser. The gas holdup simulation results in the riser tends to be less dependent on the bubble slip velocity due to the fact that the effect of the liquid velocity on the flow is far greater than the former (Šimčik *et al.,* 2011). Hence, not much difference was observed in the riser simulation results.

However, it can be seen that the Universal drag model gives a slightly better prediction with increasing height and at the top of the riser. Meanwhile, closer agreement with experimental gas holdup was also observed through the Rayleigh-Taylor drag model as shown in Figure 4.2 (b) at the top region of the downcomer. This could be attributed to the inclusion of the drag model that accounts the effect of bubble swarm (i.e., distorted and cap bubble) in the model which obtained an overall error of 41.1%. On the other hand, the Grace et al. (1976) and Tomiyama et al. (1998) drag models governed by bubble deformation performed similarly in both riser and downcomer with an overall error of 43.3% and 42.8%, respectively. It is noteworthy that the latter which differs in terms of that it's governed by Eötvös number was derived from the same data source as the former. This may be partly explain their similarities obtained from the result. In the downcomer, values predicted by both the non-spherical drag models shown lower gas holdup values with increasing height but they outperformed the Schiller and Naumann (1935) drag model. This indicates that aside from bubble swarm effect, the drag model is not limited only to the viscous regime but inclusive of irregular shaped bubbles regimes which affects the gas holdup distribution even at bubble size of 3.4 mm. This finding is of interest as some studies that adopted the spherical models have obtained conflicting results where high accuracy was obtained (Chen and Bai, 2017) but in this study, it was found otherwise.
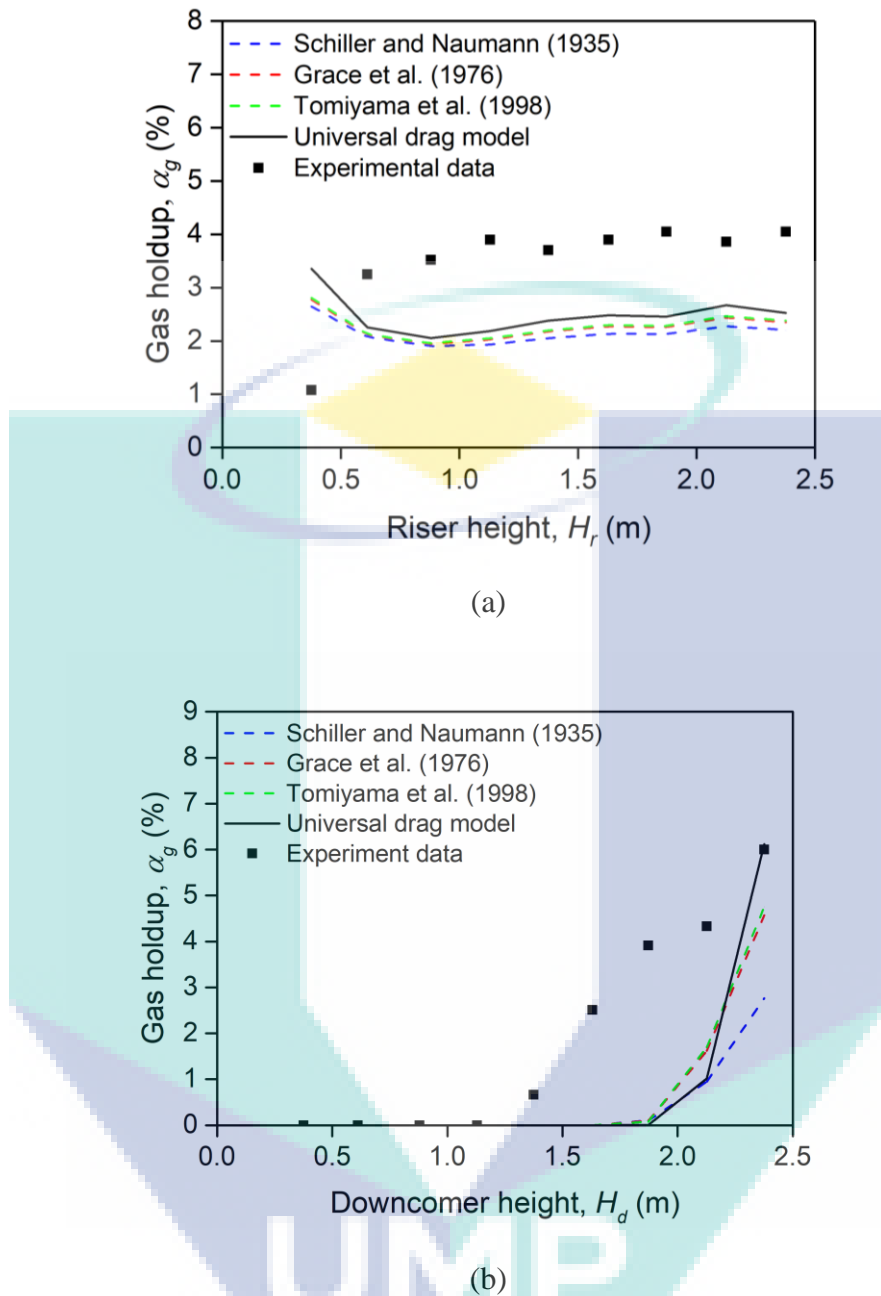
(a)

(b)

Figure 4.2:   Comparison study between different drag models on the prediction of gas holdup distribution at different heights across the (a) riser and (b) downcomer.

Source: Experimental data from Couvert (2000).

The Schiller and Naumann (1935) model which was derived based on rigid spherical particles, yielded the largest deviation from experimental measurement with an average 46.9% error in the riser and significantly lower gas holdup predicted in the downcomer. This implied less bubbles were dragged into the downcomer when the spherical drag model was considered. Vial et al. (2002) have similarly obtained a large margin of error on predicted gas holdup distribution when employing rigid spherical

particle drag model (i.e. within 57.4%) however their error was higher due to a 2D approach in their simulation. In addition, Vial et al. (2002) setup was an external airlift reactor known for being efficient in disengaging gas in the gas separator thus there is no obvious comparison on the effects of only considering the viscous regime model.

Despite the Schiller and Naumann (1935) model being a widely implemented drag model in airlift reactor CFD studies, in a non-zero downcomer the effects of bubble slip velocity in the downcomer would be relatively stronger due to its counter-current flow of the gas-liquid phases (Šimčik *et al.,* 2011). Talvy et al.'s work is based on a non-zero downcomer hence the result reflects the effect of bubble slip velocity on the gas holdup in the downcomer was captured better through the Universal drag model. Thus, the Universal drag model is employed for the remainder of this work.

4.3.2   Effect of Lift Model on Prediction of Local Gas Holdup

The effect of lift force on the prediction of gas holdup was evaluated. When the lift model is considered, slight improvements in predictive accuracy were observed in the riser as shown in Figure 4.3 (a). Chen and Bai (2017) have observed the same slight improvement in accuracy on their global gas holdup prediction when evaluating the effects of lift model however, its effects on local gas holdup were not reported.

In this study, an increase in accuracy on the local gas holdup profile was observed with increasing height in the riser through the inclusion of the Tomiyama et al. (2002) lift model with an overall error of 36.6%. Meanwhile, mild improvements were also obvious in the downcomer although there was a slightly over-prediction at the top of the downcomer as shown in Figure 4.3 (b). This suggests that the role of the lift model is more prominent at higher regions of the reactor. This is supported by Figure 4.6(b) whereby, the role of the lift model is seen to have shifted the peak towards the centre of the riser. Generally, the inclusion of the lift model did not significantly improve the results in local gas holdup at lower regions of the riser and downcomer which explains why in some studies with shorter reactors, the lift model was omitted (Balleda *et al.,* 2007; Zhang *et al.,* 2012). However, it shifted the bubble plume slightly away from the internal baffle wall which aids the dispersion of gas holdup at higher heights as shown in Figure 4.4. It was thus implemented in the following case study.
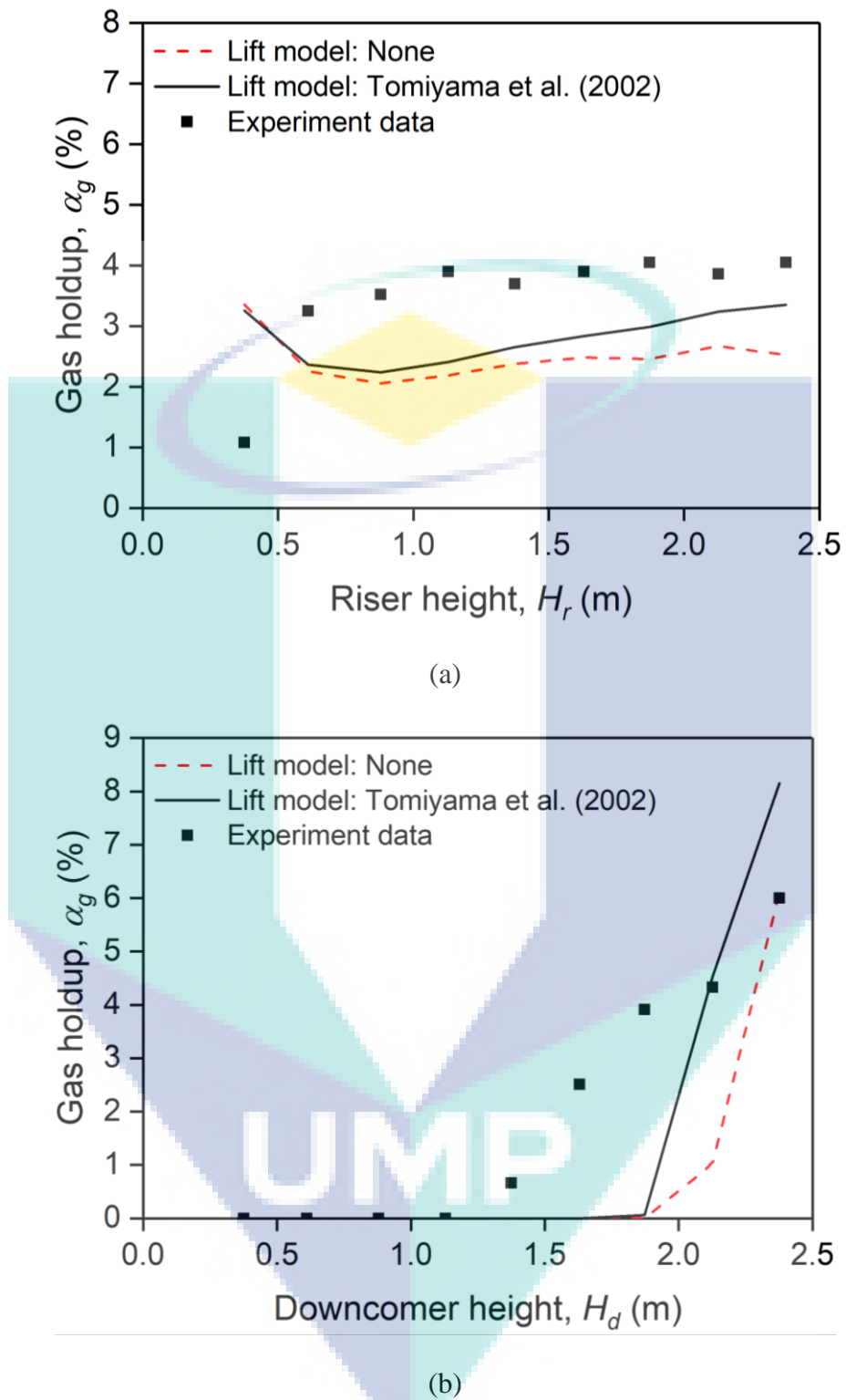
(a)

(b)

Figure 4.3   The effect of lift model on the prediction of gas holdup distribution at different heights across the (a) riser and (b) downcomer. Experimental data from Couvert (2000).
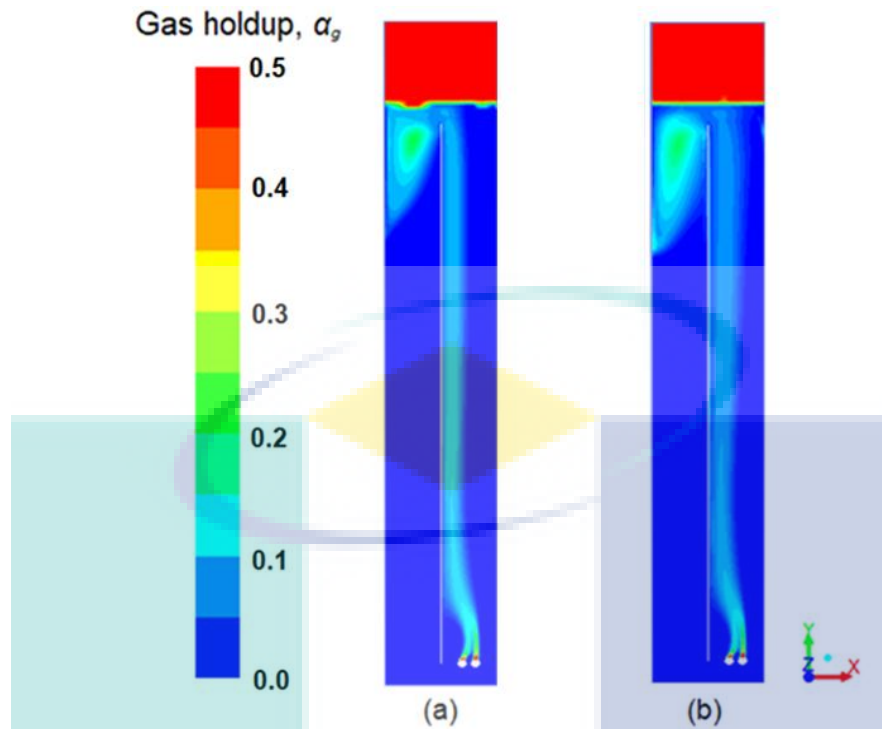
Figure 4.4   Contour plot of the gas holdup distribution across the riser at $t = 50$ s when (a) absence of lift model and (b) Tomiyama et al. (2002) lift model were employed.
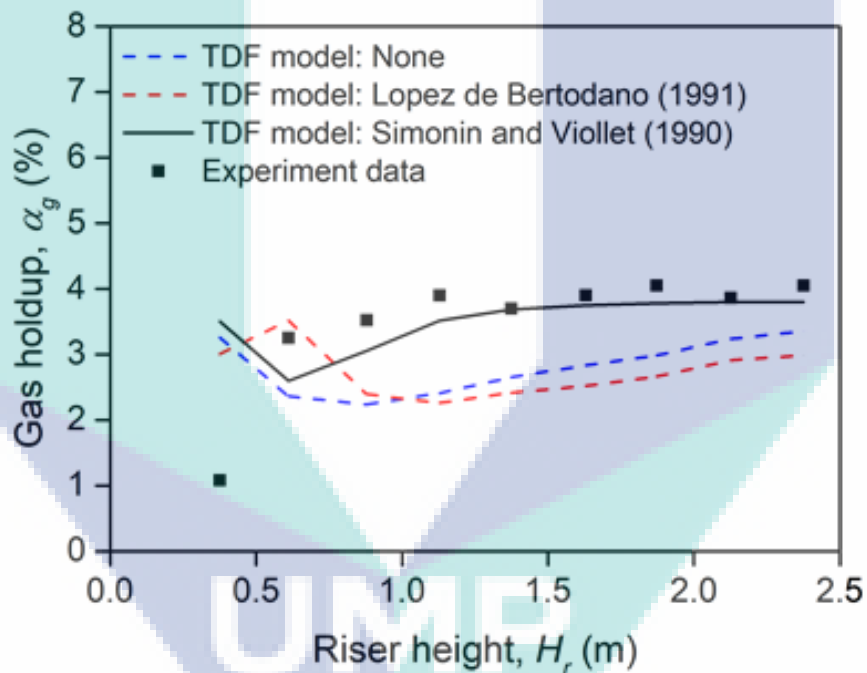
4.3.3   Comparison between Different Turbulent Dispersion Models on Prediction of Local Gas Holdup

An evaluation on the effect of turbulent dispersion force model on the prediction of gas holdup the non-zero downcomer internal airlift reactor was conducted with drag and lift model considered in this study. When all three interfacial momentum forces were employed (i.e. drag, lift and turbulent dispersion forces), results on the local gas holdup across the height of the riser and downcomer achieved significant improvements as shown in Figure 4.5. Chen and Bai (2017) study also supported that the turbulent dispersion model has led to significant improvements on the global gas holdup in comparison to the lift model within the flow regime of bubbly flow. Talvy et al. (2007) on the other hand, have shown that the inclusion of the turbulent dispersion model based on drift velocity has observed the same significant improvement in local gas holdup across the riser.

Most two-fluid model studies in internal airlift reactors that have employed the turbulent dispersion model have yet to reach an agreed consensus between the popular Lopez de Bertodano (1991) model derived based on molecular movement and drift velocity by Simonin and Viollet (1990) (Talvy *et al.,* 2007; Mohajerani *et al.,* 2012).

Hence this work is followed up with a comparison study between the two different turbulent dispersion models. A comparison between Lopez de Bertodano (1991) and Simonin and Viollet (1990) have shown slightly different improvements. The former model derived based on molecular movement improved the gas holdup result in regions near the sparger in the riser as shown in Figure 4.5 (a). The sparger region is dominated by the force of inertia (Smith, 1998). Meanwhile, the region above the sparger is known as free bubble zone region driven by buoyancy (Smith, 1998). The gas holdup in this region was under predicted as shown in Figure 4.5 (b) although some improvements were noted with increasing riser height. Regions in the gas disengagement zone above the downcomer was also over predicted as shown in Figure 4.5 (b) giving an overall error of 30.5%.

(a)

Figure 4.5   Comparison study between different turbulent dispersion models on the gas holdup distribution prediction at different heights across the (a) riser and (b) downcomer.

Source: Experimental data from Couvert (2000).
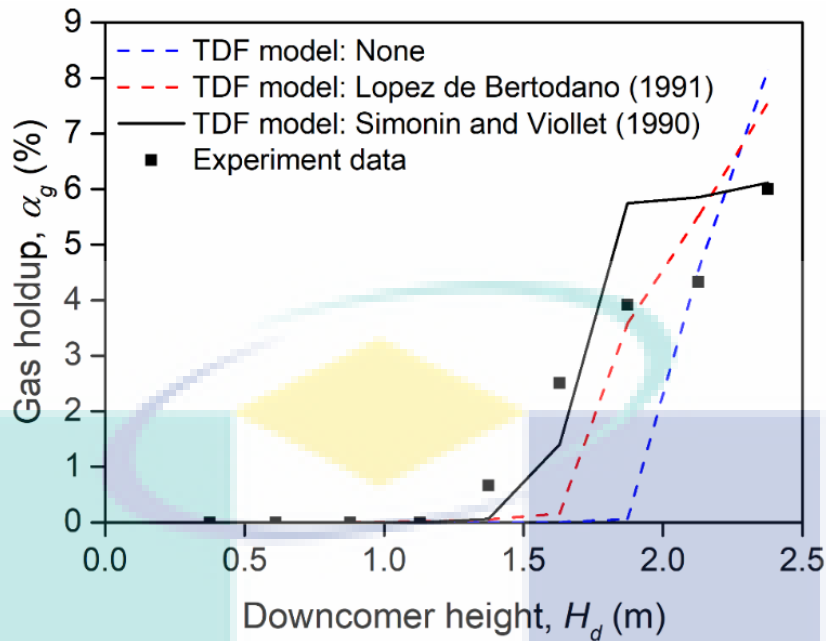
(b)

Figure 4.5   continued

This could be due to Lopez de Bertodano (1991) model which converges the dispersion term, C_{TD} to a singularity. The C_{TD} values differ based on bubble diameter and turbulence parameters which explains the wide variety of constants proposed across literature to match with experimental results. In this work, the value employed was C_{TD} = 1 seem to be inferior to the drift velocity model. Meanwhile, the drift velocity by the Simonin and Viollet (1990) model greatly improved results across the height of the riser and by far has the best accuracy in predicting the gas holdup as shown in Figure 4.5 with an overall error of 19.4%. This is similarly reported by Talvy et al.'s work who employed the drift velocity model in a 2D internal airlift reactor. The regions that were well captured were bubble zones that are predominantly plume zones consisting of shearing motions from the liquid phase (Smith, 1998). It is worth noting that the inclusion of the drift velocity have also managed to accurately predict the profiles of the gas holdup in the downcomer as shown in Figure 4.5 (b). The increase in accuracy is due to the versatility of the dispersion term introduced by Simonin and Viollet (1990) as function of properties of the two phases and turbulence. However, the model has slightly over predicted the regions near the sparger and the top region of the downcomer. The discrepancy might partly be due to measurements taken by Couvert (2000) whom employed pressure measurements to measure the gas holdup. Pressure probes tend to be intrusive to the flow

and may interfere with actual readings. The discrepancy obtained from the simulation was similar as Talvy et al. (2007) simulation was thus therefore is in good agreement with experimental results.

Meanwhile, the drift velocity by the Simonin and Viollet (1990) model greatly improved results across the height of the riser and by far has the best accuracy in predicting the gas holdup as shown in Figure 4.5 with an overall error of 19.4%. The regions that were well captured were bubble zones that are predominantly plume zones consisting of shearing motions from the liquid phase (Smith, 1998). It is worth noting that the inclusion of the drift velocity have also managed to accurately predict the profiles of the gas holdup in the downcomer as shown in Figure 4.5 (b).

The increase in accuracy is due to the versatility of the dispersion term introduced by Simonin and Viollet (1990) as function of properties of the two phases and turbulence. However, the model has slightly over predicted the regions near the sparger and the top region of the downcomer. The discrepancy might partly be due to measurements taken by Couvert (2000) whom employed pressure measurements to measure the gas holdup. Pressure probes tend to be intrusive to the flow and may interfere with actual readings. The discrepancy obtained from the simulation was similar as Talvy et al. (2007) simulation was thus therefore is in good agreement with experimental results.

Meanwhile, the drift velocity by the Simonin and Viollet (1990) model greatly improved results across the height of the riser and by far has the best accuracy in predicting the gas holdup as shown in Figure 4.5 with an overall error of 19.4%. The regions that were well captured were bubble zones that are predominantly plume zones consisting of shearing motions from the liquid phase (Smith, 1998). It is worth noting that the inclusion of the drift velocity have also managed to accurately predict the profiles of the gas holdup in the downcomer as shown in Figure 4.5 (b).
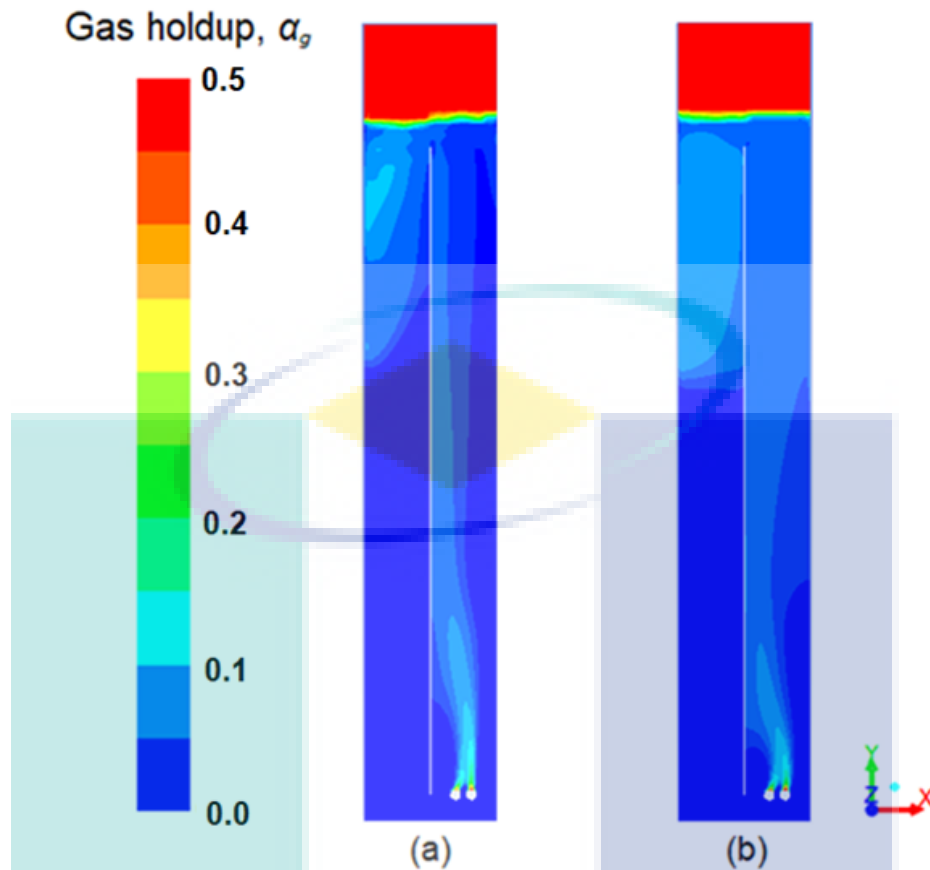
Figure 4.6   Contour plot of the gas holdup distribution across the riser at $t = 50$ s when (a) Lopez de Bertodano (1991) and (b) Simonin and Viollet (1990) were employed.

The increase in accuracy is due to the versatility of the dispersion term introduced by Simonin and Viollet (1990) as function of properties of the two phases and turbulence. However, the model has slightly over predicted the regions near the sparger and the top region of the downcomer. The discrepancy might partly be due to measurements taken by Couvert (2000) whom employed pressure measurements to measure the gas holdup. Pressure probes tend to be intrusive to the flow and may interfere with actual readings. The discrepancy obtained from the simulation was similar as Talvy et al. (2007) simulation was thus therefore is in good agreement with experimental results.

A notable difference between the two turbulent dispersion models can be visualised through the contour map of the gas holdup within Figure 4.6. It can be seen that the bubble plume is much narrower (i.e. less dispersed) and leaning towards the internal wall through the Lopez de Bertodano (1991) model. This has also resulted to a concentrated gas holdup profile in the top region of the downcomer. On the other hand, the Simonin and Viollet (1990) model shows a much more homogeneously dispersed gas

hold up profile. The implementation of the model reflects the gas holdup to be dispersed across the reactor which would be vital in minimizing dead zones.

4.3.4 Comparison between Different Bubble-induced Turbulence Models on Prediction of Local Gas Holdup

As limited studies are available on the bubble-induced turbulence which was mostly included together with the closure model, in this study the bubble-induced turbulence models were evaluated only in the presence of Universal drag model, Tomiyama et al. (1998) lift model. The evaluation of the bubble-induced turbulence models was performed through the comparison between Sato and Sekoguchi (1975) and Troshko and Hassan (2001).
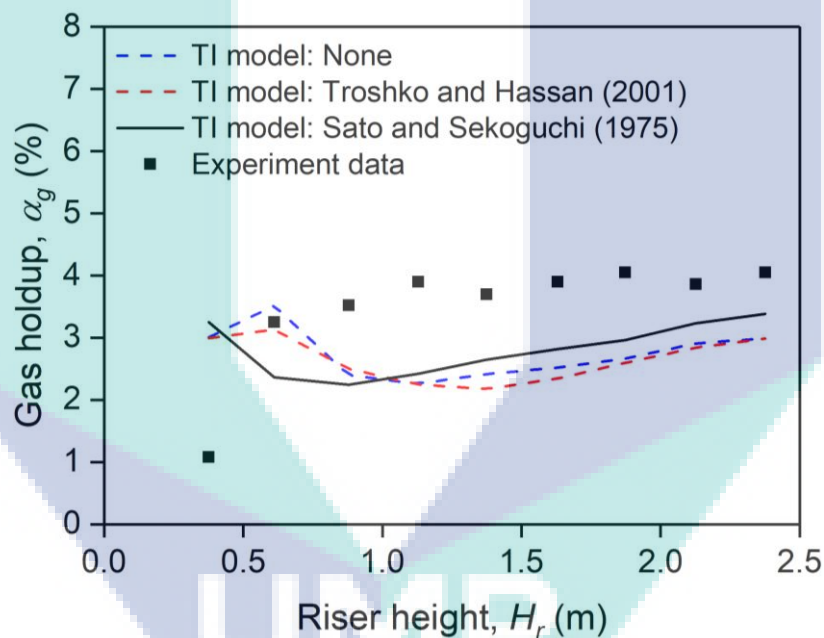
(a)

Figure 4.7   Comparison study between different bubble-induced turbulence models on the gas holdup distribution prediction at different heights across the (a) riser and (b) downcomer.

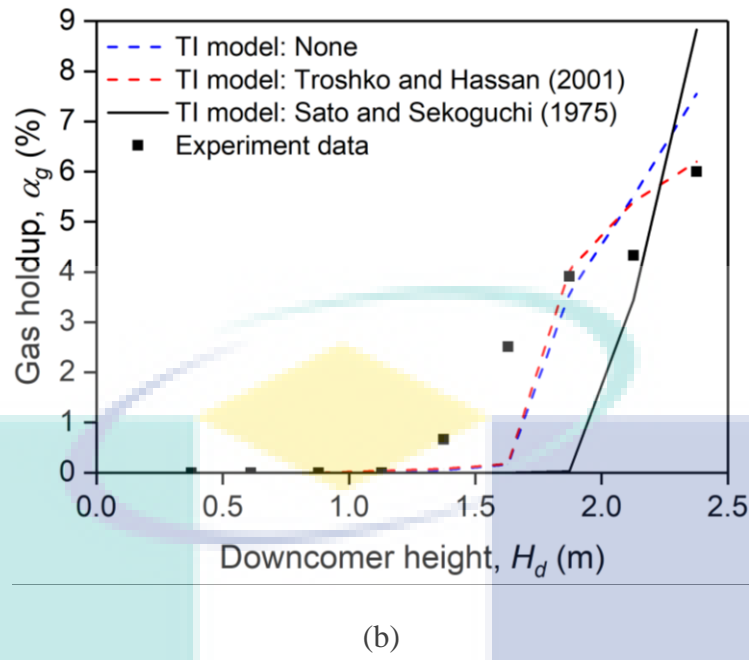Source: Experimental data obtained from Couvert (2000).

(b)

Figure 4.7   continued

According to the results, the Sato and Sekoguchi (1975) model which is introduced as an additional viscosity term has a slightly better performance in predicting the gas holdup especially in the riser with a 42.6% mean error in comparison to the Troshko and Hassan (2001) with mean error of 53.7%. However, it is notable that the gas holdup was highly under predicted in the downcomer obtaining an overall error of 41.3%. On the other hand, Troshko and Hassan (2001) obtained a slightly better predicted in the downcomer but was under predicted in the riser with an overall error of 36.6%.

4.3.5   Prediction of Radial Gas Holdup

On the other hand, Figure 4.8 illustrates the radial gas holdup profile at height 2.125 m in the riser. Figure 4.8 (a) shows that the spherical bubble drag model and bubble deformation drag models are more prone towards the internal baffle wall without accounting the effect of bubble swarm. Meanwhile, the Universal drag model is in closer agreement with experimental data where the radial gas holdup profile leans more towards the centre region of the riser with an error of 77%. On the other hand, Tomiyama et al. (2002) causes wall peaks to appear with a reduced error of 44.9%. This core peaking appears when a surge of small bubbles near the walls which was well captured by the model. This is due to the nature of the lift model whereby, the velocity fluctuations near the wall in upwards flow motion is maximal (Tomiyama et al., 2004).
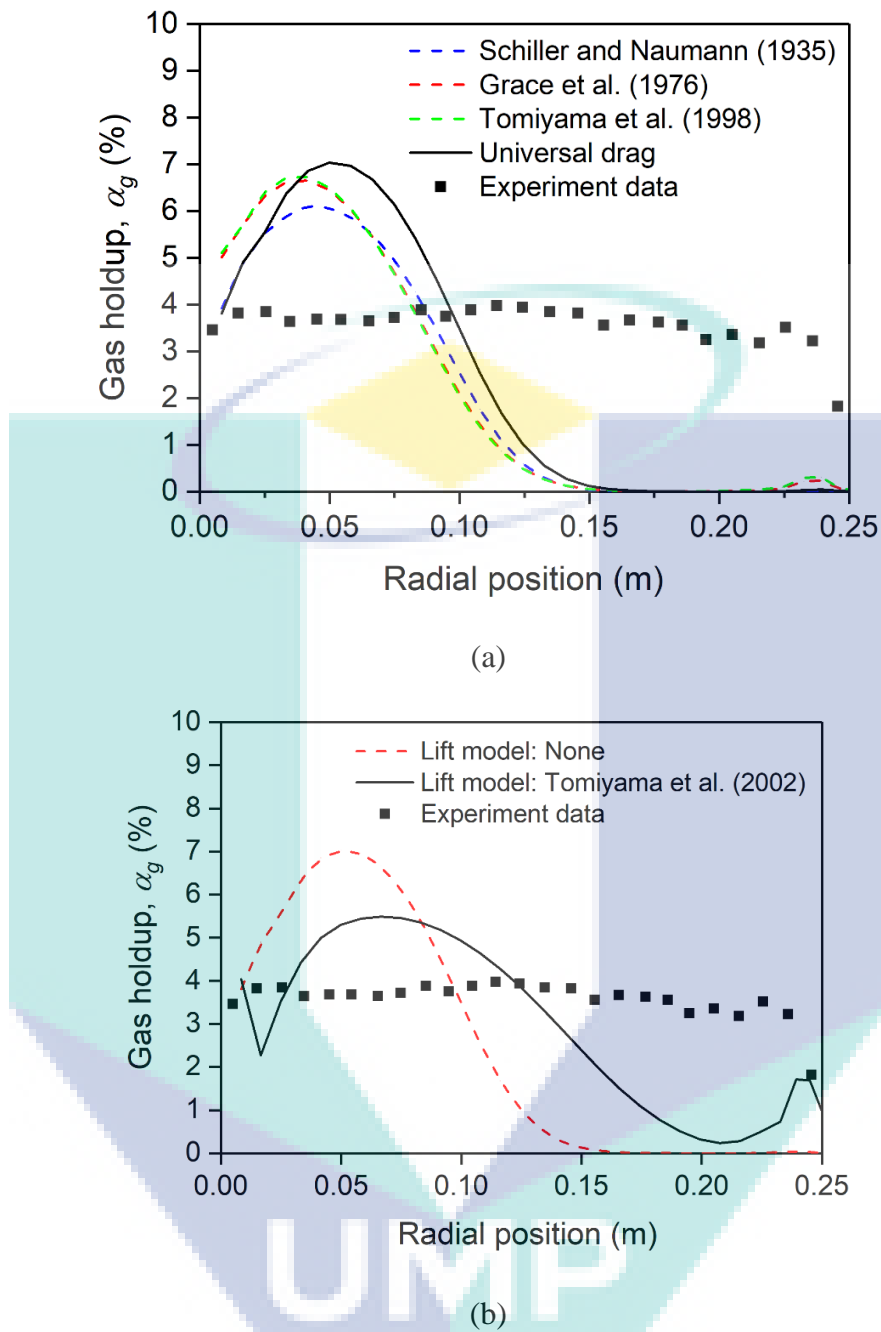
(a)

(b)

Figure 4.8   The effect of interfacial momentum forces (a) comparison of different drag models, (b) lift model, (c) comparison of different turbulent dispersion force model and (d) comparison of different bubble-induced turbulence forces on the radial gas holdup distribution at height 2.125 m in the riser.

Source: Experimental data obtained from Couvert (2000).

(c)

(d)
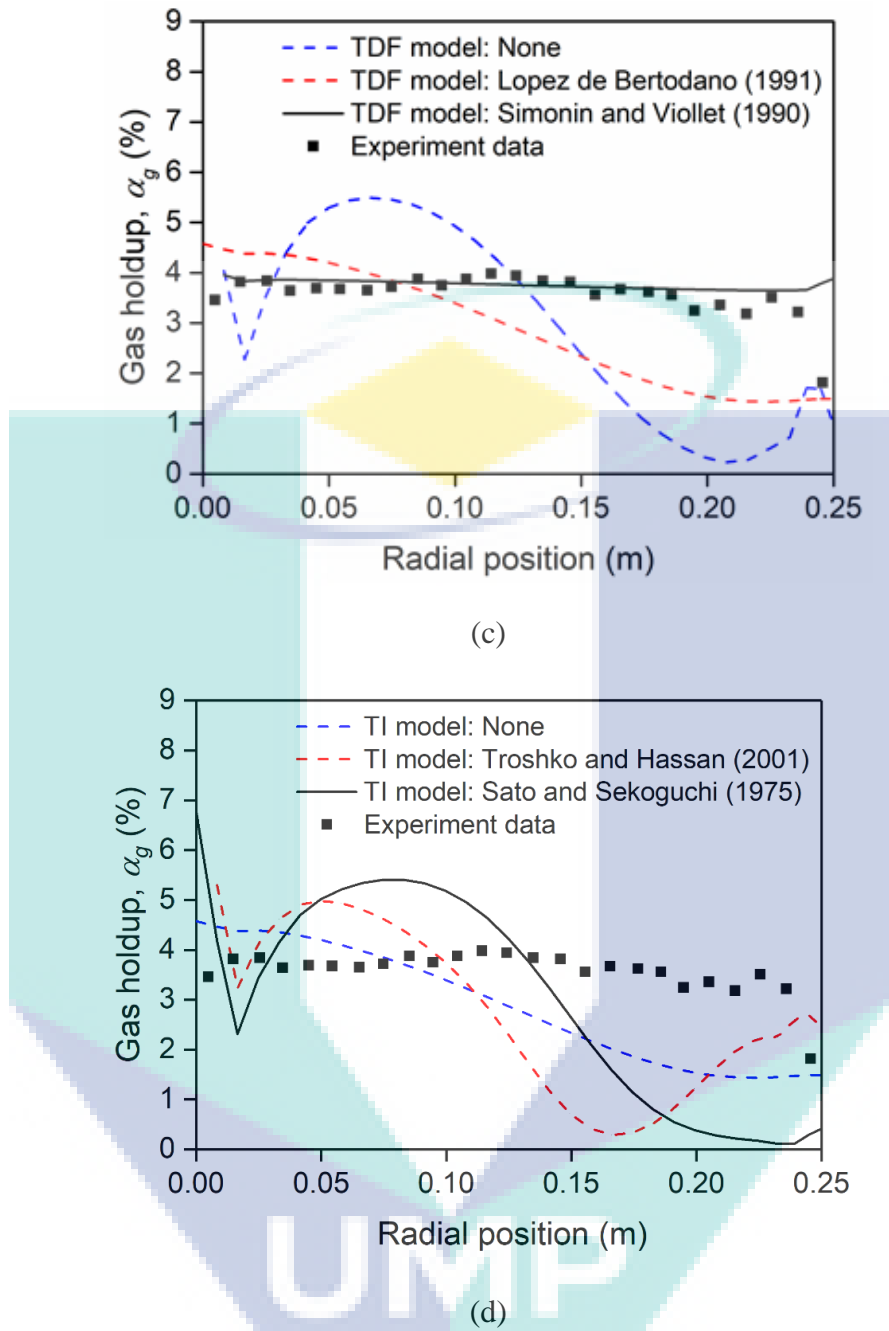
Figure 4.8   continued

Figure 4.8 further reflects on the effect of turbulent dispersion force on the radial gas holdup profiles. The inclusion of the Lopez de Bertodano (1991) model was able to slightly improve results and depress severely the radial gas holdup peaks from Figure 4.8 (b). However, the drift velocity model is proven to be better at predicting the gas holdup profiles than the Lopez de Bertodano (1991) model with an error of 6.8%. The Simonin and Viollet (1990) model was able to capture the radial gas holdup profile at higher

precision in comparison to the Lopez de Bertodano (1991) model which obtained 29.2% error. Though, at near wall regions, the drift velocity model prediction was slightly off.

An independent evaluation on the effects of the bubble-induced turbulence model in the presence of drag and lift models only, shows that Sato and Sekoguchi (1975) was able to subside the wall peaks but only obtained an accuracy of 41.3%. On the other hand, Troshko and Hassan (2001) was able to obtained slightly better prediction of the radial gas holdup with an error of 36.6%. Aside from that, the distribution of the flow is more centre than only with drag and lift models considered.

Overall results showed that the drag model with the bubble swarm correction term performed better at predicting the radial gas holdup especially in the downcomer section. Whereas the drag model that accounts bubble deformation showed slightly better predictive accuracy than the model that assume rigid spherical bubbles. The role of the lift model shifts the peak of the gas holdup towards the centre through the Tomiyama et al. (2002) lift model. By considering the turbulent dispersion model, results were in closer agreement especially through the inclusion of the drift velocity model.

4.3.6 Prediction of Axial Liquid Velocity

Figure 4.9 illustrates the axial liquid velocity profiles at height 1.125 m predicted by the drag models, lift model and turbulent dispersion force models. Figure 4.9 (a) shows that the performances of all four drag models were comparable with slight discrepancy between the experimental data. Grace et al. (1976) and Tomiyama et al. (1998) models were able to accurately predict the liquid velocity profiles but at the cost of discrepancy of the gas holdup results in Figure 1. The Universal drag predicted comparable well to the non-spherical drag models. Schiller and Naumann (1935) on the other hand, slightly over-predicted the liquid velocity. By considering lift, not much notable changes were observed in the liquid velocity.

(a)

(b)

Figure 4.9   The effect of interfacial momentum forces (a) comparison of different drag models, (b) lift model, (c) comparison of different turbulent dispersion force model and (d) comparison of different bubble-induced turbulence forces on axial liquid velocity height 1.125 m.
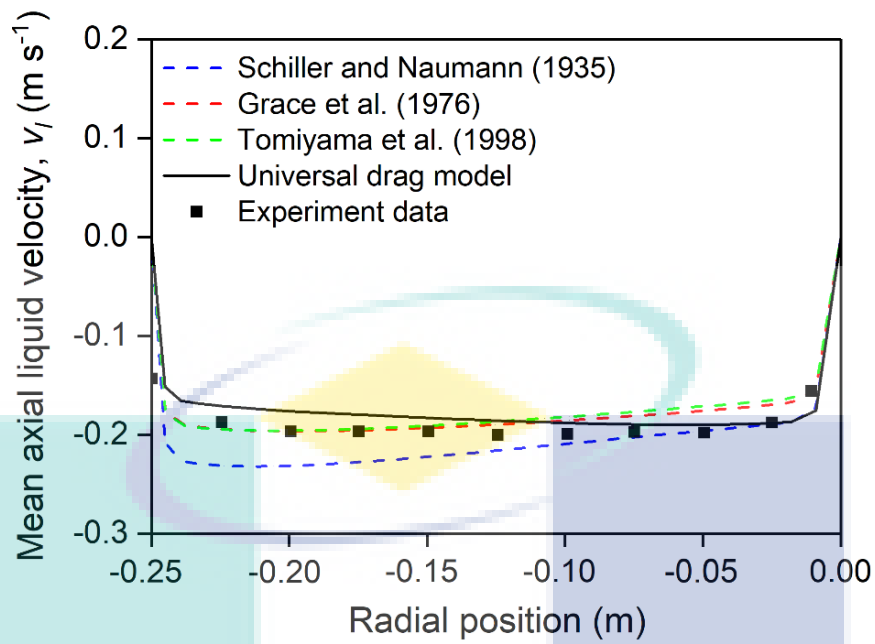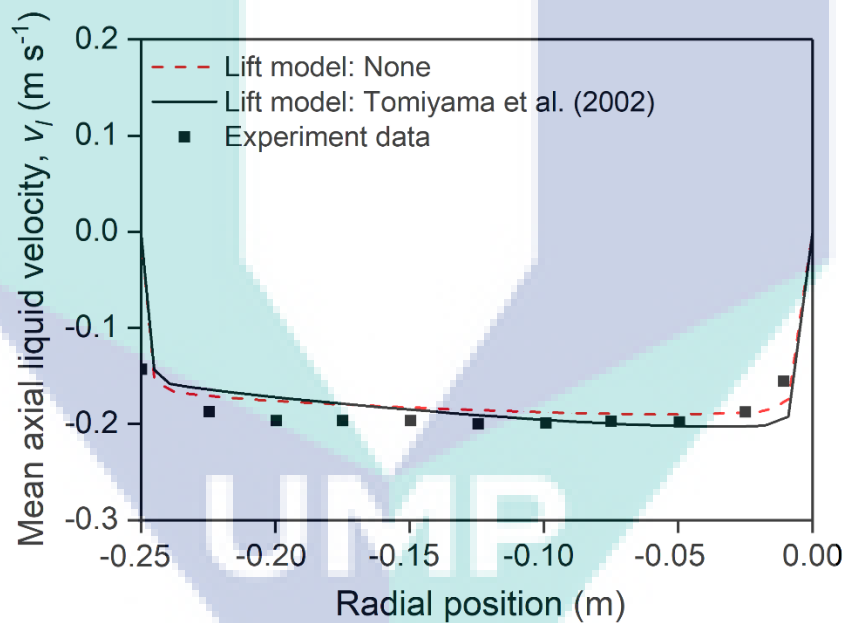
Source: Experimental data obtained from Cockx (1997).
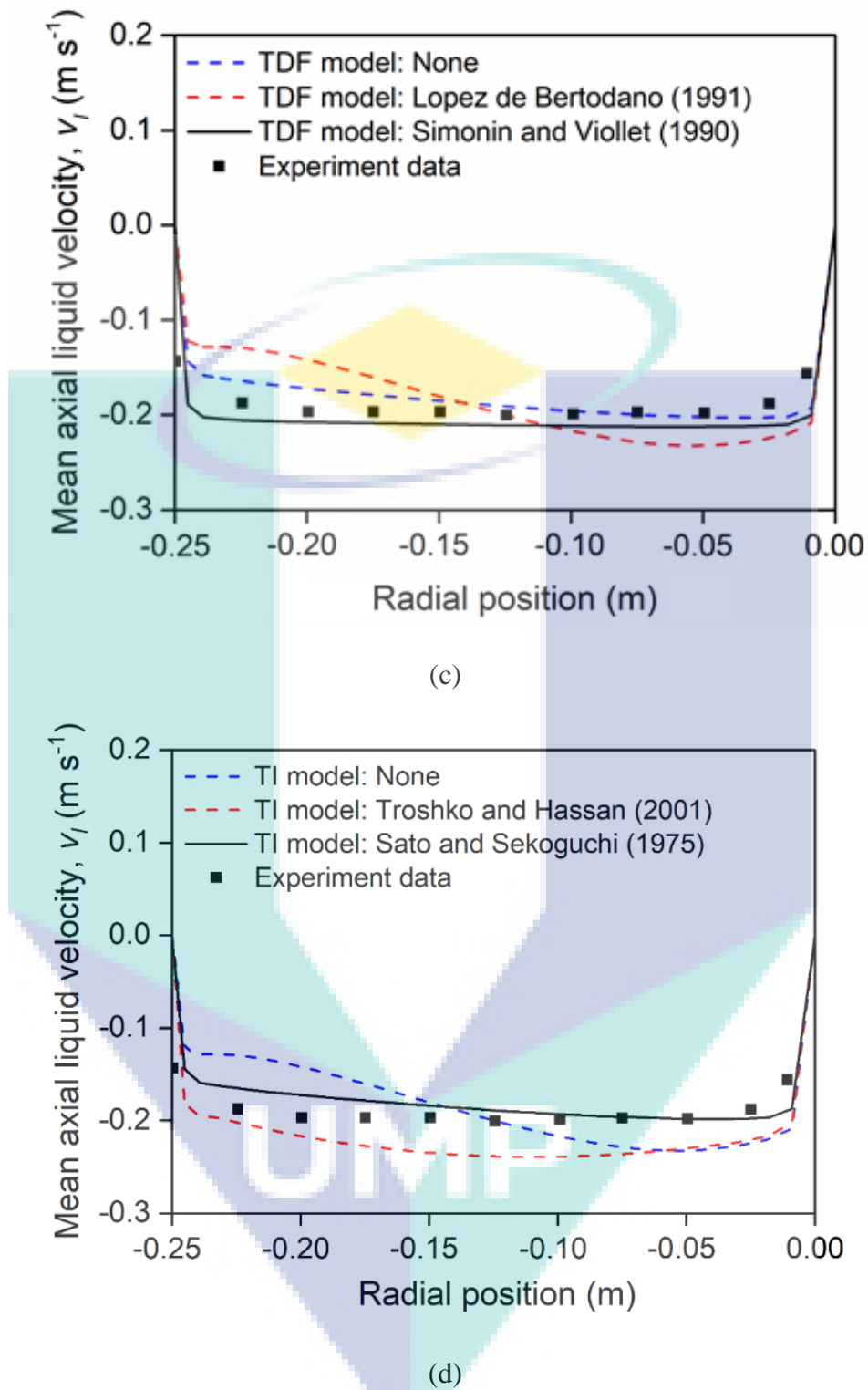
(c)

(d)

Figure 4.9   continued

The addition of the turbulent dispersion model resulted to minor increase in accuracy of the predicted liquid velocity through the Simonin and Viollet (1990) model. While the result for the Lopez de Bertodano (1991) model was slightly off. The inclusion of the turbulent dispersion model increased the accuracy of the predicted liquid velocity

signifying its importance in both the local gas holdup and liquid velocity. The bubble-induced turbulence as also lead to a minor discrepancy on the liquid velocity results leading to a slightly over predicted liquid velocity.

Overall, the predictions for all cases were reasonably good for the liquid velocity profile. Not much can be reflected from the result as the liquid velocity in the downcomer is relatively mild the effects. Thus in the following, the results in an internal airlift reactor was continued to understand the effects.

4.4 Internal Airlift Reactor with Total Gas Disengagement

In this part of the study, the closure model assessment was also extended into zero downcomer internal airlift reactor whereby CFD simulation was carried and validated experimental data obtained from LDA measurements on a lab scale airlift reactor rig. In this work, the comparisons between different drag models, effects of lift model were assessed.

4.4.1 Comparison between Different Drag Models

The effect of different drag models (i.e. Schiller and Naumann, 1935; Tomiyama et al. 1998 and Universal drag) is being studied by comparing the predicted mean axial liquid velocities with experimental measured data obtained from LDA as shown in Figure 4.10. The lift model and the turbulent dispersion were enabled for this case study. $0 < r/R < 1.0$ shows the dimensionless width of the internal airlift reactor where $0 < r/R < 0.3$ refers to the width of the downcomer region and $0.4 < r/R < 1.0$ refers to the width of the riser region.

It can be seen Schiller and Naumann (1935), a drag coefficient as a function of Reynolds number performed poorly with an overall error of 59.4%. It only performs fairly at height, $Y_1 = 0.20$ m which is the region most nearest to the sparger. Beyond that, the discrepancy became even larger with increasing height. It is worth noting that Schiller and Naumann (1935) model assumes spherical bubbles which neglects deformation of the bubble surface. On the other hand, both drag coefficients by Tomiyama et al. (1999) and Universal drag governed by the Eötvös number and different flow regimes, respectively were in closer agreement with experimental data obtained from LDA.
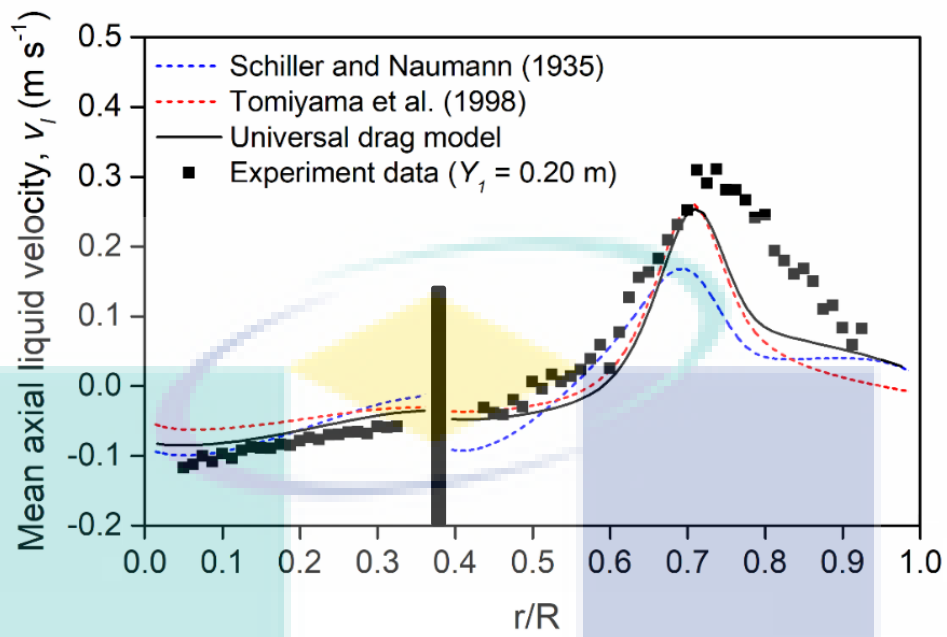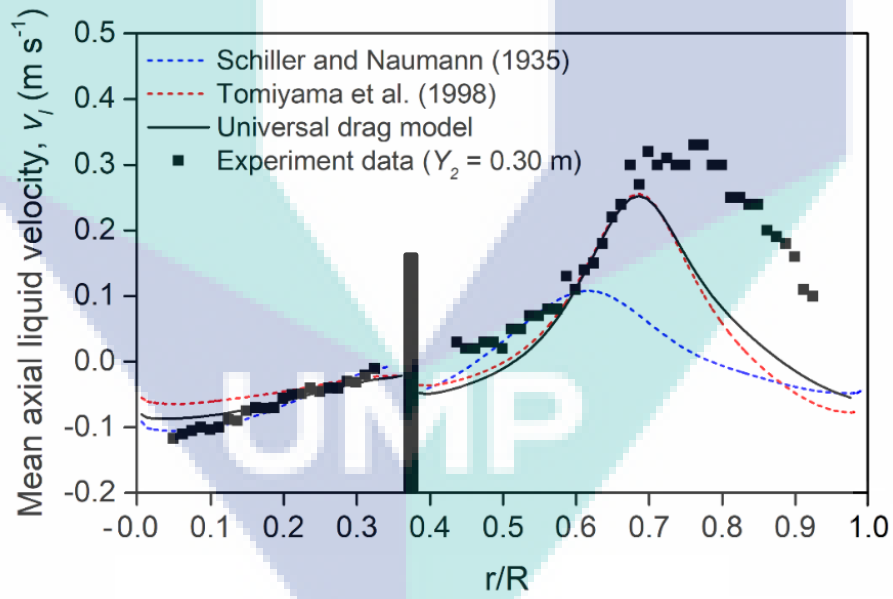
Figure 4.10   The effect of different drag models on the mean axial liquid velocity compared with experimental data obtained from LDA at three different heights, (a) Y_1 = 0.20m, (b) Y_2 = 0.30m and (c) Y_3 = 0.38m at sparger position (X_A = 0.125 m).
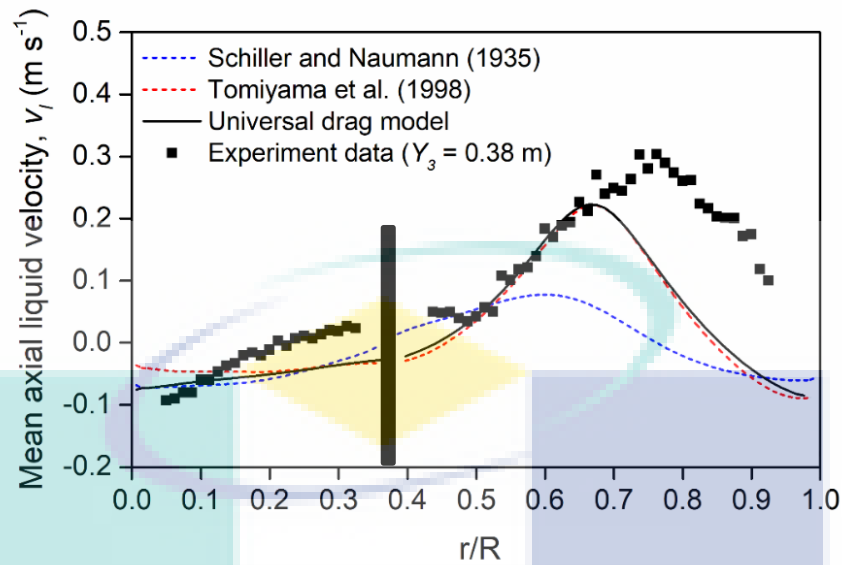
(c)

Figure 4.10   continued

The Tomiyama et al. (1998) included the bubble Reynolds number and an additional Eötvös number in its expression whereby it considers the terminal velocities that are affected by gravity and surface tensions due to bubble deformation. The model was able to significantly improve predictions of the axial liquid velocity within the riser but was slightly off in the downcomer with an overall error of 58.7%.

Amongst the drag models, the Universal drag is best fitted with the experimental results in both the riser and downcomer although it only gives a slight improvement in accuracy in comparison to the Tomiyama et al. (1998) model with an overall error of 53.4%. This slight improvement is notably observed in both the riser and downcomer. This result suggests that the drag model as a function of Rayleigh-Taylor instability and the inclusion of bubble swarm is more accurate. Hence, the Universal drag model is being implemented for the evaluation on the effect of considering the lift model.

4.4.2   The Effect of Lift Model

The effect of lift model on the predictive accuracy of the mean axial liquid velocity is studied with Universal drag and turbulent dispersion force enabled as illustrated in Figure 4.11.

When the lift effect is neglected, it is observed that the discrepancy between the simulation results with experimental result is minimal with an overall error of 52.7%. This indicates that drag force plays a dominant role amongst the interfacial momentum forces.

When lift force is enabled, the radial gas profile peak and magnitude of the axial liquid velocity is higher. This is attributed to the consideration of lift force, drifting the bubbles tangentially from its flow direction, heading towards the centre of the riser. From the results it can be seen the role of the lift force more prominent with increasing height across the airlift reactor. Although the difference in peaks here are not that substantial, it is worth noting that the effect of the lift model is deem more significant at higher superficial gas velocity as the bubble sizes are polydisperse in nature (Tabib et al., 2008).
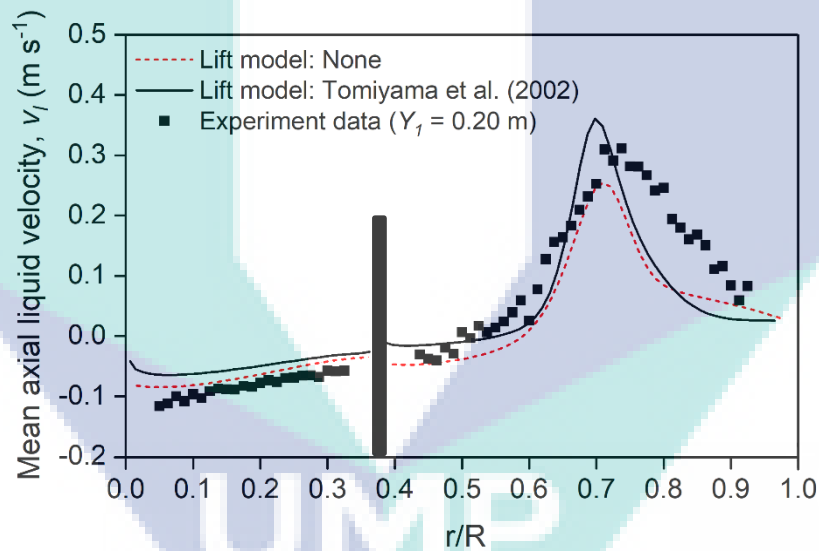

(a)

Figure 4.11   The effect of lift model on the mean axial liquid velocity compared with experimental data obtained from LDA at three different heights, (a) $Y_1 = 0.20$ m, (b) $Y_2 = 0.30$ m and (c) $Y_3 = 0.38$ m at sparger position ($X_A = 0.125$ m).

(b)

(c)

Figure 4.11   continued

It is observable for all case studies that the riser at height $Y_2 = 0.30$ m and both the riser and downcomer height at $Y_3 = 0.38$ m, the prediction accuracy of the mean axial liquid velocity in the riser is far off although the trend is present. The combination of drag force and lift model leaves room for further improvement in the accuracy at those heights. Those are the position at which a swarm of bubbles are dispersed at. However, it is worth noting that the liquid velocity within the regions of the downcomer was well predicted indicated that the closure model may be suitable as well for the zero downcomer

configuration as Talvy et al. (2007) only measurement of the liquid velocity is located at mid height of the downcomer (i.e. 1.125 m).

4.5 Effect of Sparger Position on the Flow Field within the Internal Airlift Reactor

An influence on the sparger position was also being evaluated in this study. Spargers are known to influence the flow field through the dispersion of the bubbles and energy distribution of the airlift reactor. However, there has yet to be a study which evaluates the position of the sparger over the internal airlift reactor.

(a)
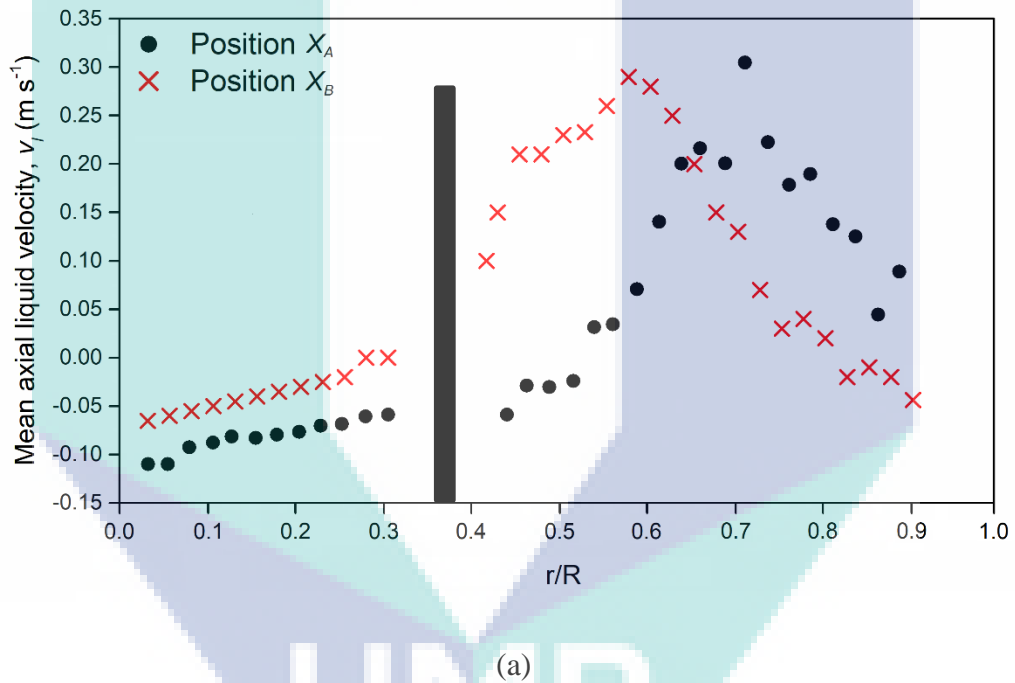
Figure 4.12   The effect sparger on the mean axial liquid velocity compared with experimental data obtained from LDA at three different heights, (a) $Y_1 = 0.20$ m, (b) $Y_2 = 0.30$ m and (c) $Y_3 = 0.38$ m at sparger position ($X_A = 0.125$ m and $X_B = 0.075$ m).
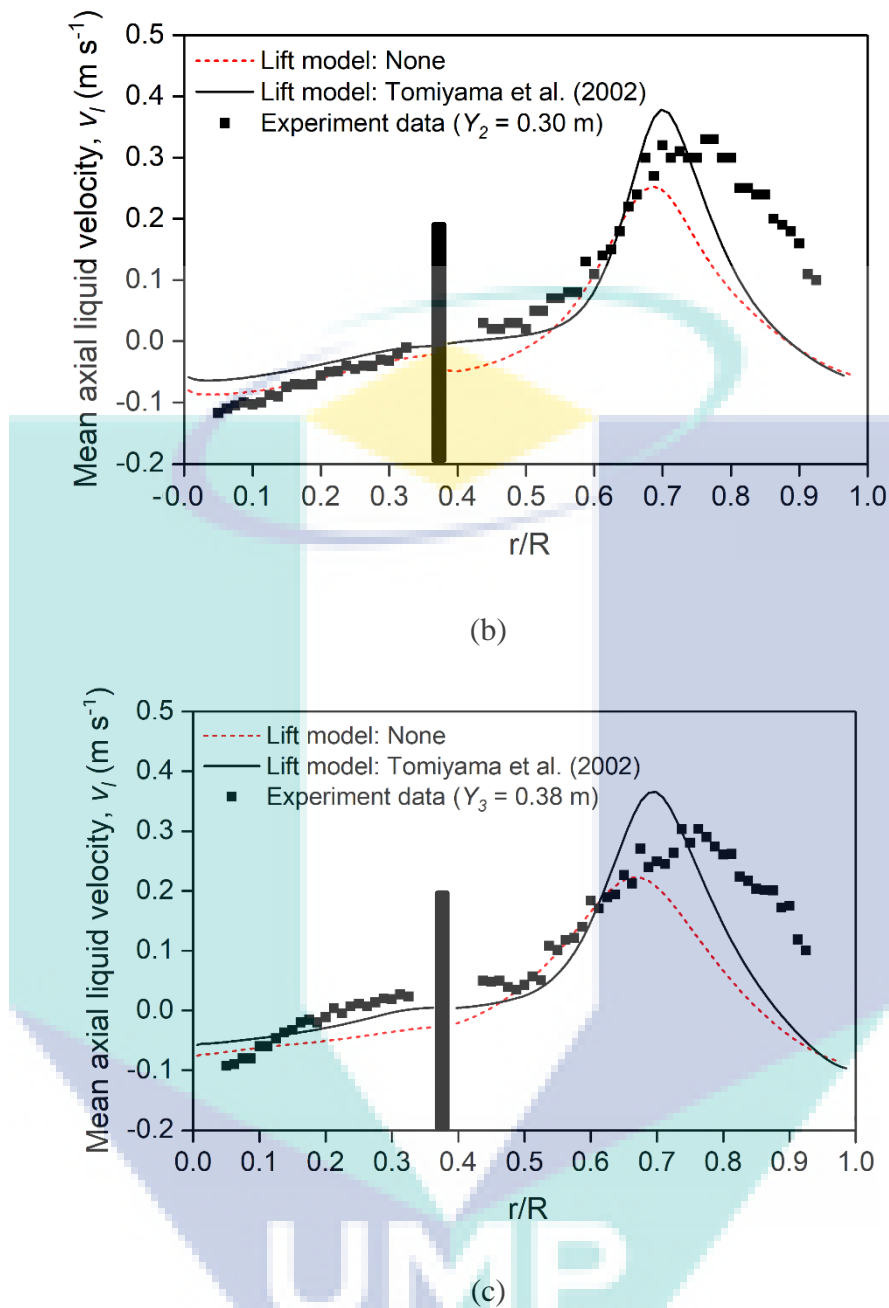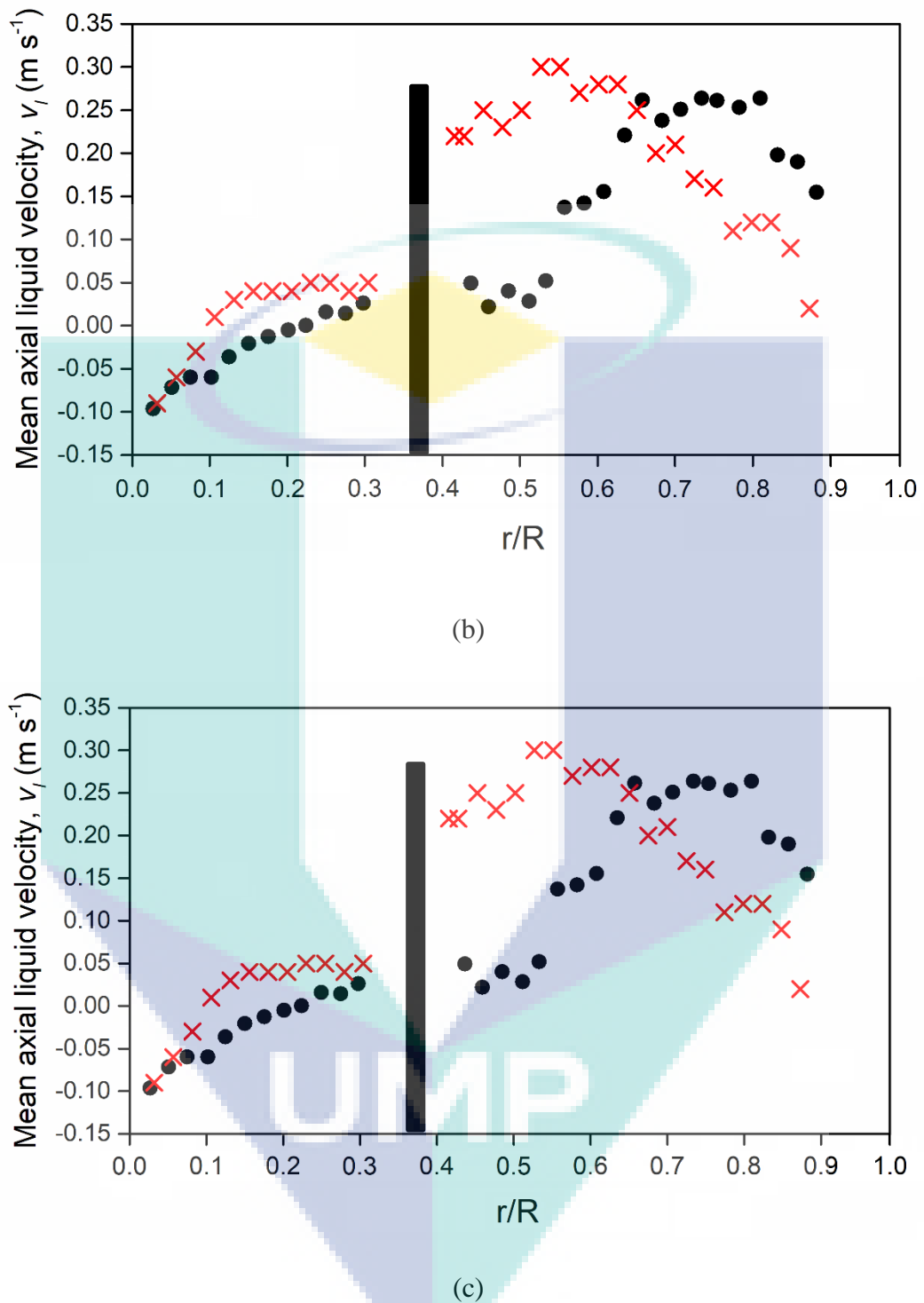
Figure 4.12   continued

LDA techniques was adopted to obtain the mean flow quantities of the axial liquid velocity. The sparger was placed in two positions denoted as X_A at position of 0.125 m which is at the centre of the riser and X_B at the position of 0.075 m which is placed nearer to the baffle wall of the internal airlift reactor. Overall we can observe that the measured

axial liquid velocity differ between both positions in terms of their axial velocity distribution. The magnitude of the axial velocities for both sparger positions are almost similar across the height (i.e. $Y_1 = 0.20$ m, $Y_2 = 0.30$ m and $Y_3 = 0.38$ m) of the riser $0.4 < r/R < 1.0$. However, it can be seen that the axial liquid velocity in the downcomer is slightly lower as shown at height $Y_1 = 0.20$ m and $Y_2 = 0.30$ m at $0.0 < r/R < 0.3$. This would indicate that when the sparger is placed closer to the wall, the circulation flow will be lower in the downcomer.

Recirculation of the flow field is also more evident when sparger was at position $X_B = 0.075$ m. At $0.1 < r/R < 0.3$ across height $Y_1 = 0.20$ m and $Y_2 = 0.30$ m, the positive values of mean axial liquid velocity indicates an up flow occurs near the baffle wall in the downcomer which is absence in sparger at position $X_B = 0.125$ m. Moreover, due to the position of the sparger X_B being close to the wall, recirculation is also occurring more in the riser as shown at $0.8 < r/R < 0.9$ in Figure 4.12 (a). At height $Y_3 = 0.38$ m the flow is more vigorous spreading above the riser and downcomer. This region is known as the gas disengagement zone. It can be seen that, the velocity profile in the downcomer in Figure 4.12 (c) is much steeper than the sparger position in X_A. All these elements indicate that, the sparger position at X_B would be too energy inefficient as more velocity recirculation are occurring instead of flowing according to the direction of the bulk fluid. The sparger position in X_A is by far most suitable as it has higher liquid velocity circulation (i.e. evident from the magnitude of the liquid velocity in the downcomer) and also has a more controlled flow.

CHAPTER 5

CONCLUSION

5.1   Conclusions

CFD model is a useful tool to predict the gas-liquid bubbly flow field within the internal airlift reactor through the two-fluid model. A robust closure model which accounts the momentum exchange forces would be required to complete the two-fluid model. The closure model which were being evaluated in this study (i.e. drag, lift, turbulent dispersion and bubble-induced turbulence) would be crucial to obtain an accurate prediction on the gas holdup in the internal airlift reactor. The objectives of this study have been attained through the findings from the assessment and comparison studies of the closure model as summarised as shown below:

i.   Evaluation on the closure model showed that the drag model only was underpredicted by two-folds. The spherical drag model through the Schiller and Naumann (1935) obtain similar predictions with other drag models in the riser but obtained major discrepancy in the downcomer due to counter-current flow. Meanwhile, the lift model was noticeably significant with increasing height of the internal airlift reactor. The turbulent dispersion model is crucial for the prediction of gas distribution. Meanwhile the bubble-induced turbulence cause discrepancy in the results.

ii.   The closure model has been validated in through two internal airlift reactor configurations with partial gas disengaged and total gas disengagement. It was found that in the partial gas disengaged internal airlift reactor the inclusion of the Universal drag model, Tomiyama et al. (20020 and turbulent dispersion model through the drift velocity Simonin and Viollet (1990) were able to predict the

surface-averaged gas holdup, radial gas holdup and liquid velocity within 19.4%, 6.8% and 13.5% mean error, respectively. Meanwhile, in the total gas disengagement internal airlift reactor axial liquid velocity predicted across the riser and downcomer managed to obtain 52.7% through the inclusion of the Universal drag model, Tomiyama et al. (2002) lift model and Simonin and Viollet (1990) turbulent dispersion model.

iii. The influence of the sparger position on the gas-liquid internal airlift reactor was being evaluated and had been found that at position, $X_A = 0.125$ m which is at the centre position of the riser, gives a higher magnitude of liquid velocity meanwhile position $X_B = 0.075$ m is energy intensive as an occurrence of liquid recirculation appears within the downcomer at height $Y_2 = 0.30$ m. Sparger position $X_B = 0.075$ m tends to be more vigorous as evidence in the liquid velocities spread across $Y_3 = 0.38$ m. position, $X_A = 0.125$ m is far more suitable in order to have a more efficient flow and unnecessary recirculation and dead zones especially for bioprocesses.

The main contributions of this thesis is the development of a modelling strategy using the two-fluid model to simulate the hydrodynamics within bubbly flow in gas-liquid internal airlift reactors at homogeneous regime. The closure models (i.e. drag, lift and turbulent dispersion) proposed were able to predict the mean flow quantities with good agreement with experimental data. Aside from that, the employment of the drag model was also elucidated to play a significant role in both the gas holdup in the downcomer and axial liquid velocity in the riser. On the other hand, the effect of sparger position was also studied using LDA and was found to be energy efficient when located in the middle at the bottom of the riser.

5.2   Recommendations

It is desired that in the future studies to extend the CFD modelling approach to be more applicable in industrial scale up therefore here are the recommendations that can be done:

i. Extend the measured LDA mean quantities to turbulent quantities for more realistic validation for the CFD model. Turbulent quantities affects the bubbles size and mixing which are both important in mass transfer processes.

ii. Bubble dynamic which is governed by bubble coalescence and breakage can be accounted in future studies to model an accurate bubble size distribution. The bubble size distribution will be able to increase the accuracy of the mass transfer predicted

iii. Case studies on novelty airlift reactors for applications in wastewater treatments which would be energy saving and efficient mixing. Increment in population and industrial plants in Malaysia would require advancement in technology for economical pre-treatment before being discharged into sewages. Mixing time and mass transfer models can be included to complete the CFD model for various applications in industrial what-if analysis.

REFERENCES

Amooghin, A.E., Jafari, S., Sanaeepur, H. and Kargari, A. (2015). Computational fluid dynamics simulation of bubble coalescence and breakup in an internal airlift reactor: Analysis of effects of a draft tube on hydrodynamics and mass transfer. *Applied Mathematical Modelling*, *39*, 1616-1642.

Asadi, A., Zinatizadeh, A.A. and Van Loosdrecht, M. (2016). High rate simultaneous nutrients removal in a single air lift bioreactor with continuous feed and intermittent discharge regime: Process optimization and effect of feed characteristics. *Chemical Engineering Journal*, *301*, 200-209.

Auton, T.R. (1987). The lift force on a spherical body in a rotational flow. *Journal of Fluid Mechanics*, *183*, 199-218.

Balleda, A., Pushpavanam, S. and Deshpande, A. (2007). Experimental and numerical investigation of liquid circulation induced by a bubble plume in a baffled tank. *Chemical Engineering Science*, *62*, 4689-4704.

Bannari, R., Bannari, A., Selma, B. and Proulx, P. (2011). Mass transfer and shear in an airlift bioreactor: Using a mathematical model to improve reactor design and performance. *Chemical Engineering Science*, *66*, 2057-2067.

Becker, S., Sokolichin, A. and Eigenberger, G. (1994). Gas—liquid flow in bubble columns and loop reactors: Part II. Comparison of detailed experiments and flow simulations. *Chemical Engineering Science*, *49*, 5747-5762.

Bednarz, A., Weber, B. and Jupke, A. (2017). Development of a CFD model for the simulation of a novel multiphase counter-current loop reactor. *Chemical Engineering Science*, 161, 350-359.

Behin, J. (2010). Modeling of modified airlift loop reactor with a concentric double-draft tube. *Chemical Engineering Research and Design*, *88*, 919-927.

Behin, J., and Ahmadi, A. (2010). Mixing parameters for an airlift bioreactor considering constant cross sectional area of riser to downcomer: Effect of sparging gas location. *Korean Journal of Chemical Engineering*, 27, 1226-1232.

Behin, J. and Farhadian, N. (2013). Residence time distribution measurements in a two dimensional rectangular airlift reactor by digital image processing. *Experimental Thermal and Fluid Science*, *51*, 244-250.

Bel Fdhila, R. and Simonin, O. (1992). Eulerian prediction of a turbulent bubbly flow downstream of a sudden pipe expansion. *In Proceedings 5th Workshop on Two-Phase Flow Predictions*, 264.

Bello, R.A., Robinson, C.W. and Moo- Young, M. (1984). Liquid circulation and mixing characteristics of airlift contactors. *The Canadian Journal of Chemical Engineering*, *62*, 573-577.

Benemann, J.R. (2009). Microalgae biofuels: A brief introduction. *Benemann Associates*

and MicroBio Engineering, Walnut Creek, CA.

Blažej, M., Kiša, M. and Markoš, J. (2004). Scale influence on the hydrodynamics of an internal loop airlift reactor. *Chemical Engineering and Processing: Process Intensification*, *43*, 1519-1527.

Blocken, B., Stathopoulus, T. and van Beeck, J.P.A.J. (2016). Pedestrian-level wind conditions around buildings: Review of wind-tunnel and CFD techniques and their accuracy for wind comfort assessment. *Building and Environment*, 100, 50-81.

Burns, A.D., Frank, T., Hamill, I. and Shi, J.M. (2004). The Favre averaged drag model for turbulent dispersion in Eulerian multi-phase flows. In *5th International Conference on Multiphase Flow.*

Buwa, V.V., Deo, D.S. and Ranade, V.V. (2006). Eulerian–Lagrangian simulations of unsteady gas–liquid flows in bubble columns. *International Journal of Multiphase Flow*, *32*, 864-885.

Cao, C., Dong, S. and Guo, Q. (2007). Experimental and Numerical Simulation for Gas−Liquid Phases Flow Structure in an External-Loop Airlift Reactor. *Industrial & Engineering Chemistry Research*, *46*, 7317-7327.

Chao, Y., Ishida, T., Sugano, Y. and Shoda, M. (2000). Bacterial cellulose production by Acetobacter xylinum in a 50- l internal- loop airlift reactor. *Biotechnology and Bioengineering*, *68*, 345-352.

Chen, J., Yang, N., Ge, W. and Li, J. (2008). Modeling of regime transition in bubble columns with stability condition. *Industrial & Engineering Chemistry Research*, *48*, 290-301.

Chen, L. and Bai, Z. (2017). CFD simulation of the hydrodynamics in an industrial scale cyclohexane oxidation airlift loop reactor. *Chemical Engineering Research and Design*, *119*, 33-46.

Chisti, M.Y. and Moo-Young, M. (1987). Airlift reactors: characteristics, applications and design considerations. *Chemical Engineering Communications*, *60*, 195-242.

Chisti, M.Y. and Moo-Young, M. (1988). Gas holdup in pneumatic reactors. *Chemical Engineering Journal*, *38*, 149-152.

Chisti, M.Y., Halard, B. and Moo-Young, M. (1988). Liquid circulation in airlift reactors. *Chemical Engineering Science*, *43*, 451-457.

Chisti, Y. (1998). Pneumatically agitated bioreactors in industrial and environmental bioprocessing: hydrodynamics, hydraulics and transport phenomena. *Applied Mechanics Reviews*, *51*, 33-112.

Chisti, Y. (2008). Biodiesel from microalgae beats bioethanol. *Trends in Biotechnology*, *26*, 126-131.

Chisti, Y. and Moo-Young, M. (1993). Improve the performance of airlift

reactors. *Chemical Engineering Progress*, *89*, 38-38.

Clift, R. (1978). Bubbles. Drops and Particles. *Academic Press*.

Cockx, A., Line, A., Roustan, M., Do-Quang, Z. and Lazarova, V. (1997). Numerical simulation and physical modeling of the hydrodynamics in an air-lift internal loop reactor. *Chemical Engineering Science*, *52*, 3787-3793.

Couvert, A., Bastoul, D., Roustan, M. and Chatellier, P. (2004). Hydrodynamic and mass transfer study in a rectangular three-phase air-lift loop reactor. *Chemical Engineering and Processing: Process Intensification*, *43*, 1381-1387.

Datta, S., Christena, L.R. and Rajaram, Y.R.S. (2013). Enzyme immobilization: An overview on techniques and support materials. *Biotech*, *3*, 1-9.

Davarnejad, R., Bagheripoor, E. and Sahraei, A. (2012). CFD simulation of scale influence on the hydrodynamics of an internal loop airlift reactor. *Engineering*, *4*, 668.

Deen, N. (2001). An experimental and computational study of fluid dynamics in gas-liquid chemical reactors. Aalborg University.

Dhanasekharan, K.M., Sanyal, J., Jain, A. and Haidari, A. (2005). A generalized approach to model oxygen transfer in bioreactors using population balances and computational fluid dynamics. *Chemical Engineering Science*, *60*, 213-218.

Dhaouadi, H., Poncin, S., Hornut, J.M., Wild, G., Oinas, P. and Korpijarvi, J. (1997). Mass transfer in an external-loop airlift reactor: experiments and modeling. *Chemical Engineering Science*, *52*, 3909-3917.

Dijkhuizen, W., Roghair, I., Annaland, M.V.S. and Kuipers, J.A.M. (2010). DNS of gas bubbles behaviour using an improved 3D front tracking model - drag force on isolated bubbles and comparison with experiments. *Chemical Engineering Science*, *65*, 1415-1426.

Drew, D.A. and Lahey Jr, R.T. (1979). Application of general constitutive principles to the derivation of multidimensional two-phase flow equations. *International Journal of Multiphase Flow*, *5*, 243-264.

Elghobashi, S.E. and Abou- Arab, T.W. (1983). A two- equation turbulence model for two- phase flows. *The Physics of Fluids*, *26*, 931-938.

Garcia-Ochoa, F., and Gomez, E. (2004). Theoretical prediction of gas–liquid mass transfer coefficient, specific area and hold-up in sparged stirred tanks. *Chemical Engineering Science*, *59*, 2489-2501.

Garcia-Ochoa, F. and Gomez, E. (2009). Bioreactor scale-up and oxygen transfer rate in microbial processes: an overview. *Biotechnology Advances*, *27*, 153-176.

Gimbun, J., Rielly, C.D. and Nagy, Z.K. (2009). Modelling of mass transfer in gas–liquid stirred tanks agitated by Rushton turbine and CD-6 impeller: A scale-up study. *Chemical Engineering Research and Design*, *87*, 437-451.

Gosman, A.D., Lekakou, C., Politis, S., Issa, R.I. and Looney, M.K. (1992). Multidimensional modeling of turbulent two- phase flows in stirred vessels. *AIChE Journal*, *38*, 1946-1956.

Grace, J.R. (1976). Shapes and velocities of single drops and bubbles moving freely through immiscible liquids. *Chemical Engineering Research and Design*, *54*, 167-173.

Granata, T. (2017). Dependency of microalgal production on biomass and the relationship to yield and bioreactor scale-up for biofuels: A statistical analysis of 60+ years of algal bioreactor data. *BioEnergy Research*, *10*, 267-287.

Groen, J.S., Oldeman, R.G.C., Mudde, R.F. and Van Den Akker, H.E.A. (1996). Coherent structures and axial dispersion in bubble column reactors. *Chemical Engineering Science*, *51*, 2511-2520.

Gumery, F., Ein-Mozaffari, F. and Dahman, Y. (2009). Characteristics of local flow dynamics and macro-mixing in airlift column reactors for reliable design and scale-up. *International Journal of Chemical Reactor Engineering*, 7(*1*), 1-47.

Hekmat, A., Amooghin, A.E. and Moraveji, M.K. (2010). CFD simulation of gas–liquid flow behaviour in an air-lift reactor: determination of the optimum distance of the draft tube. *Simulation Modelling Practice and Theory*, *18*, 927-945.

Hills, J.H. (1976). The Operation of a bubble column at high throughputs I. Gas holdup measurement. *Chemical Engineering Journal*, *12*, 89-99.

Hosseini, N. S., Shang, H., Ross, G. M., & Scott, J. A. (2016). Comparative analysis of top-lit bubble column and gas-lift bioreactors for microalgae-sourced biodiesel production. *Energy Conversion and Management*, *130*, 230-239.

Huang, Q., Yang, C., Yu, G. and Mao, Z. S. (2010). CFD simulation of hydrodynamics and mass transfer in an internal airlift loop reactor using a steady two-fluid model. *Chemical Engineering Science*, *65*, 5527-5536.

Ishii, M. and Zuber, N. (1979). Drag coefficient and relative velocity in bubbly, droplet or particulate flows. *AIChE Journal*, *25*, 843-855.

Issa, R.I. and Oliveira, P.J. (1993). Modelling of turbulent dispersion in two phase flow jets. *In Engineering Turbulence Modelling and Experiments*, 947-957.

Jakobsen, H.A., Sannæs, B.H., Grevskott, S. and Svendsen, H.F. (1997). Modeling of vertical bubble-driven flows. *Industrial and Engineering Chemistry Research*, *36*, 4052-4074.

Jia, X., Wen, J., Feng, W. and Yuan, Q. (2007). Local hydrodynamics modeling of a gas-liquid-solid three-phase airlift loop reactor. *Industrial and Engineering Chemical Resources, 46*, 5210-5220.

Jiang, X., Yang, N. and Yang, B. (2016). Computational fluid dynamics simulation of hydrodynamics in the riser of an external loop airlift reactor. *Particuology*, 27, 95-101.

Jones, S. M., and Harrison, S. T. (2014). Aeration energy requirements for lipid production by Scenedesmus sp. in airlift bioreactors. *Algal Research*, *5*, 249-257.

Jones, S. T., and Heindel, T. J. (2010). Hydrodynamic considerations in an external loop airlift reactor with a modified downcomer. *Industrial & Engineering Chemistry Research*, *49*, 1931-1936.

Kadic, E. and Heindel, T.J. (2014). An introduction to bioreactor hydrodynamics and gas-liquid mass transfer. *John Wiley & Sons*.

Karamanev, D.G. and Nikolov, L.N. (1992). Free rising spheres do not obey Newton's law for free settling. *AIChE Journal*, 38, 1843-1846.

Karcz, J., Musiał, M., Bitenc, M. and Domański, M. (2013). CFD modelling of the fluid flow characteristics in an external-loop air-lift reactor. *Chemical Engineering*, *32*.

Kataoka, I. and Serizawa, A. (1989). Basic equations of turbulence in gas-liquid two-phase flow. *International Journal of Multiphase Flow*, *15*, 843-855.

Kawase, Y., and Moo-Young, M. (1990). Mathematical models for design of bioreactors: Applications of: Kolmogoroff's theory of isotropic turbulence. *The Chemical Engineering Journal*, *43*, B19-B41.

Kawase, Y., Tsujimura, M. and Yamaguchi, T. (1995). Gas hold-up in external-loop airlift bioreactors. *Bioprocess Engineering*, *12*, 21-27.

Kilonzo, P.M., Margaritis, A., Bergougnou, M.A., Yu, J. and Ye, Q. (2007). Effects of geometrical design on hydrodynamic and mass transfer characteristics of a rectangular-column airlift bioreactor. *Biochemical Engineering Journal*, *34*, 279-288.

Kleinstreuer, C. (2003). Two-phase flow: theory and applications. *CRC Press*.

Koide, K., Kimura, M., Nitta, H. and Kawabata, H. (1988). Liquid circulation in bubble column with draught tube. *Journal of Chemical Engineering of Japan*, 21, 393-399.

Kolev N.I. (2005). Multiphase Flow Dynamics 2: Thermal and Mechanical Interactions. Berlin, Germany: *Springer*.

Lahey, J.R.T., De Bertodano, M.L. and Jones J.O.C. (1993). Phase distribution in complex geometry conduits. *Nuclear Engineering and Design*, *141*, 177-201.

Launder, B.E. and Spalding, D.B. (1974). The numerical computation of turbulent flow Computer methods in applied mechanics and engineering. Надійшла до редакції.

Law, D., Battaglia, F. and Heindel, T.J. (2008). Simulating Gas-Liquid Flows in an External Loop Airlift Reactor. In ASME 2008 International Mechanical Engineering Congress and Exposition. *American Society of Mechanical Engineers*, 395-403.

Lefrancois, L., Mariller, C.G. and Mejane, J.V. (1955). Effectionnements aux procedes

de cultures forgiques et de fermentations industrielles. *Brevet d'Invention*, France, (1), 102.

Lestinsky, P., Vayrynen, P., Vecer, M. and Wichterle, K. (2012). Hydrodynamics of airlift reactor with internal circulation loop: experiment vs. CFD simulation. *Procedia Engineering*, *42*, 892-907.

Li, G.Q., Yang, S.Z., Cai, Z.L. and Chen, J.Y. (1995). Mass transfer and gas-liquid circulation in an airlift bioreactor with viscous non-Newtonian fluids. *The Chemical Engineering Journal and the Biochemical Engineering Journal*, *56*, 101-107.

Liao, J., Ziegenhein, T. and Rzehak, R. (2016). Bubbly flow in an airlift column: A CFD study. *Journal of Chemical Technology and Biotechnology*, 91, 2904-2915.

Lin, T.J. and Chen, P.C. (2005). Studies on hydrodynamics of an internal-loop airlift reactor in gas entrainment regime by particle image analyzer. *Chemical Engineering Journal*, *108*, 69-79.

Lopez, B.M. (1991). *Turbulent bubbly flow in a triangular duct* (Doctoral dissersation). Troy, New York: Rensselaer Polytechnic Institute.

Lucas, D. and Tomiyama, A. (2011). On the role of the lateral lift force in poly-dispersed bubbly flows. *International Journal of Multiphase Flow*, *37*, 1178-1190.

Luo, H.P. and Al-Dahhan, M.H. (2011). Verification and validation of CFD simulations for local flow dynamics in a draft tube airlift bioreactor. *Chemical Engineering Science*, *66*, 907-923.

Luo, L., Yuan, J., Xie, P., Sun, J. and Guo, W. (2013). Hydrodynamics and mass transfer characteristics in an internal loop airlift reactor with sieve plates. *Chemical Engineering Research and Design*, *91*, 2377-2388.

Mahmood, K. A., Wilkinson, S. J., and Zimmerman, W. B. (2015). Airlift bioreactor for biological applications with microbubble mediated transport processes. *Chemical Engineering Science*, *137*, 243-253.

Massart, A., Mirisola, A., Lupant, D., Thomas, D. and Hantson, A.L. (2014). Experimental characterization and numerical simulation of the hydrodynamics in an airlift photobioreactor for microalgae cultures. *Algal Research*, *6*, 210-217.

McClure, D.D., Dolton, T.P., Barton, G.W., Fletcher, D.F. and Kavanagh, J.M. (2017). Hydrodynamics and mixing in airlift contactors: Experimental work and CFD modelling. *Chemical Engineering Research and Design*, *127*, 154-169.

Merchuk, J.C. and Gluz, M. (1999). Bioreactors, Air-lift reactors. *Gas*, *1*, 2.

Merchuk, J.C. and Siegel, M.H. (2007). Air-lift reactors in chemical and biological technology. *Journal of Chemical Technology and Biotechnology*, *41*, 105-120.

Mirón, A.S., Garcıa, M.C.C., Gómez, A.C., Camacho, F.G., Grima, E.M. and Chisti, Y. (2003). Shear stress tolerance and biochemical characterization of Phaeodactylum

tricornutum in quasi steady-state continuous culture in outdoor photobioreactors. *Biochemical Engineering Journal*, *16*, 287-297.

Masood, R.M.A. and Delgado, A. (2014). Numerical investigation of the interphase forces and turbulence closure in 3D square bubble columns. *Chemical Engineering Science*, 108, 154-168.

Mohajerani, M., Mehrvar, M. and Ein- Mozaffari, F. (2012). CFD analysis of two–phase turbulent flow in internal airlift reactors. *The Canadian Journal of Chemical Engineering*, 90, 1612-1631.

Montoya, G., Lucas, D., Baglietto, E. and Liao, Y. (2016). A review on mechanisms and models for the churn-turbulent flow regime. *Chemical Engineering Science*, *141*, 86-103.

Moraveji, M. K., Sajjadi, B., Jafarkhani, M., and Davarnejad, R. (2011). Experimental investigation and CFD simulation of turbulence effect on hydrodynamic and mass transfer in a packed bed airlift internal loop reactor. *International Communications in Heat and Mass Transfer*, *38*, 518-524.

Mudde, R.F., Groen, J.S. and Van Den Akker, H.E.A. (1997). Liquid velocity field in a bubble column: LDA experiments. *Chemical Engineering Science*, *52*, 4217-4224.

Mudde, R.F., Groen, J.S. and Van Den Akker, H.E.A. (1998). Application of LDA to bubbly flows. *Nuclear Engineering and Design*, *184*, 329-338.

Oey, R.S., Mudde, R.F. and Van Den Akker, H.E. (2003). Numerical simulations of an oscillating internal- loop airlift reactor. *The Canadian Journal of Chemical Engineering*, *81*, 684-691.

Oldshue, J.Y. (1983). Fluid mixing technology. *McGraw-Hill*.

Paul, E.L., Atiemo-Obeng, V.A. and Kresta, S.M. (Eds.). (2004). Handbook of industrial mixing: science and practice. *John Wiley & Sons*.

Pirouzi, A., Nosrati, M., Shojaosadati, S. A., and Shakhesi, S. (2014). Improvement of mixing time, mass transfer, and power consumption in an external loop airlift photobioreactor for microalgae cultures. *Biochemical Engineering Journal*, 87, 25-32.

Popovic, M. K., and Robinson, C. W. (1989). Mass transfer studies of external- loop airlifts and a bubble column. *AIChE journal*, *35*, 393-405.

Ranade, V.V., Perrard, M., Xuereb, C., Le Sauze, N. and Bertrand, J. (2001). Influence of gas flow rate on the structure of trailing vortices of a Rushton turbine: PIV measurements and CFD simulations. *Chemical Engineering Research and Design*, 79, 957-964.

Rayi, N. K., & Ananthula, V. V. (2014). Biodegradation of phenolic wastewater in a bubble column bioreactor with internal draft tube.

Roy, S., Dhotre, M.T. and Joshi, J.B. (2006). CFD simulation of flow and axial dispersion in external loop airlift reactor. *Chemical Engineering Research and Design*, *84*, 677-690.

Roy, S., Dhotre, M.T., and Joshi, J. B. (2006). CFD simulation of flow and axial dispersion in external loop airlift reactor. *Chemical Engineering Research and Design*, *84*, 677-690.

Rzehak, R., Ziegenhein, T., Kriebitzsch, S., Krepper, E., and Lucas, D. (2017). Unified modeling of bubbly flows in pipes, bubble columns, and airlift columns. *Chemical Engineering Science*, 157, 147-158.

Sato, Y., Sadatomi, M. and Sekoguchi, K. (1981). Momentum and heat transfer in two-phase bubble flow-I. Theory. *International Journal of Multiphase Flow*, *7*, 167-177.

Schiller, L. and Naumann, A. (1935). A drag coefficient correlation. *Zeitschrift des Vereins Deutscher Ingenieure*, *77*, 318-320,

Schwarz, M.P. and Turner, W.J. (1988). Applicability of the standard k-ϵ turbulence model to gas-stirred baths. *Applied Mathematical Modelling*, *12*, 273-279.

Shoda, M. and Sugano, Y. (2005). Recent advances in bacterial cellulose production. *Biotechnology and Bioprocess Engineering*, *10*, 1.

Siegel, M.H. and Robinson, C.W. (1992). Application of airlift gas-liquid-solid reactors in biotechnology. *Chemical Engineering Science*, *47*, 3215-3229.

Siegel, M.H., Merchuk, J.C. and Schugeri, K. (1986). Air-lift reactor analysis: interrelationships between riser, downcomer, and gas-liquid separator behaviour, including gas recirculation effects. *AIChE Journal*, 32(*10*), 1585-1596.

Silva, M.K., d'Ávila, M.A. and Mori, M. (2011). CFD modelling of a bubble column with an external loop in the heterogeneous regime. *The Canadian Journal of Chemical Engineering*, *89*, 671-681.

Šimčík, M., Mota, A., Ruzicka, M.C., Vicente, A. and Teixeira, J. (2011). CFD simulation and experimental measurement of gas holdup and liquid interstitial velocity in internal loop airlift reactor. *Chemical Engineering Science*, *66*, 3268-3279.

Simonin, O. and Viollet, P.L. (1990). Modelling of turbulent two-phase jets loaded with discrete particles. *Phenomena in Multiphase Flows*, 259-269.

Smith, B.L. (1998). On the modelling of bubble plumes in a liquid pool. *Applied Mathematical Modelling*, *22*, 773-797.

Sokolichin, A., Eigenberger, G. and Lapin, A. (2004). Simulation of buoyancy driven bubbly flow: established simplifications and open questions. *AIChE Journal*, *50*, 24-45.

Stiriba, Y., Gourich, B. and Vial, C. (2017). Numerical modeling of ferrous iron oxidation in a split-rectangular airlift reactor. *Chemical Engineering Science*, 170, 705-719.

Tabib, M.V., Roy, S.A. and Joshi, J.B. (2008). CFD simulation of bubble column—An analysis of interphase forces and turbulence models. *Chemical Engineering Journal*, *139*, 589-614.

Talvy, S., Cockx, A. and Line, A. (2005). Global modelling of a gas–liquid–solid airlift reactor. *Chemical Engineering Science*, *60*, 5991-6003.

Talvy, S., Cockx, A. and Line, A. (2007). Modeling hydrodynamics of gas–liquid airlift reactor. *AIChE Journal*, *53*, 335-353.

Tan, W.S., Dai, G.C., Ye, W. and Shen, J.P. (1995). Local flow behavior of the liquid phase in an airlift bioreactor for potential use in animal cell suspension cultures. *The Chemical Engineering Journal and The Biochemical Engineering Journal*, 57, 31-36.

Tomiyama, A. (2004). Drag, lift and virtual mass forces acting on a single bubble. *In 3rd International Symposium Two-Phase Flow Modeling and Experimentation Pisa*.

Tomiyama, A., Kataoka, I., Zun, I. and Sakaguchi, T. (1998). Drag coefficients of single bubbles under normal and micro gravity conditions. *JSME International Journal Series B Fluids and Thermal Engineering*, *41*, 472-479.

Tomiyama, A., Tamai, H., Zun, I. and Hosokawa, S. (2002). Transverse migration of single bubbles in simple shear flows. *Chemical Engineering Science*, *57*, 1849-1858.

Troshko, A.A. and Hassan, Y.A. (2001). A two-equation turbulence model of turbulent bubbly flows. *International Journal of Multiphase Flow*, *27*, 1965-2000.

van Baten, J.M., Ellenberger, J. and Krishna, R. (2003). Using CFD to Describe the Hydrodynamics of Internal Air- lift Reactors. *The Canadian Journal of Chemical Engineering*, *81*, 660-668.

Vial, C., Poncin, S., Wild, G. and Midoux, N. (2002). Experimental and theoretical analysis of the hydrodynamics in the riser of an external loop airlift reactor. *Chemical Engineering Science*, 57, 4745-4762.

Wellek, R.M., Agrawal, A.K. and Skelland, A.H.P. (1966). Shape of liquid drops moving in liquid media. *AIChE Journal*, *12*, 854-862.

Wilkinson, P.M. (1991). *Physical aspects and scale-up of high pressure bubble columns* (Doctoral dissertation). Groningen, Netherlands: Rijksuniversiteit Groningen.

Zhang, D.Z. and VanderHeyden, W.B. (2002). The effects of mesoscale structures on the macroscopic momentum equations for two-phase flows. *International Journal of Multiphase Flow*, *28*, 805-822.

Zhang, T., Wei, C., Feng, C. and Zhu, J. (2012). A novel airlift reactor enhanced by funnel internals and hydrodynamics prediction by the CFD method. *Bioresource Technology*, *104*, 600-607.

Zhang, T., We, C., Ren, Y., Feng, C., and Wu, H. (2017). Advances in airlift reactors: modified design and optimization of operation conditions. *Reviews in Chemical Engineering*, *33*, 163-182.

Zhang, T., Wei, C., Feng, C., Ren, Y., Wu, H. and Preis, S. (2019). Advances in characteristics analysis, measurement methods and modelling of flow dynamics in airlift reactors. *Chemical Engineering & Processing: Process Intensification, 144*, 107633.

Zhou, G. (1998). Characteristics of turbulence energy dissipation and liquid-liquid dispersions in an agitated tank. University of Alberta.

Ziegenhein, T., Zalucky, J., Rzehak, R. and Lucas, D. (2016). On the hydrodynamics of airlift reactors, Part I: Experiments. *Chemical Engineering Science*, *150*, 54-65.

Znad, H., Báleš, V. and Kawase, Y. (2004). Modeling and scale up of airlift bioreactor. *Computers & Chemical Engineering*, *28*, 2765-2777.

Žun, I. (1980). The transverse migration of bubbles influenced by walls in vertical bubbly flow. *International Journal of Multiphase Flow*, *6*, 583-588.

LIST OF PUBLICATIONS

Journal

1. Liew, S.Y., Lam, Z.Y., Gimbun, J. (2017). Experimental measurement and CFD simulation on the hydrodynamics of an internal-loop airlift reactor. *MATEC Web of Conferences*, 111(*1002*): 1-9. Scopus.

2. Liew, S.Y., Gimbun, J. (2017). CFD simulation on the hydrodynamics in gas-liquid airlift reactor. *Chemical Product and Process Modeling*, 12(*4*): 1-11. Scopus and ESCI ISI indexed.

3. Gimbun, J., Liew S.Y., Nagy, Z.K., Rielly, C.D. (2016). Three-way coupling simulation of a gas-liquid stirred tank using a multi-compartment population balance model. *Chemical Product and Process Modelling*, 11(3): 205-216. Scopus and ESCI ISI indexed.

Conference/Exhibition

1. Liew, S.Y., Lam Z.Y., Gimbun, J. Experimental measurement and CFD simulation on the hydrodynamics of an internal-loop airlift reactor. *FluidsChE 2017*, 4-6 April 2017, Kota Kinabalu, Sabah.

2. Liew, S.Y., Gimbun, J. CFD simulation of hydrodynamics in gas-liquid airlift reactor (Paper ID: PS30). *SOMChE 2016*, 1-3 December 2016, Miri, Sarawak.

3. Gimbun, J., Liew, S.Y., Nagy, Z.K., Rielly, C.D. Three-way coupling simulation of a gas-liquid stirred tank using a multi-compartment population balance model. *FluidsChE 2015*, 25-27 November 2015, Pulau Langkawi, Kedah